

technical steel research

Steel products and applications for building, construction and industry

Large web openings for service integration in composite floors

(1) C. Müller, O. Hechler, (2) A. Bureau, D. Bitar, D. Joyeux,
(3) L. G. Cajot, T. Demarco, (4) R. M. Lawson, S. Hicks, P. Devine,
(5) O. Lagerqvist, E. Hedman-Pétursson, E. Unosson, (6) M. Feldmann

(1) **RWTH** – Mies-van-der-Rohe Straße 1, D-52074 Aachen

(2) **CTICM** – Domaine de Saint-Paul, 102, route de Limours, F-78471 Saint-Rémy-lès-Chevreuse

(3) **ProfilArbed** – 66, rue de Luxembourg, L-4221 Esch-sur-Alzette

(4) **The Steel Construction Institute** – Silwood Park, Ascot SL5 7QN, Berkshire, United Kingdom

(5) **University of Luleå** – S-97 187 Luleå

(6) **Universität Kaiserslautern** – Postfach 3049, D-67653 Kaiserslautern

Contract No 7210-PR/315
1 July 2001 to 31 December 2003

Final report

Directorate-General for Research

LEGAL NOTICE

Neither the European Commission nor any person acting on behalf of the Commission is responsible for the use which might be made of the following information.

***Europe Direct is a service to help you find answers
to your questions about the European Union***

**Freephone number (*):
00 800 6 7 8 9 10 11**

(* Certain mobile telephone operators do not allow access to 00 800 numbers or these calls may be billed.

A great deal of additional information on the European Union is available on the Internet. It can be accessed through the Europa server (<http://europa.eu>).

Cataloguing data can be found at the end of this publication.

Luxembourg: Office for Official Publications of the European Communities, 2006

ISBN 92-79-01723-3

ISSN 1018-5593

© European Communities, 2006
Reproduction is authorised provided the source is acknowledged.

Printed in Luxembourg

PRINTED ON WHITE CHLORINE-FREE PAPER

Foreword

This report is subdivided into the following parts:

Part 1 contains a summary, general information on the project and a brief description of the works performed.

In **Part 2** test reports, analyses, evaluations and design models are presented in detail.

Design recommendations and predesign aids are given in **Part 3** of the report.

The **CD ROM** enclosed to the report contains:

- Part 1, Part 2 and Part 3 of the report in pdf-format
- a computer software for the design of steel and composite beams with single large web openings
- an interactive document including hypertext links for the predesign of cellular steel and composite beams fabricated from rolled I-sections; design aids such as loading tables are presented in terms of graphs and tables

Summary

The aim of the project "Large web openings for service integration in composite floors" was to experimentally and theoretically investigate the behaviour of steel and composite beams with web openings.

Therefore the works performed in the frame of this project have been subdivided into the following main topics:

- design of steel and composite beams with multiple regular or single large web openings under normal (cold) conditions
- design software for steel and composite beams with single large web openings and design aids for steel and composite cellular beams
- design of steel and composite beams with multiple regular web openings under fire conditions
- improved manufacture of cellular beams

Concerning the design of steel and composite beams with multiple regular or single large web openings under normal (cold) conditions the following tests were performed:

- 3 large scale tests on composite beams with multiple regular web openings with the aim to study:
 - the composite action at the supports of simply supported beams
 - the behaviour of elongated openings
 - the influence of load introduction via secondary beams
 - the influence of highly asymmetrical steel sections
- 1 large scale test on a pure steel beam to study the effect of different types of stiffening of web openings
- 8 large scale tests on steel and composite beams with unstiffened and stiffened single large web openings in order to study:
 - the various failure modes
 - the influence of the size and the position of single large web openings
 - the influence of the concrete slab
 - the influence of different types of stiffening

All tests could be verified by adequate Finite Element simulations, so that it was possible to perform further parameter studies in order to obtain information in areas not covered by the test programme. Further on extensive Finite Element analyses were performed to get information on the influence of non-centrally placed web openings leading to a simplified theory for the buckling resistance of web posts and an alternative compression field or strut model combining compression and bending in the web post.

For composite beams with multiple regular web openings the following main conclusions can be drawn:

- in general the failure mode of local instability, i.e. web post buckling, should not be decisive and be avoided by stiffening if necessary; ring stiffeners have been proven to be the most effective way of stiffening
- the influence of the load introduction via secondary beams is negligible, if minimum requirements (e.g. for the reinforcement, the strength of the secondary beams and its connection to the main girder, etc.) are met

- the influence of asymmetry is not as critical as first thought and the limitation given in the codes is too conservative
- the stiffness of beams is largely influenced by multiple regular web openings leading to larger deflections; thus the serviceability limit state is often governing the design

For steel and composite beams with unstiffened and stiffened single large web openings the summary of the conclusions is as follows:

- in general the adequate position of single large web openings should be chosen carefully in order to avoid premature failure due to local effects
- for the shear buckling verification a more accurate formula has been developed in terms of a reduction factor to the shear buckling resistance of webs without openings
- for the design model for the Vierendeel mechanism more beneficial limits for the cross sectional classification of the Tee section are proposed
- concerning elongated openings it could be verified that these can be treated in the same way as rectangular web openings
- the lateral torsional buckling check according to EN 1994-1-1 has been extended to cases with single large web openings; further on conditions are defined where no lateral torsional buckling check is necessary
- for semi-continuous joints recommendations for the position of the web opening were developed to guarantee that the joint behaviour is not influenced

A complete design guidance in terms of a step by step procedure has been elaborated giving a generalised method applicable to hot rolled and fabricated steel sections with discrete and regular openings. New aspects incorporated in this design guidance are

- the treatment of bending and tension interaction effects in the bottom Tee section
- the consideration of highly asymmetric sections
- the treatment of local composite effects at large web openings

Re-calculations of some of the experiments performed have been carried out showing that the procedure leads to satisfactory and conservative results.

A further outcome of the project is the development of a design software. This software designs and analyses composite and non-composite beams, under distributed and/or point loads and covers:

- composite and non-composite construction
- use of standard deck profiles, user defined decks or a solid slab
- propped and unpropped construction (of both the beam and the decking)
- use as an edge or an internal beam
- circular, rectangular and elongated openings, with or without stiffeners
- additional point loads and additional uniformly distributed loads
- use of normal weight and light weight concrete
- use of headed shear connectors (including Hilti HVB shear connectors)
- groups of shear connectors along the beam

The background of the software is documented in terms of an engineering logic.

Also a predesign tool for steel and composite cellular beams has been elaborated. It is presented in terms of a specific document including hypertext links to graphs and tables giving some general guidance on the predesign, the range of depth for cellular beams, section properties and loading tables. This simple and efficient tool has been developed on the basis of 50000 case studies on doubly symmetric cellular beams fabricated from European I-profiles for spans up to 24 m.

To study the behaviour of cellular composite beams under fire conditions two fire tests on specimens similar to those tested under normal (cold) conditions were carried out:

- an unloaded test in order to study the influence of the web openings and the way of application of the fire protection on the heat distribution
- a loaded test to investigate the influence of the web openings on the fire resistance

For both tests a sprayed fire protection has been used.

As conclusion from the test and the accompanying simulations on the heat distribution it can be stated that in general the inner edge of openings should be protected in order to avoid a specific assessment of the temperature field. The simple approach using massivity factors leads to safe-sided results.

Concerning the fire resistance under loading the comparison of the test result with numerical simulations leads to a good correlation as the failure mode, the time to failure and the vertical displacement could be reproduced. First thoughts on a very simple approach for the design of the fire protection thickness have been presented. Nevertheless there is only one test available and further investigations will be necessary.

Concerning the improvement of the manufacture of cellular beams the main focus was on the optimisation of the welding procedure of the web posts. The investigations have been performed in two steps.

In the first step 13 small scale tests on plates representing the web posts were carried out with different welding procedures, configurations and parameters with the aim to minimise the deformations from welding. It can be concluded that the two sided welding, without chamfering for web thicknesses smaller than 12 mm and with chamfering for web thicknesses greater than 12 mm, are the most efficient and economic solutions.

In the second step 8 real scale tests on short beams with symmetric and asymmetric cross sections loaded mainly in shear were made. If, from the overall design, full penetration butt weld were not necessary the welds were carried out as partial penetration butt welds in order to optimise the welding procedure and the consumption of the weld material. The test results could be verified by Finite Element analyses and further parameter studies were carried out.

As conclusion it can be stated that in many cases full penetration butt weld are not necessary, so that even chamfering can be avoided.

Contents	Page
1 Introduction and general	11
1.1 Project objectives	11
1.2 Ways and means	11
2 Contribution from RWTH	13
2.1 Introduction	13
2.2 Description of test programme	13
2.2.1 General arrangements	13
2.2.2 Test 1	14
2.2.3 Test 2A	15
2.2.4 Test 2B	17
2.2.5 Test 3	18
2.2.6 Test 4	19
2.3 Fabrication and execution	20
2.4 Testing	20
2.4.1 General	20
2.4.2 Experimental results	22
2.5 Numerical Simulations	29
2.5.1 General	29
2.5.2 Comparison between simulations and tests on composite beams	31
2.5.3 Comparison of test results and FE analysis	31
2.5.4 Parametric Studies	34
2.6 Summary and conclusion	39
2.7 Design recommendations	41
2.8 Literature	42
3 Contribution from CTICM	43
3.1 General	43
3.2 Predesign tools for cellular beams	44
3.2.1 Introduction	44
3.2.2 Steel cellular beams	44
3.2.3 Composite cellular beams	49
3.3 Fire behaviour of cellular beams	51
3.3.1 Experimental results on the unloaded beam	53
3.3.2 Experimental results on the loaded beam	55
3.3.3 Numerical mechanical behaviour of the loaded beam	57
3.3.4 Analysis	60

3.3.5	Conclusion	62
3.4	References	63
4	Contribution from PROFILARBED-RESEARCH	65
4.1	Summary	65
4.2	ACB ARCELOR Cellular Beams fabrication	65
4.3	Fabrication of the test specimen	65
4.4	Improvement of the welding procedures for cellular beams	66
4.4.1	Actual assembling procedure for cellular beams	66
4.4.2	Small scale tests	67
4.4.3	Large scale tests	72
5	Contribution from SCI	87
5.1	Finite Element analysis of web post buckling	87
5.2	Design guidance for composite beams with large openings for services	88
5.2.1	Existing publications	88
5.2.2	Scope of publication	89
5.2.3	Design codes	89
5.2.4	Material strengths	89
5.3	ARCELOR web post buckling tests	90
5.3.1	Symmetric Beams	90
5.3.2	Asymmetric Beams	91
5.3.3	Conclusions	91
5.4	Engineering logic for the analysis and design software	92
5.5	Design Software	102
5.6	References	105
6	Contribution from UNIV LULEA	107
6.1	General	107
6.2	Main objectives	107
6.3	Slender web beams	108
6.3.1	Test results	108
6.3.2	Shear buckling	109
6.3.3	Vierendeel bending	112
6.3.4	Web-post buckling	113
6.4	Elongated circular openings	113
6.5	Beams in compression including lateral restraints - Lateral torsional buckling of composite beams with web openings	114
6.6	Semi-continuous joints	119
6.7	References	120

1 Introduction and general

1.1 Project objectives

Currently, no design recommendations exist at a European level to permit design of large web openings in composite beams without particular tests for the individual purpose.

Within this project the following issues concerning steel and composite beams and composite floors with web openings have been studied by tests and theoretical investigations:

- behaviour under normal conditions (effects from web buckling, bending resistance, shear resistance, additional deflection from the web openings, effects of local composite action)
- behaviour under fire conditions including the effects from fire protection
- improvement of the manufacturing process of beams with single and regular web openings

On the basis of the results from the experimental and theoretical investigations design recommendations as well as simplified design aids have been elaborated. Further a computer software for the design of steel and composite beams with single web openings has been developed.

1.2 Ways and means

The works performed in the frame of the project have been subdivided into 5 working packages with several sub-tasks; for each working package one partner acted as the working package coordinator.

WP 1: Tests on composite beams with web openings (WP coordinator: RWTH)

- 1.1 Review existing tests and their performance. Identify unexpected performance and gaps in current tests.
- 1.2 Identify new test series to complement existing tests and to provide test information in areas of current practice.
- 1.3 Set up tests on composite beams, based on the objectives identified in 1.2.
- 1.4 Analyse the performance of these tests.
- 1.5 Prepare test reports.

WP 2: Improved manufacture of beams with web openings (WP coordinator: PROFILARBED)

- 2.1 Review current manufacturing processes.
- 2.2 Address improved manufacturing techniques.
- 2.3 Address requirements for connections.
- 2.4 Tests on modified or improved weld details and on distortion due to welding.
- 2.5 Address the use of high strength steel (S460) for perforated beams and the associated manufacturing requirements.

WP 3: Fire resistance of perforated beams (WP coordinator: PROFILARBED)

- 3.1 Review the methods in Eurocode 3 and 4 Parts 1.2 for establishing the fire resistance and fire protection required for steel and composite beams.
- 3.2 Identify fire tests on perforated beams.
- 3.3 Plan and execute fire tests.
- 3.4 Develop design rules for steel and composite beams with perforated webs taking account of the temperature distribution in the web and bottom flange in comparison to solid web beams. Prepare these rules in accordance with EC3 and EC4 Parts 1.2.
- 3.5 Prepare simplified design tables for perforated beams.

WP 4: Preparation of design guidance and software (WP coordinator: SCI)

- 4.1 Back-analyse all tests in accordance with the proposed design method. Present model factors to demonstrate the level of safety of the proposed method.
- 4.2 Prepare draft recommendations.
- 4.3 Prepare simplified design tables.
- 4.4 Prepare resp. extend existing computer software for analysis of steel and composite beams with large web openings.
- 4.5 Investigate practical issues of service integration for the cases identified above.
- 4.6 Prepare design recommendations.

WP 5: Special cases (WP coordinator: UNIV LULEA)

- 5.1 Develop design rules for slender web beams, including:
 - tension field action
 - vertical stiffeners
- 5.2 Develop design rules for elongated circular openings.
- 5.3 Develop design rules for beams subject to compression, including lateral restraints.
- 5.4 Develop design rules for semi-continuous construction through end-plate connections.

2 Contribution from RWTH

2.1 Introduction

The objectives of work package 1 “Tests on Composite Beams with Web Openings” has been to analyse the behaviour of composite beams with multiple regular web openings under “normal” conditions. Preliminary existing solutions have been reviewed to identify experimental investigations providing test information in areas of current practice. Consequently the following test programme has been fixed.

Test 1, Test 2 and Test 3 are tests on composite beams using metal sheets as a common composite slab system. Also a common concrete grade is used. Test 4 is a test on a pure steel beam. The following tests have been agreed:

- Test 1 is the basic test with the main focus on the composite action in the end cell; Test 1 could be extended to 2 tests 1A and 1B. After the expected failure at an opening at one end the specimen could be fixed and the test could be continued until failure at the opening at the other end.
- Test 2A investigates elongated openings; Test 2B tests the load introduction via secondary beams. The distance of the shear studs is kept similar to Test 1 or 3.
- Test 3 has an highly asymmetrical section ($A_{f,b} : A_{f,t} = 1 : 4$).
- Test 4 investigates the behaviour of stiffened openings.

This report presents a short summary of each single test. Furthermore this document includes a rough overview of numerical analyses of the tests performed. In addition an extract of the parametrical studies with the focus on the influence of material properties, geometry and load introduction on the failure load and failure mechanism are enclosed. Finally the conclusions derived from the test programme are given.

2.2 Description of test programme

2.2.1 General arrangements

The following arrangements for all tests have been agreed:

- All steel parts are in grade S355.
- One row of shear studs $\varnothing 19 \times 100$ with a distance of 150 mm has been applied.
- The composite slab consists of steel sheet and concrete topping.
- The overall slab thickness is 130 mm.
- The width of the slab has been chosen to 1,8 m, i.e. larger than the effective width $L/4$.
- Concrete grade C25/30 is used.
- HOLORIB[®] steel sheets HR 51 / 150 with a thickness of 1,25 mm are applied.
- For Test 1 and 3 the minimum reinforcement of 0,4 % in longitudinal and transversal direction is applied.
- For Test 2 the reinforcement for a “good design” is used.
- Stiffeners are provided at support and under each point of load introduction.
- The test specimens were propped during erection.

For Test 1 and Test 3 the sheets have been orientated perpendicular to the beam, for Test 2 parallel to the beam. In both cases the sheets have primarily been punched and afterwards put over the shop-welded studs.

2.2.2 Test 1

The scope of Test 1 is to study a basic test with multiple regular web openings to which the further tests can be related to. Additionally the composite slab has been left away at one of the supports to investigate the composite action in the end cell.

Thus a simply supported composite beam with regular web openings has been chosen, see Figure 2-1. It has been loaded by four point loads P as close as possible to $1/8$, $3/8$, $5/8$ and $7/8$ L to simulate a uniformly distributed load.

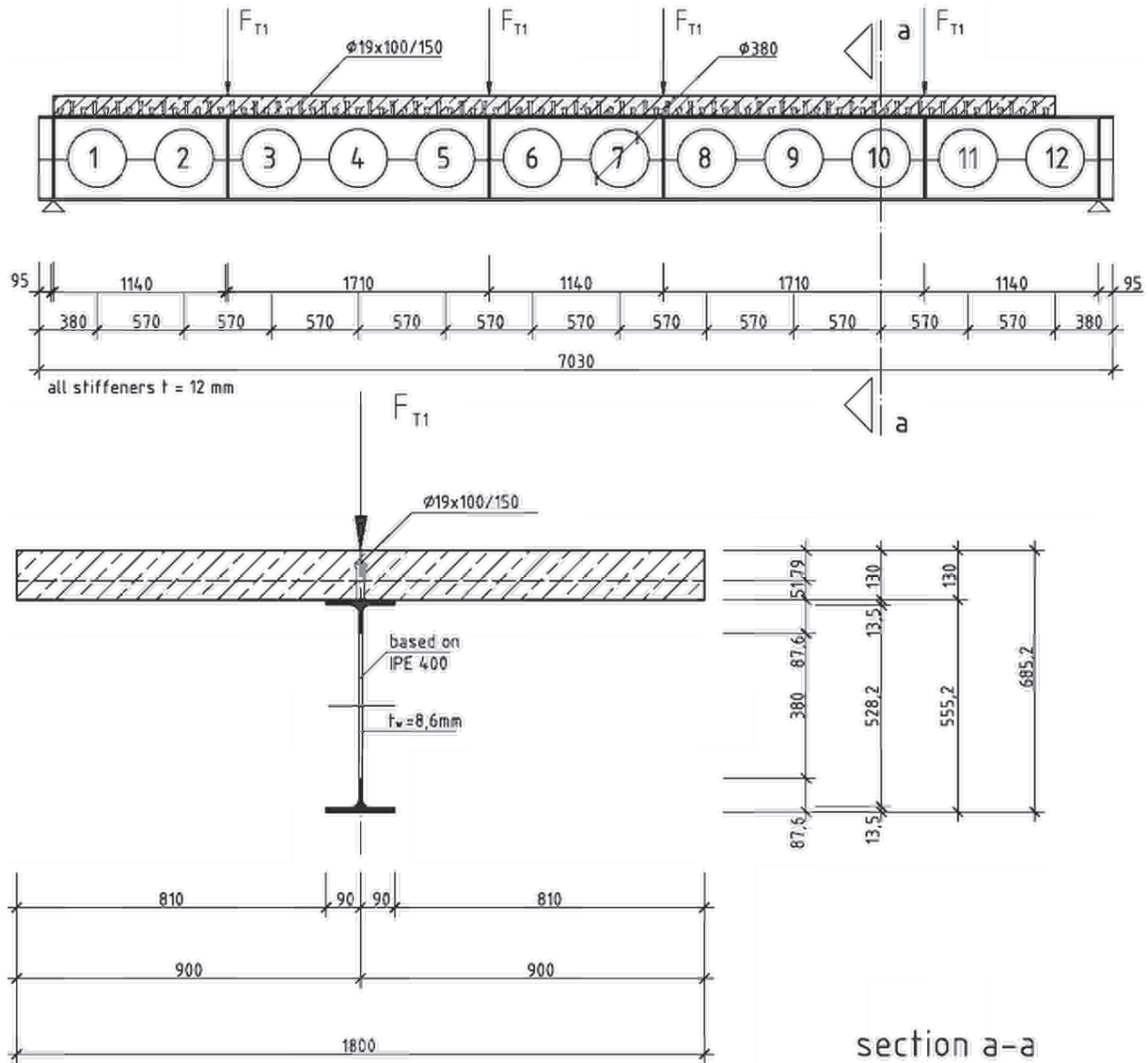


Figure 2-1: Longitudinal section, cross section and loading - Test 1

The symmetrical cross section of the beam has been based on IPE 400 profiles; twelve regular openings have uniformly been distributed along the beam span.

Further more Test 1 has been divided into 2 tests to achieve more information about the composite action in the end cell:

- Test 1A
- Test 1B (reloading after failed opening has been closed on non-concreted side)

For test 1B the test specimen from Test 1A has been fixed by a transversal plate, see Figure 2-2, closing opening 11 and 12 to avoid repeated failure on this side of the specimen.



Figure 2-2: Sealed openings 11 and 12 - Test 1B

2.2.3 Test 2A

The scope of Test 2A is to study the behaviour of an elongated opening. The opening is located in the area of moment and shear interaction.

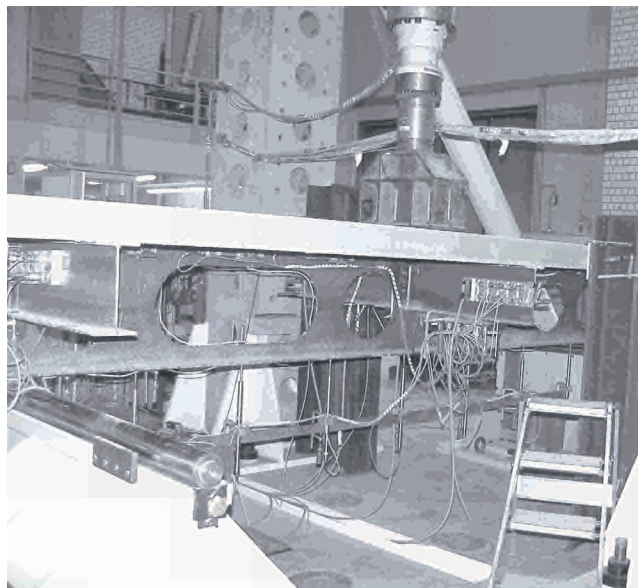


Figure 2-3: Test set-up - Test 2A

Therefore a simply supported composite beam with one elongated opening and several circular web openings has been selected for Test 2A, see Figure 2-4. It has been loaded by a single point load P centric over the cross section at midspan.

The beam has got a symmetrical cross section identical to test 1 and ten regular openings have uniformly been distributed along the beam span interrupted by one elongated opening, see Figure 2-4 and Figure 2-5. The elongated opening is gained by the fusion of two regular openings and is situated in the middle of the overall beam.

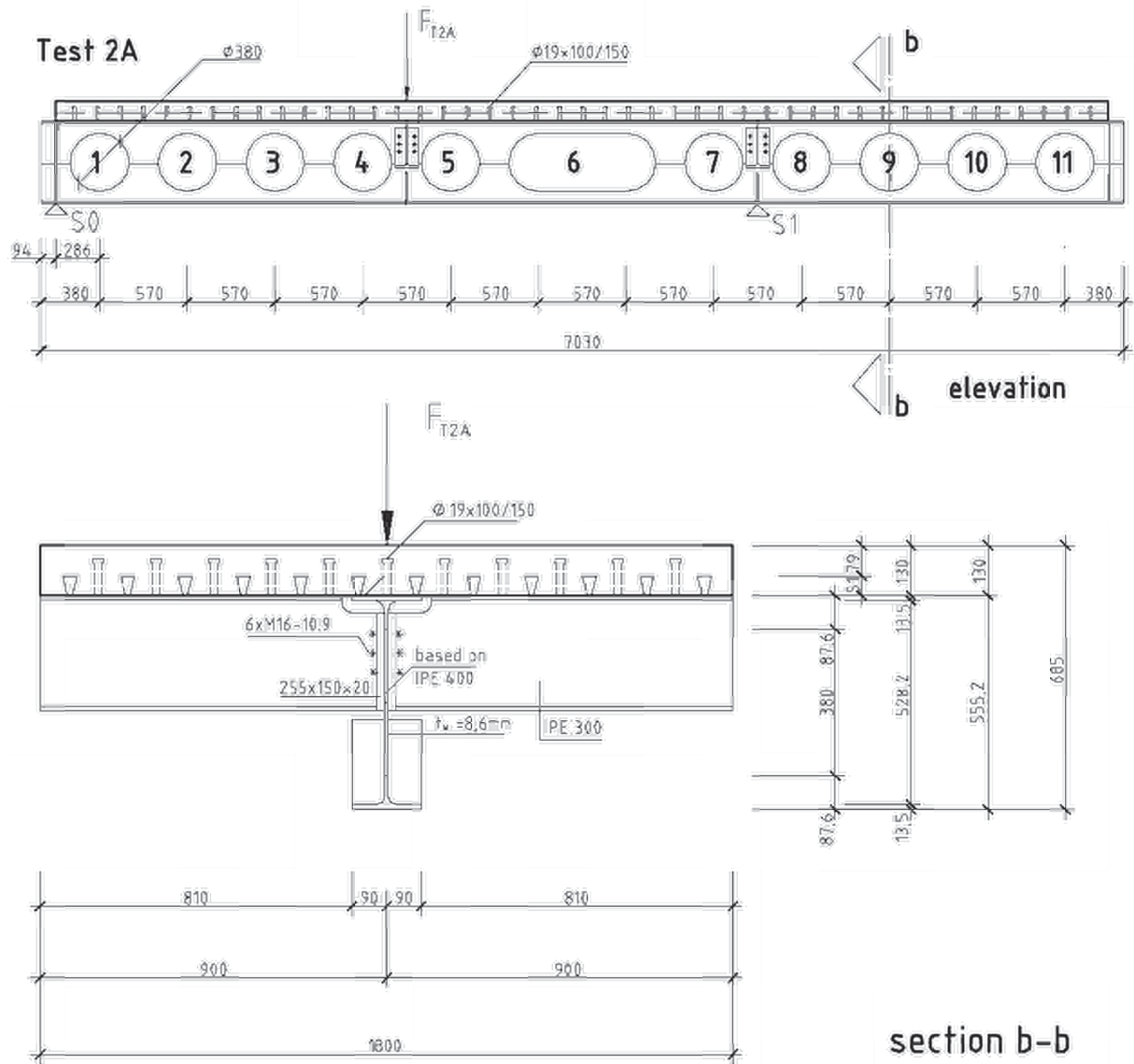


Figure 2-4: Longitudinal section, cross section and loading - Test 2A

2.2.4 Test 2B

The scope of Test 2B is to study the influence of the load introduction via secondary beams on composite beams with regular web openings whereas the secondary beams are also in composite action. The beams are connected by end plates.

The test specimen of Test 2B is the same as for Test 2A under varying load and support conditions.

Hence Test 2B has been a simply supported composite beam with one elongated opening and several circular web openings. It has been loaded by 4 point loads P introduced via secondary beams, Figure 2-5.

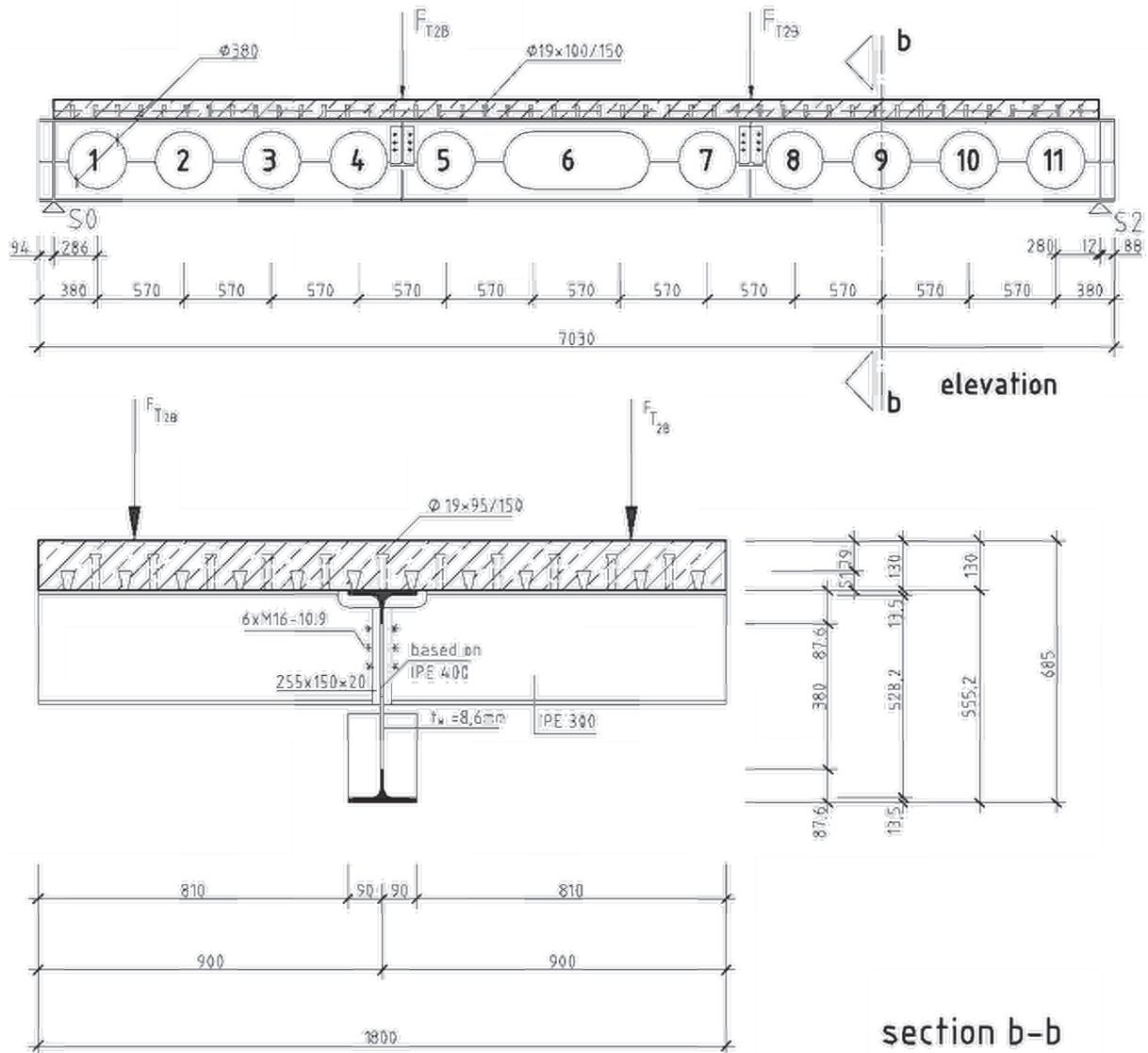


Figure 2-5: Longitudinal section, cross section and loading - Test 2B

2.2.5 Test 3

The scope of Test 3 is to study the behaviour of an highly asymmetrical steel section with web openings as a composite beam.

Additionally the composite slab has been left away at one of the supports to check the composite action in the end cell.

Consequently Test 3 has been a simply supported composite beam with 12 regular web openings. It has been loaded by four point loads P as close as possible to $1/8$, $3/8$, $5/8$ and $7/8$ L to simulate a uniformly distributed load, see Figure 2-6.

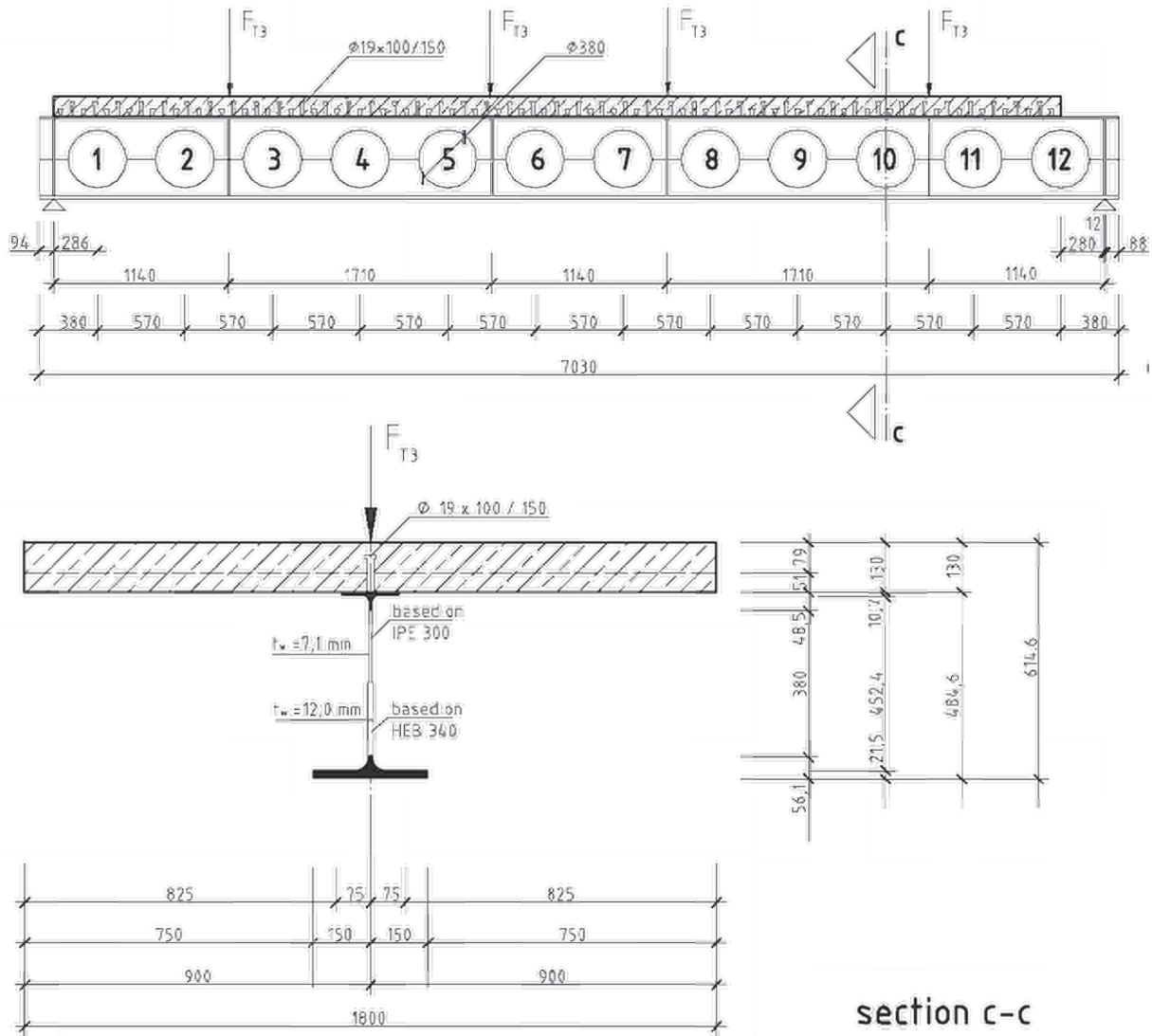


Figure 2-6: Longitudinal section, cross section and loading - Test 3

The beam consisted of an asymmetrical steel section with $A_{f,b} / A_{f,t} > 3$ (here 4:1), greater than allowed according to ENV 1994-1-1: 1992, see Figure 2-7. The upper chord has been made of an IPE 300, the lower chord of an HEB 340. Twelve regular openings have uniformly been distributed along the beam span.

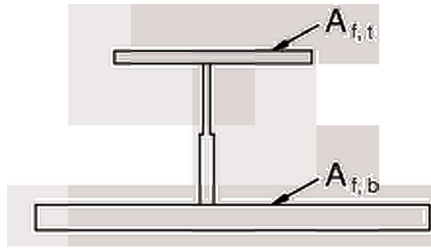


Figure 2-7: Ratio upper flange to lower flange - Test 3

2.2.6 Test 4

The scope of Test 4 is to check the behaviour of ring-stiffened, half-closed or closed circular web openings.

The test is performed as a 3-point bending test of a pure steel beam, see Figure 2-8, Figure 2-9 and Figure 2-10. 6 circular openings have uniformly been distributed along the beam span.

Ring stiffeners have been provided at opening 1 to 3, openings 4 and 5 are half-closed by infills and opening 6 is fully closed by an infill.

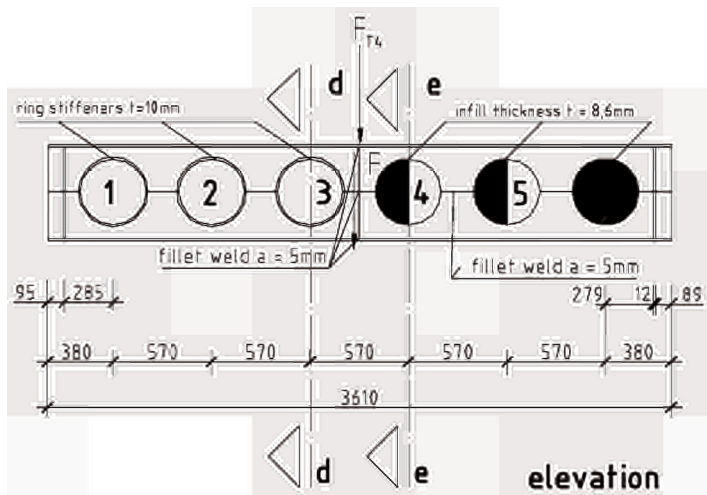


Figure 2-8: Longitudinal section and loading - Test 4

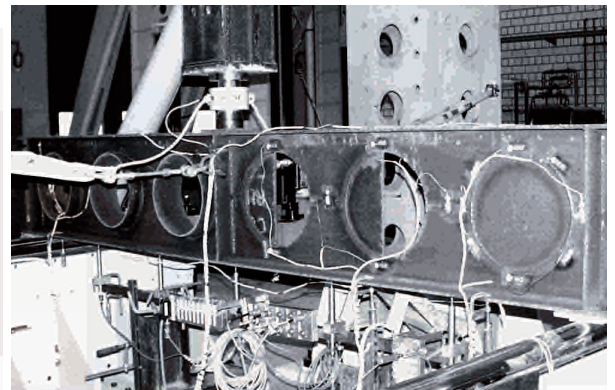


Figure 2-9: Test set-up - Test 4

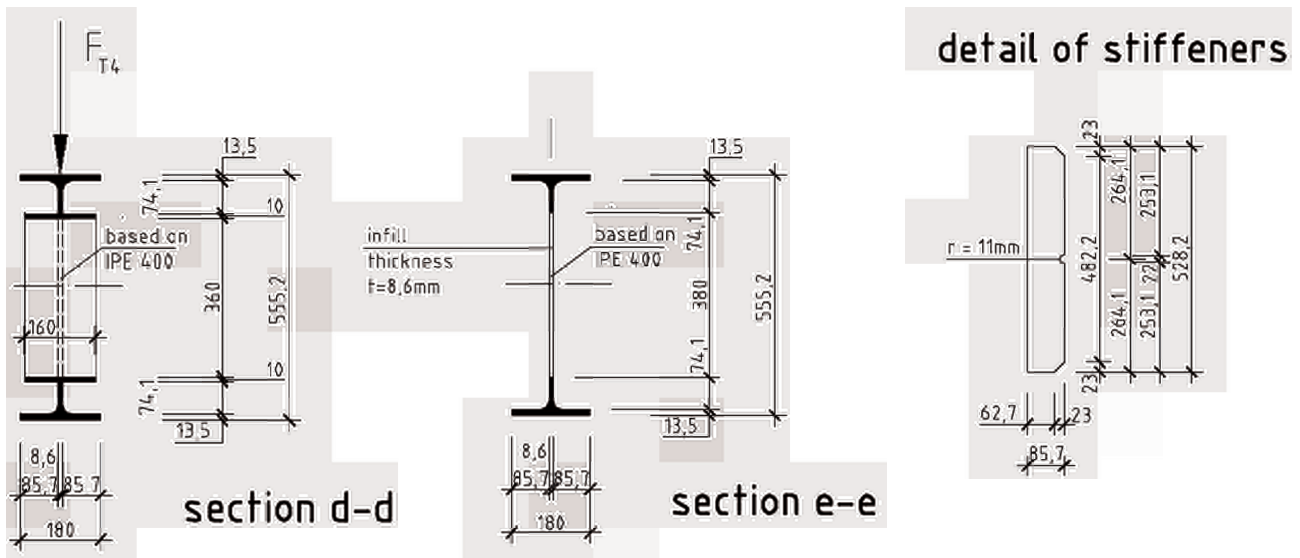


Figure 2-10: Cross section and loading - Test 4

2.3 Fabrication and execution

All girders have been fabricated by PROFILARBED, Luxembourg. The test specimen have been reinforced and concreted in the laboratories of the University of Kaiserslautern.

All tests have been carried out at the “Labor für konstruktiven Ingenieurbau”, University of Kaiserslautern, Germany.

2.4 Testing

2.4.1 General

Each test has been an ultimate limit state test. The test procedure comprises the execution of load cycles at certain load levels to exclude slippage of the load introduction and supports as well as friction in the shear joint and structure if existing. Additionally the vertical deflections, inclination and strains have been measured to guaranty a detailed evaluation of each test. As examples the following test set-ups of Test 1 and Test 4 are shown in Figure 2-11 and Figure 2-12.

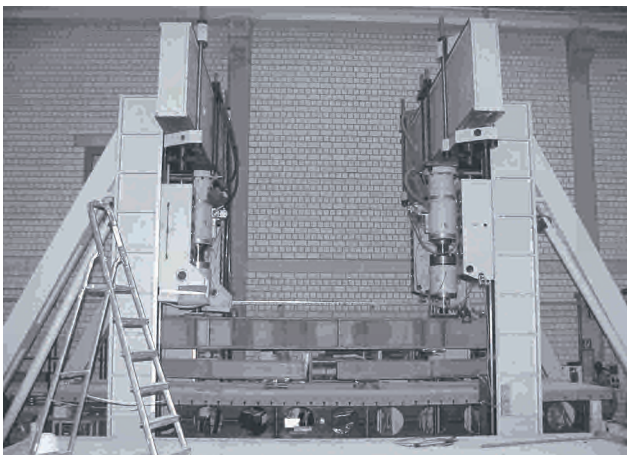


Figure 2-11: Experimental set-up - Test 1

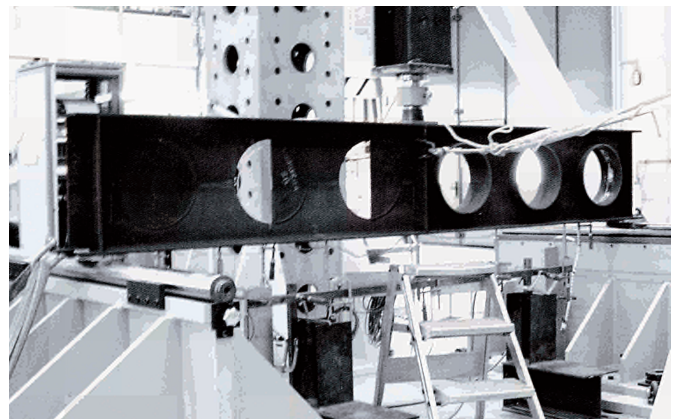


Figure 2-12: Experimental set-up - Test 4

Table 2-1 summarises the experimental results:

Table 2-1: Experimental results

Test	Failure Load	Failure criterium	Remarks
Test 1A	805,6 kN	Flexural web post buckling between 11 th and 12 th opening	<ul style="list-style-type: none"> – Uplifting of concrete chord – Vierendeel mechanism at opening 2 and 11 could be identified before failure – The Vierendeel mechanism has slightly been more developed at opening 11 than at opening 2 – Unequal slippage at the different supports
Test 1B	843,7 kN	Failure due to web post buckling between 1 st and 2 nd opening	<ul style="list-style-type: none"> – Vierendeel mechanism at opening 2 could be identified before failure
Test 2A	481,2 kN	no failure	<ul style="list-style-type: none"> – stopped at a load level of 481,2 kN to avoid any influence on Test 2B by excessive cracking of the concrete chord – Vierendeel mechanism could be identified at a load level of 337 kN by uplifting of the concrete chord
Test 2B	780,4 kN	Stopped due to excessive yielding of the bottom T-section at the elongated openings at midspan	<ul style="list-style-type: none"> – Slight lifting up of the sheets at 530 kN at midspan over the elongated opening – Longitudinal cracks on top of the concrete chord due to transversal bending at a load level of 600 kN
Test 3	658,0 kN	Web post buckling between 11 th and 12 th opening	<ul style="list-style-type: none"> – The web post buckling shape has been influenced by the different web thicknesses – Vierendeel mechanism at opening 2 and 11 before failure – Vierendeel mechanism at opening 2 has slightly been less deformed than at opening 11 – Unequal slippage at the different supports
Test 4	793,0 kN	Vierendeel mechanism at opening 4	<ul style="list-style-type: none"> – Weld cracked at upper part of the half-moon stiffener along the perimeter – Half-moon stiffener buckled due to deformations of the opening – Upper flange is extensively deformed

2.4.2 Experimental results

Diagrams of the measurements as well as photographs of the failure mechanism are given in the following figures.

2.4.2.1 Test 1A

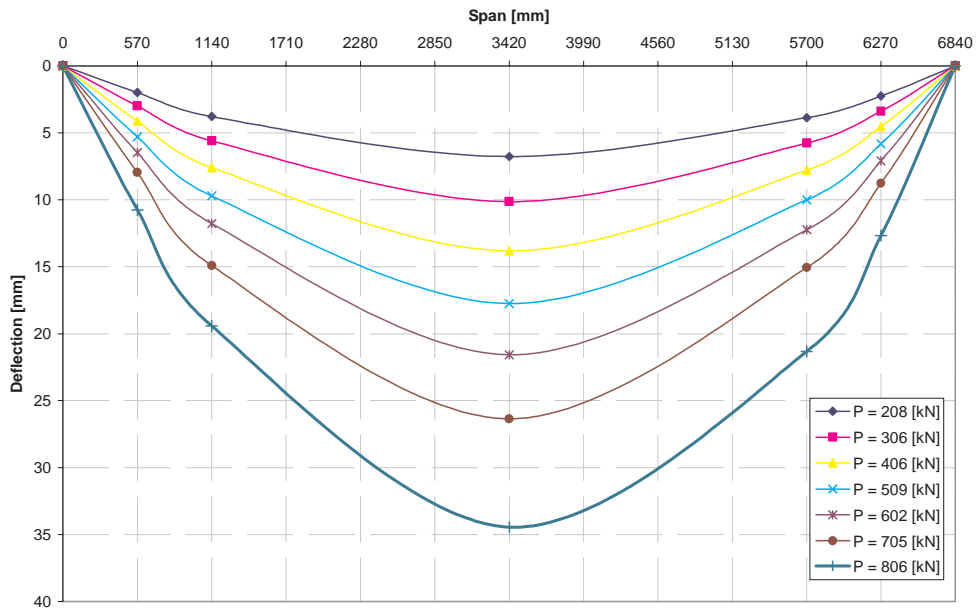


Figure 2-13: Deflection to length - Test 1A

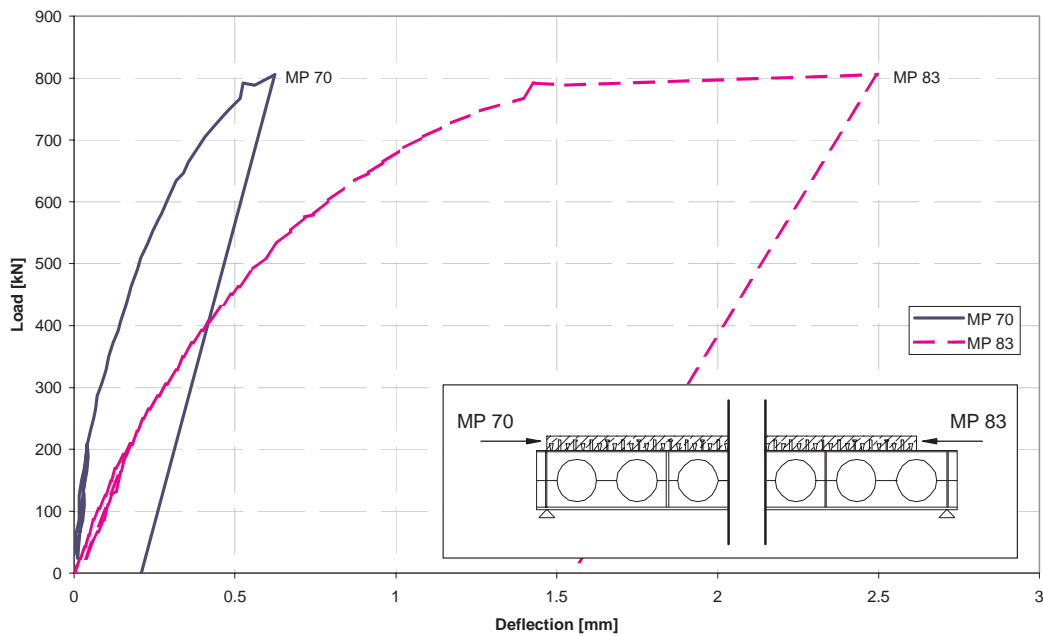


Figure 2-14: Slippage at end span - Test 1A

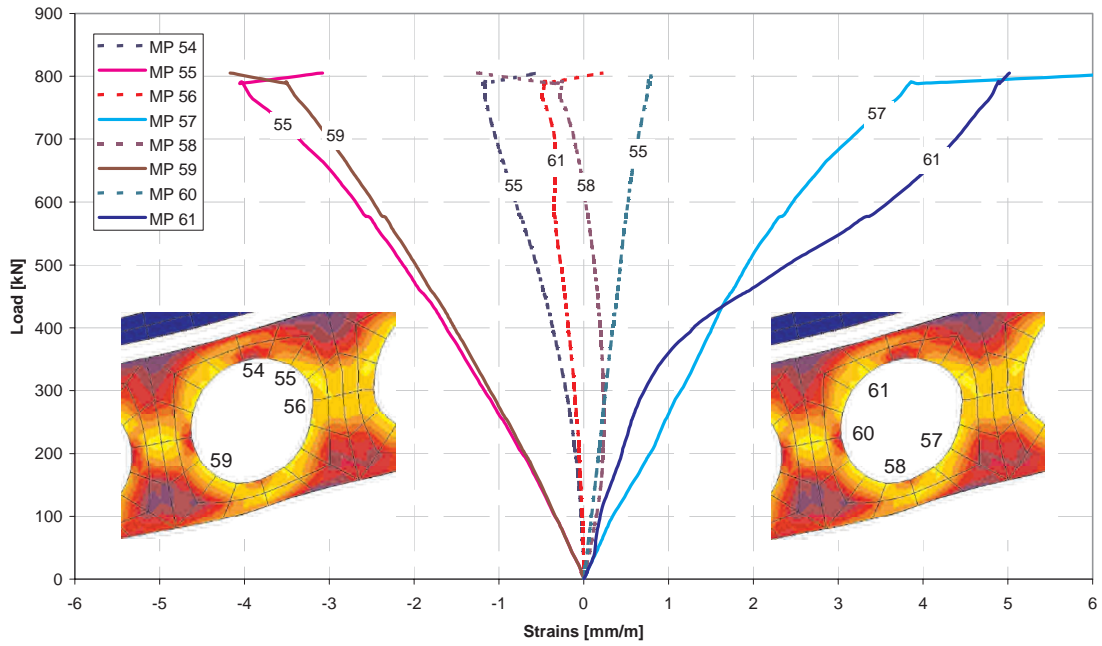


Figure 2-15: Strains around 11th opening in tangential direction - Test 1A



Figure 2-16: Flexural web post buckling between opening 11 and 12 - Test 1A



Figure 2-17: Vierendeel mechanism at 11th opening - Test 1A

2.4.2.2 Test 2A

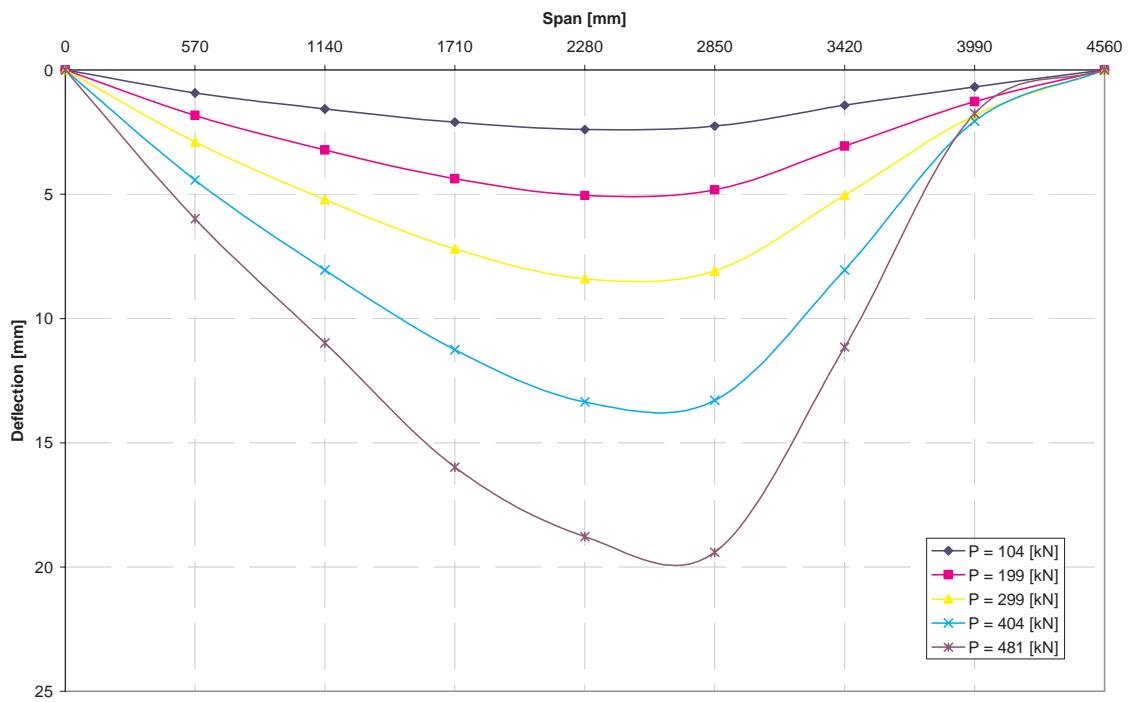


Figure 2-18: Deflection to length - Test 2A

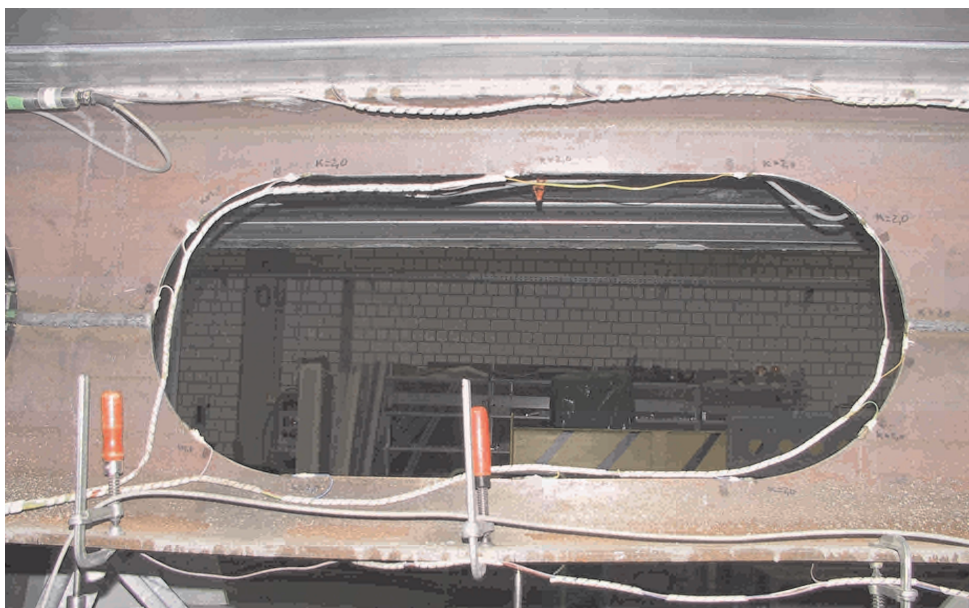


Figure 2-19: Vierendeel mechanism at elongated opening - Test 2A

2.4.2.3 Test 2B

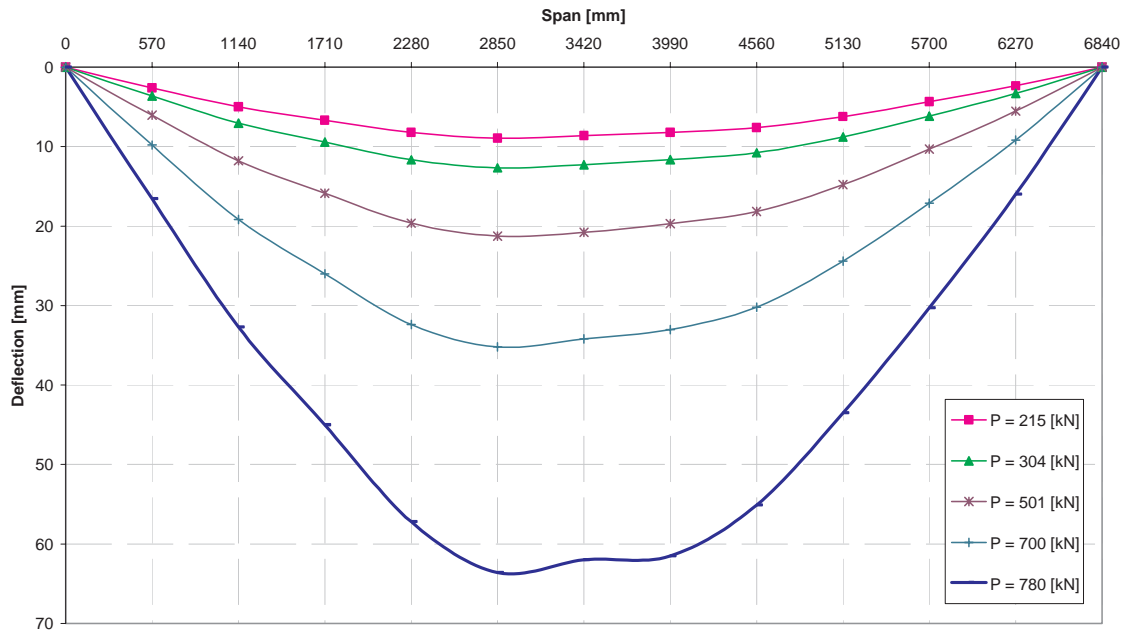


Figure 2-20: Deflection to length - Test 2B

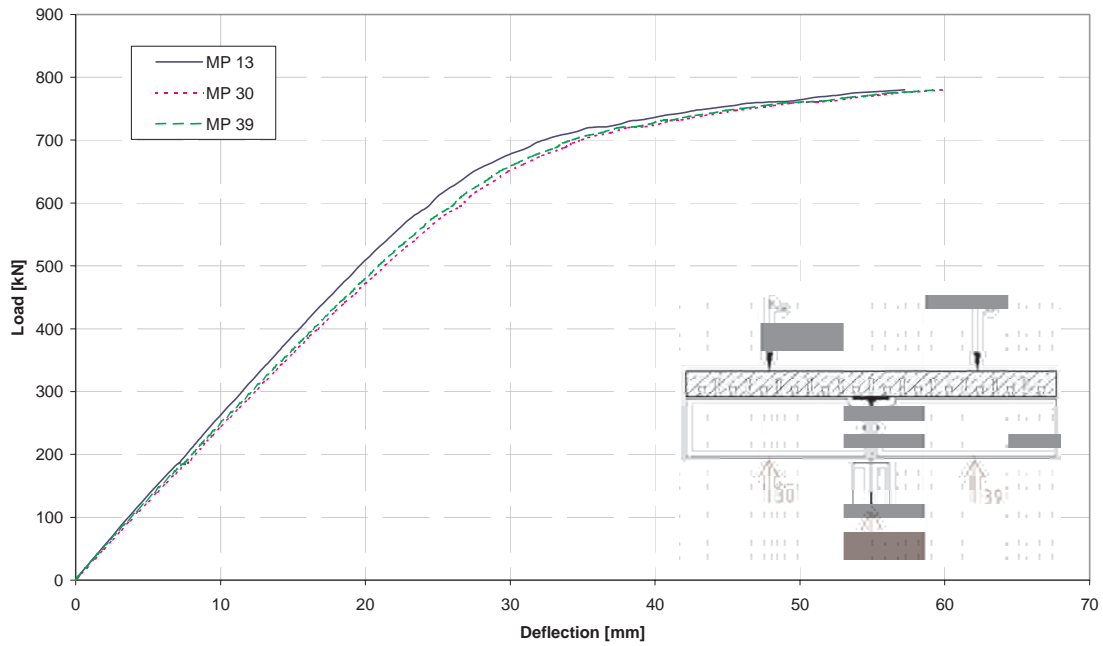


Figure 2-21: Deflection at load introduction - Test 2B

2.4.2.4 Test 3

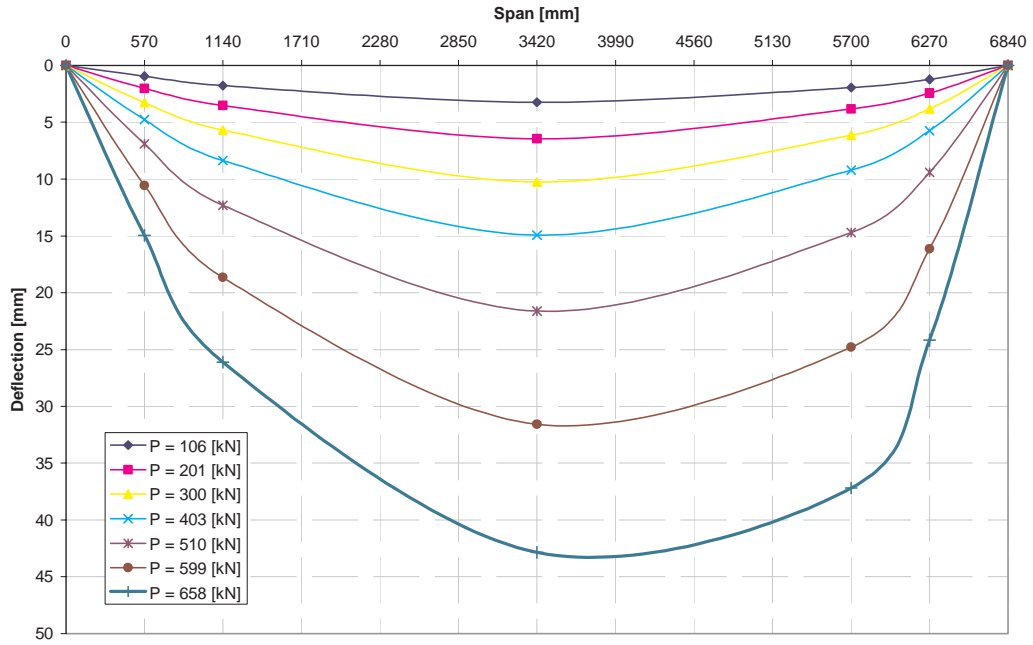


Figure 2-22: Deflection to length - Test 3

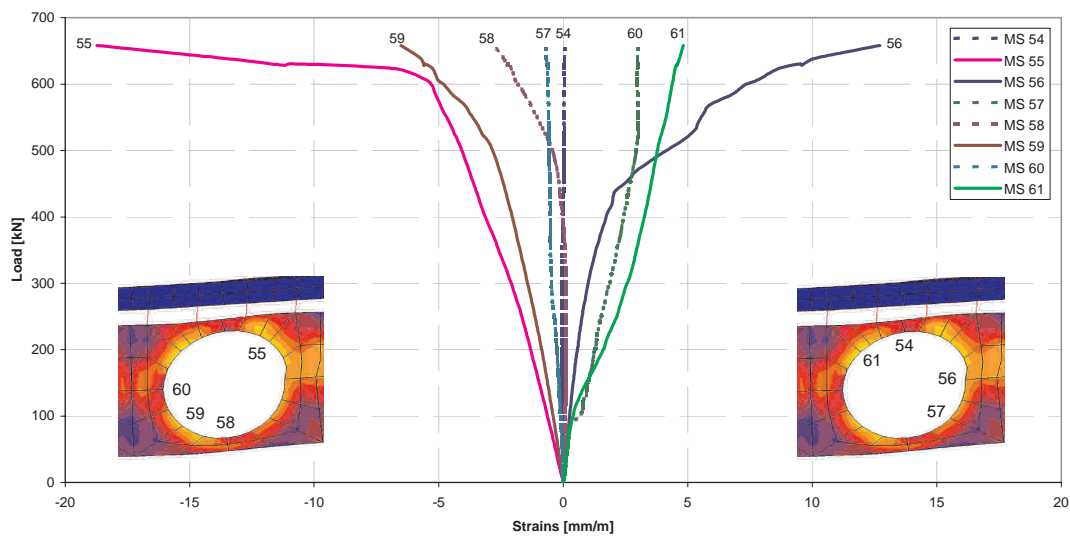


Figure 2-23: Strains around 11th opening in tangential direction - Test 3

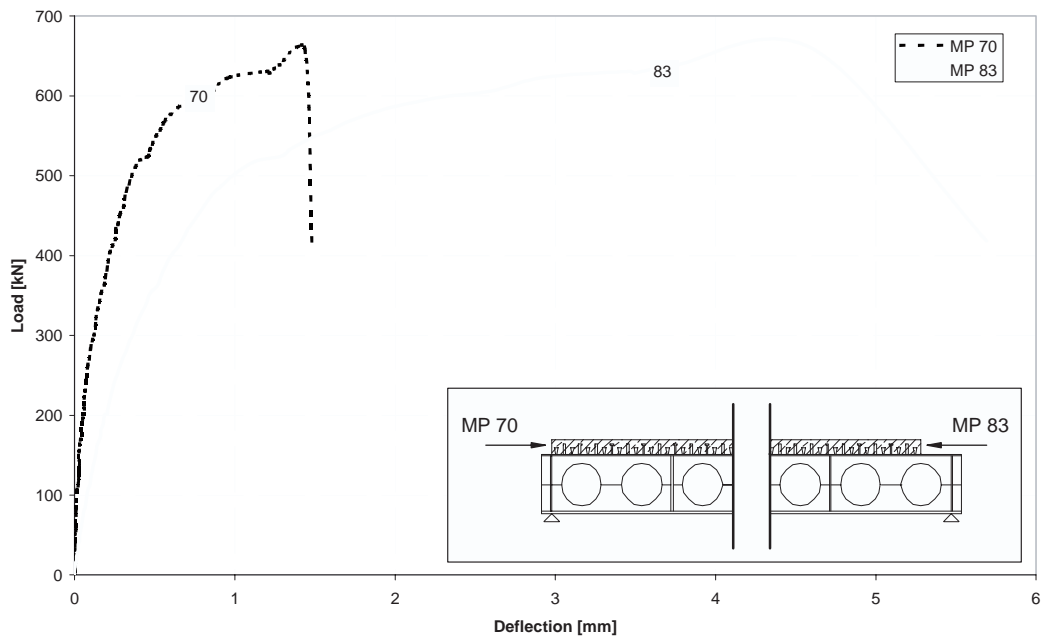


Figure 2-24: Slippage at end span - Test 3



Figure 2-25: Web post buckling - Test 3



Figure 2-26: Vierendeel mechanism - Test 3

2.4.2.5 Test 4

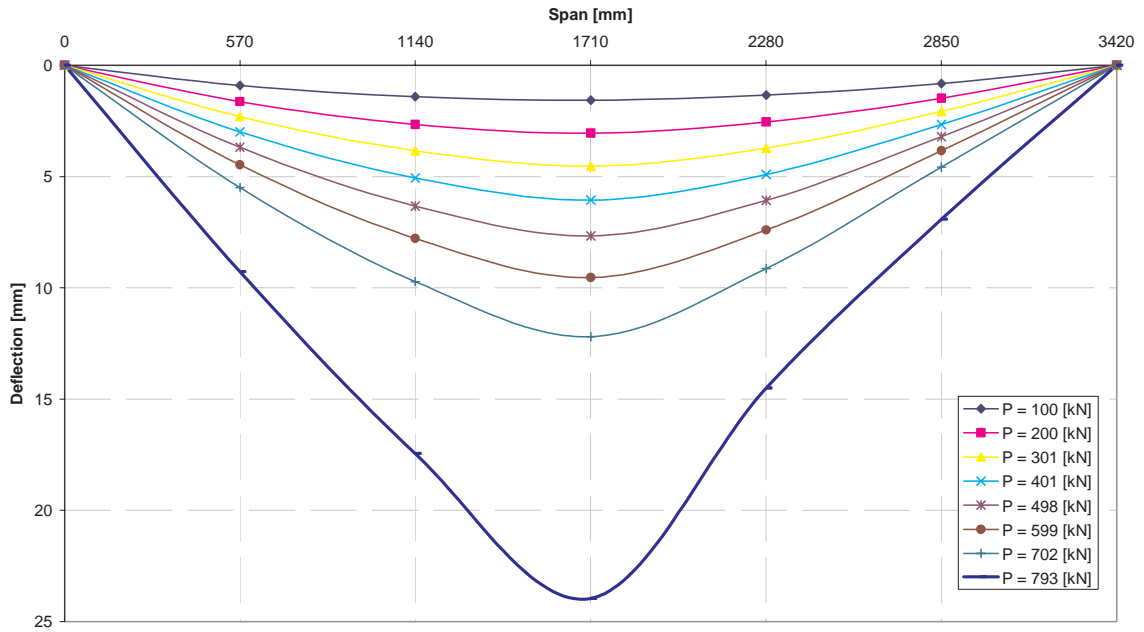


Figure 2-27: Deflection over length - Test 4

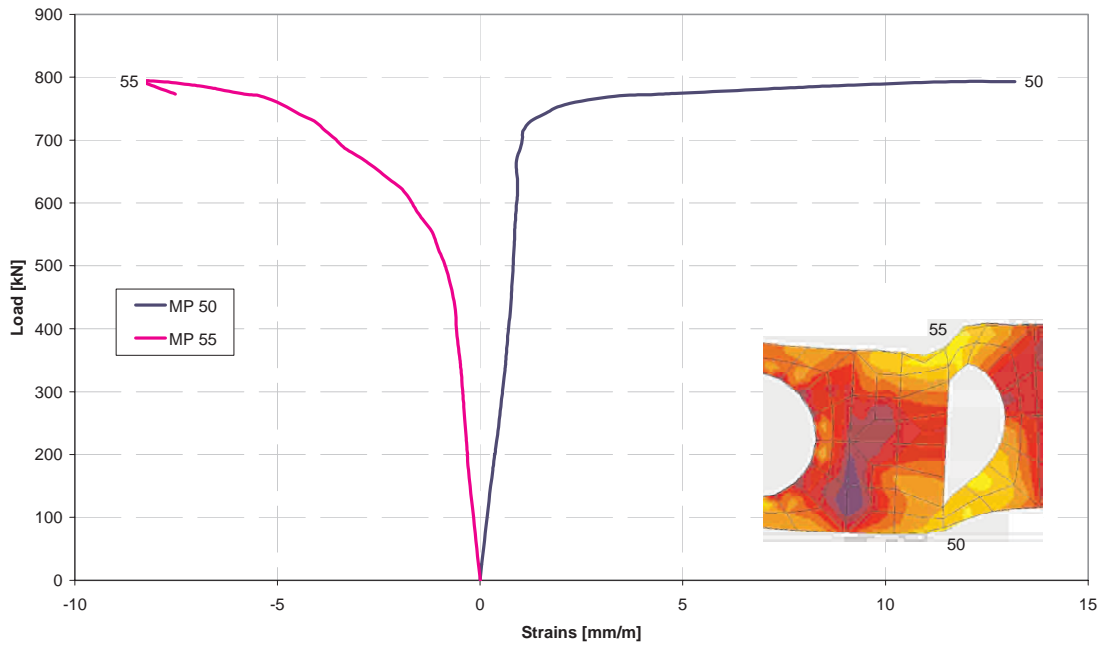


Figure 2-28: Strains at opening 4 in longitudinal direction - Test 4

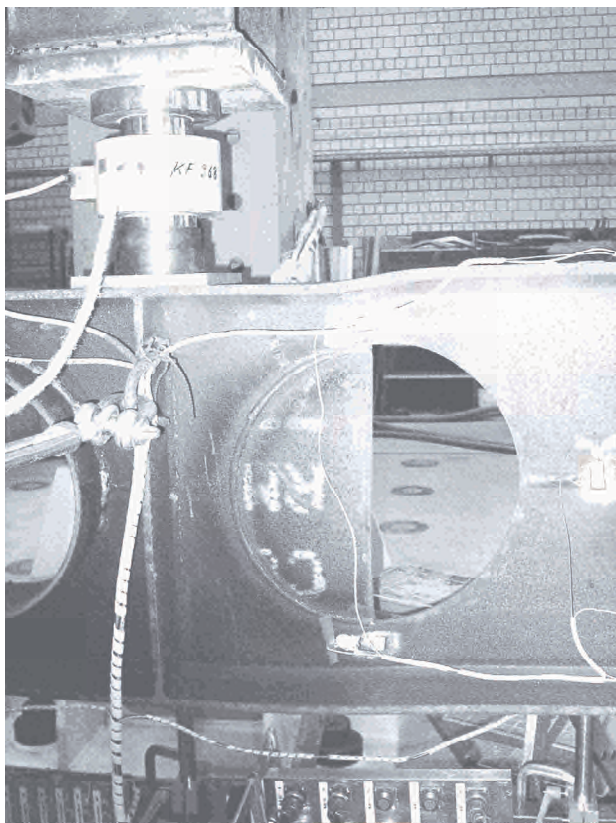


Figure 2-29: Deformations at opening 4 - Test 4

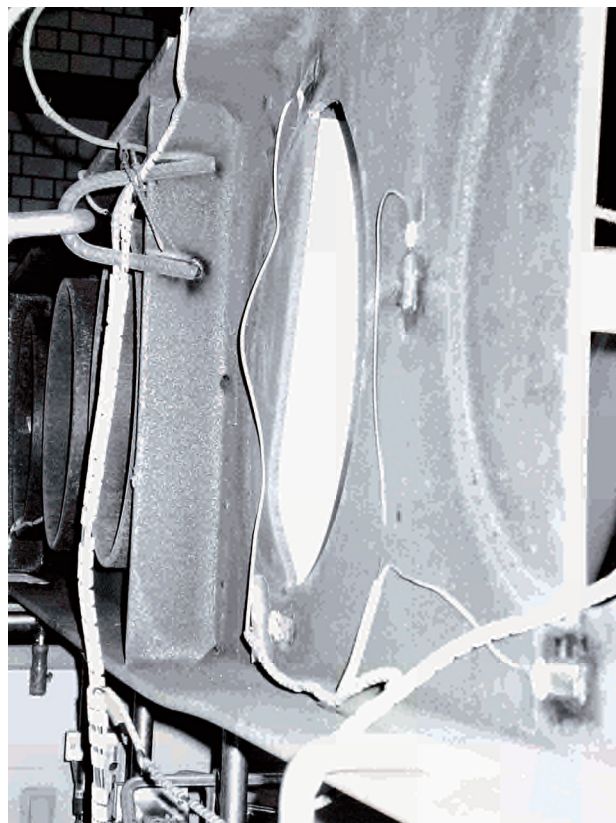


Figure 2-30: Buckling of half-moon stiffener at opening 4 - Test 4

2.5 Numerical Simulations

2.5.1 General

To intensify the analysis of the test results and to enlarge the experiences concerning composite beams with cellular openings numerical simulations have been performed.

The numerical simulation of the non-linear behaviour of composite members has to consider the particular behaviour of the following elements:

- Steel member
- Concrete slab
- Steel sheets
- Reinforcement
- Shear connectors

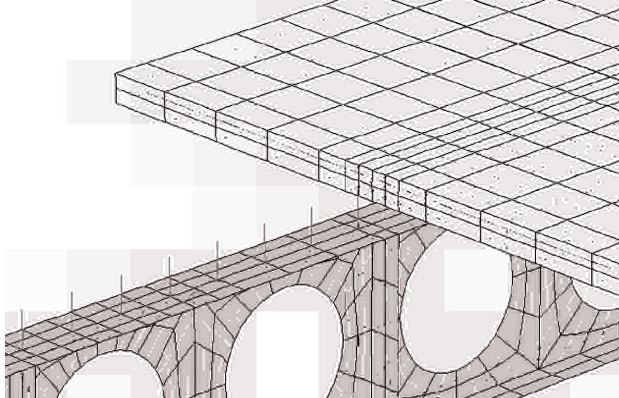
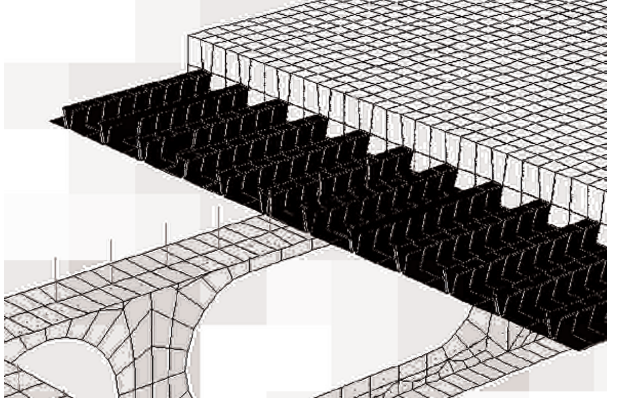
The software MARC/MENTAT [1] used for the numerical simulation works allows to describe and to combine various material laws.

The steel parts are fully modelled taking the geometry as well as the non-linear material behaviour into account. As the concrete slab is mainly under compression and the slab itself has hardly any influence on the shear bearing capacity it has been possible to generate the concrete chord itself using simplified assumptions for the discretisation. Local failure of the concrete therefore is not been considered in the analysis whereas the global influence has been regarded.

The load-slip behaviour for the shear connectors of the composite beams has been taken into account using springs with non-linear behaviour obtained by the Standard Push-Out Test.

The following Table 2-2 shows a short description of each model and the used assumptions and simplifications.

Table 2-2: Discretisation of the models

Test 1A / 1B and Test 3		Test 2A / 2B	
			
Concrete slab	<ul style="list-style-type: none"> – Three dimensional 20-node-brick elements – Linear Mohr-Coulomb – Measured geometry 	Concrete slab	<ul style="list-style-type: none"> – Three dimensional 8-node-brick elements – Linear Mohr-Coulomb – Measured geometry
HOLORIB sheets	<ul style="list-style-type: none"> – Transversal – Not generated 	HOLORIB sheets	<ul style="list-style-type: none"> – Longitudinal – Quadratic 4-Node Thick Shell Elements – Von Mises
Shear connectors	<ul style="list-style-type: none"> – Springs with non-linear behaviour 	Shear connectors	<ul style="list-style-type: none"> – Springs with non-linear behaviour
Steel beam	<ul style="list-style-type: none"> – Quadratic 8-Node Thick Shell Elements – Von Mises – Measured geometry 	Steel beam	<ul style="list-style-type: none"> – Quadratic 8-Node Thick Shell Elements – Von Mises – Measured geometry
Initial Imperfection	<ul style="list-style-type: none"> – First (positive) Eigenmode ($h_w / 250$) 	Initial Imperfection	<ul style="list-style-type: none"> – First (positive) Eigenmode ($h_w / 250$)

Test 4, as a pure steel beam, has completely been modelled by Quadratic 8-Node Thick Shell Elements taking the measured geometries into account. To obtain the realistic failure behaviour an initial imperfection according to the first (positive) Eigenmode has been applied for the analysis.

The boundary conditions for the models have been adjusted to the support condition and loading of each test, also regarding lateral restraint at the load introduction.

As the analyses have been carried out taking geometric non-linearity into account the change in structural behaviour and loss of structural stability has fully been considered.

2.5.2 Comparison between simulations and tests on composite beams

A comparison between the calculated and the measured deflections and strains as well as the failure mechanisms are given in Table 2-3. These investigations show, that it is possible to model composite beams with regular web openings with good agreement to the real behaviour.

Table 2-3: Comparison of results

		Test	FEM	Test / FEM [%]
Test 1A	Load P [kN]	806	789	98
Test 1B	Load P [kN]	852	877	103
Test 2A	Load P [kN]	481	546	113
Test 2B	Load P [kN]	780	794	102
Test 3	Load P [kN]	659	649	98
Test 4	Load P [kN]	793	808	102

In the case of Test 2A the discrepancy between the FE-analysis and the test behaviour is acceptable due to the fact, that the main focus of the FE-generation has been on Test 2B, where load introduction via secondary beams has been investigated. The divergence can be explained by not properly reflected local effects like uplift of the concrete chord, cracking of the concrete etc. by the model chosen.

2.5.3 Comparison of test results and FE analysis

The following figures show the comparison of the load deflection curves and the failure modes observed from the tests and the results from the FE analyses.

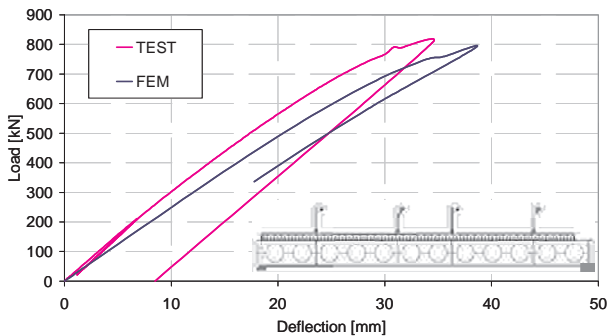


**Figure 2-31: Load-deflection curve
- Test 1A**

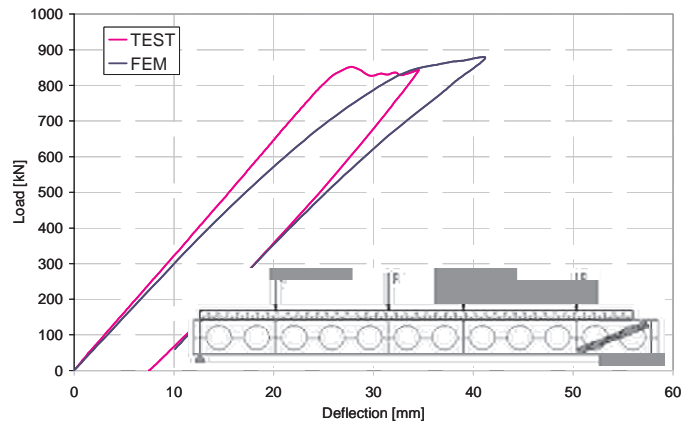


**Figure 2-32: Load-deflection curve
- Test 1B**

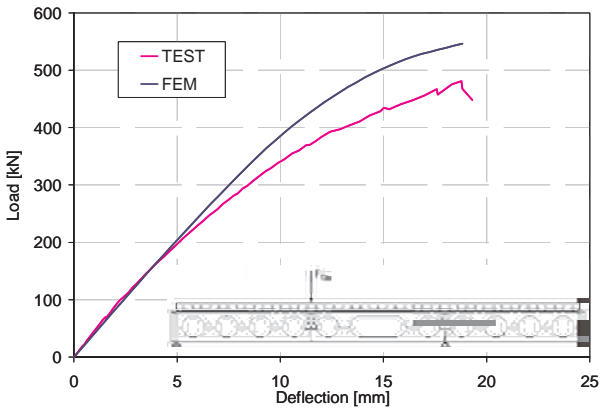


Figure 2-33: Load-deflection curve - Test 2A

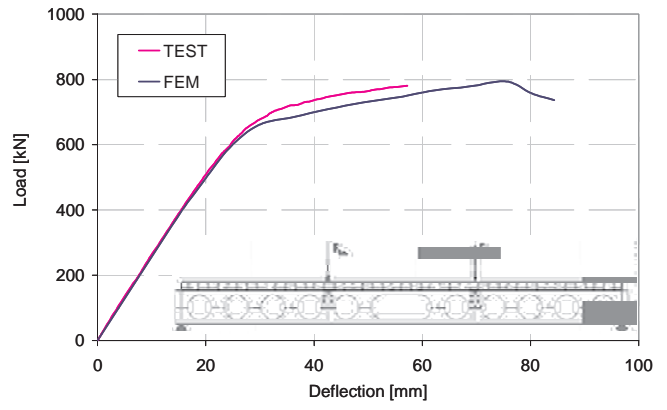


Figure 2-34: Load-deflection curve - Test 2B

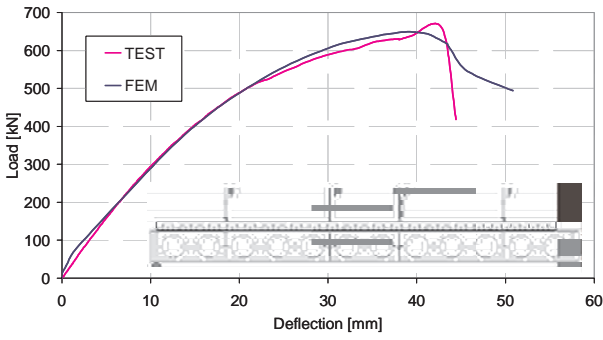


Figure 2-35: Load-deflection curve - Test 3

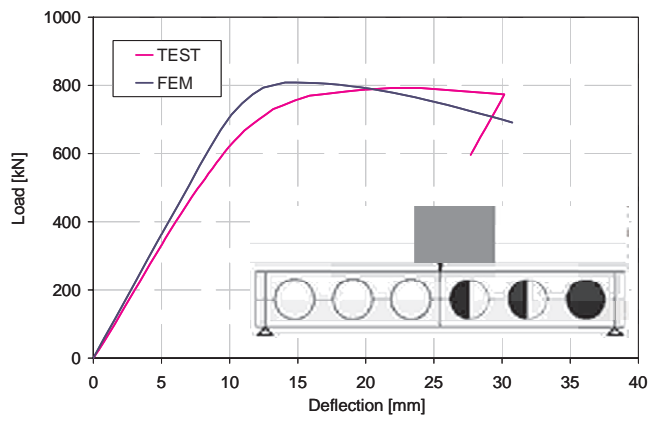
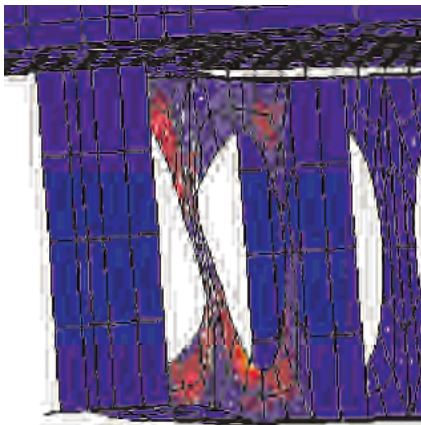


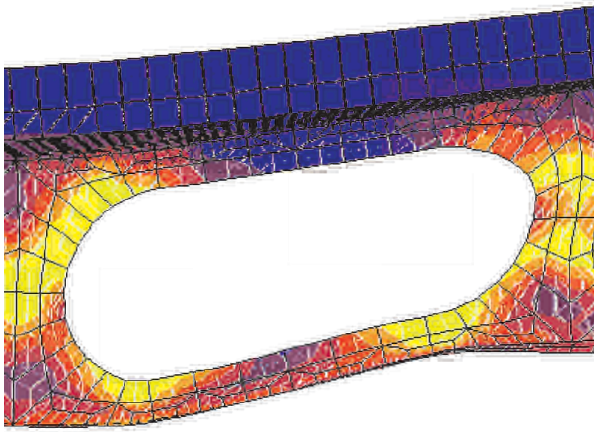
Figure 2-36: Load-deflection curve - Test 4



Scaling Factor 2



Figure 2-37: FEM failure mode - Test 1A **Figure 2-38: Test failure mode - Test 1A**



Scaling Factor 10

Figure 2-39: FEM failure mode - Test 2A

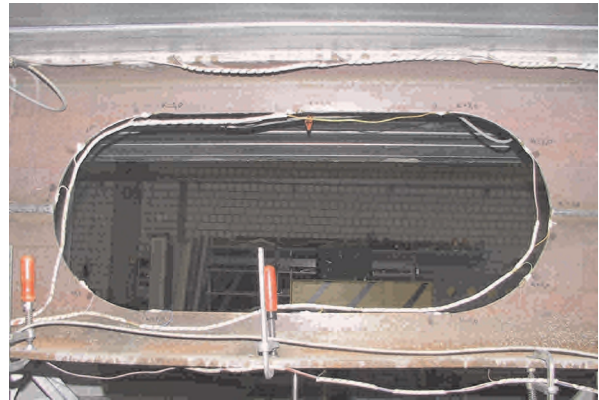
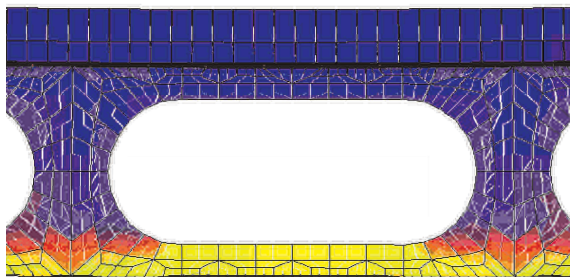


Figure 2-40: Test failure mode - Test 2A

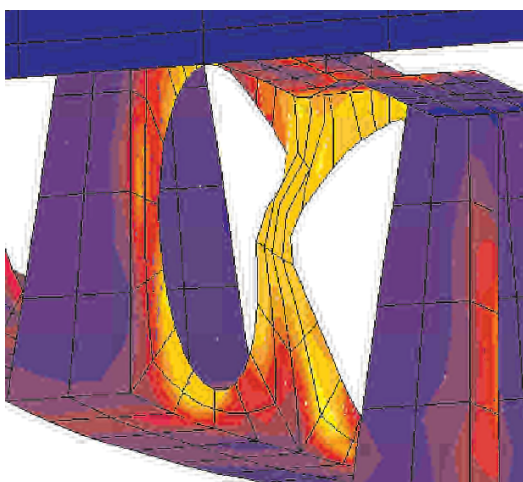


Scaling Factor 1

Figure 2-41: FEM failure mode - Test 2B



Figure 2-42: Test failure mode - Test 2B

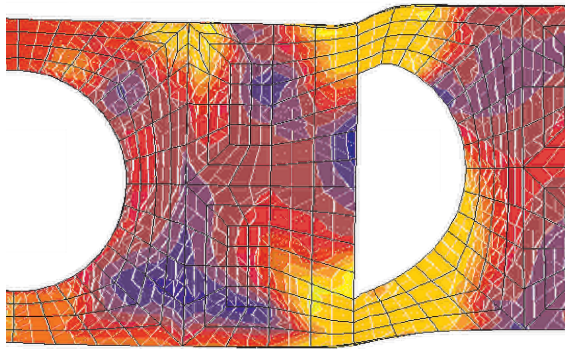


Scaling Factor 2

Figure 2-43: FEM failure mode - Test 3



Figure 2-44: Test failure mode - Test 3



Scaling Factor 2

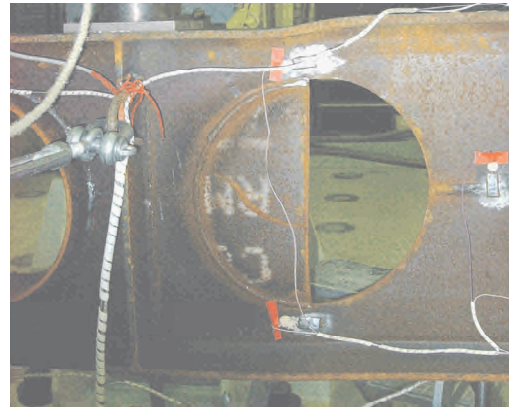


Figure 2-45: FEM failure mode - Test 4

Figure 2-46: Test failure mode - Test 4

2.5.4 Parametric Studies

2.5.4.1 Influence of the material properties

Accompanying the re-calculation of the tests parametrical studies have been carried out with the aim to enlarge the understanding of the test results. The main focus of the studies has been on the influence of the material properties on the failure load and mechanism. Therefore the FE-models calibrated to the tests have been recalculated with varying steel and concrete properties generally used in construction.

The following tables and figures summarise the outcome of the parametrical study on the material properties:

Table 2-4: Summary of parametric study on material properties – Test 1A

Test	Concrete f_{ck} [N/mm ²]	Steel f_{yk} [N/mm ²]	Failure load F [kN]	Failure mechanism
Test 1A	measured (42)	measured (451/489)	789	Web Post Buckling
Test 1A	20	265	494	Web Post Buckling
Test 1A	20	400	670	Web Post Buckling
Test 1A	20	460	721	Web Post Buckling
Test 1A	40	265	503	Web Post Buckling
Test 1A	40	400	688	Web Post Buckling
Test 1A	40	460	721	Web Post Buckling
Test 1A	80	265	506	Web Post Buckling
Test 1A	80	400	707	Web Post Buckling
Test 1A	80	460	739	Web Post Buckling
Test 1A	without concrete	measured (451/489)	749	Web Post Buckling
Test 1A	without concrete	265	398	Vierendeel
Test 1A	without concrete	400	667	Web Post Buckling

Table 2-5: Summary of parametric study on material properties – Test 2A

Test	Concrete f_{ck} [N/mm ²]	Steel f_{yk} [N/mm ²]	Failure load F [kN]	Failure mechanism
Test 2A	measured (40)	measured (383/474)	640	Vierendeel
Test 2A	20	235	408	Vierendeel
Test 2A	20	355	497	Vierendeel
Test 2A	20	460	552	Vierendeel
Test 2A	40	235	439	Vierendeel
Test 2A	40	355	531	Vierendeel
Test 2A	40	460	586	Vierendeel
Test 2A	60	235	462	Vierendeel
Test 2A	60	355	557	Vierendeel
Test 2A	60	460	611	Vierendeel

Table 2-6: Summary of parametric study on material properties – Test 2B

Test	Concrete f_{ck} [N/mm ²]	Steel f_{yk} [N/mm ²]	Failure load F [kN]	Failure mechanism
Test 2B	measured (40)	measured (383/474)	794	Web Post Buckling
Test 2B	20	235	498	Web Post Buckling
Test 2B	20	355	657	Positive Moment
Test 2B	20	460	760	Positive Moment
Test 2B	40	235	482	Positive Moment
Test 2B	40	355	617	Web Post Buckling
Test 2B	40	460	729	Web Post Buckling
Test 2B	60	235	494	Positive Moment
Test 2B	60	355	628	Web Post Buckling
Test 2B	60	460	739	Web Post Buckling

Table 2-7: Summary of parametric study on material properties – Test 3

Test	Concrete f_{ck} [N/mm ²]	Steel f_{yk} [N/mm ²]	Failure load F [kN]	Failure mechanism
Test 3	measured (30,2)	measured (408/467/488/453)	649	Web Post Buckling
Test 3	20	235	414	Web Post Buckling
Test 3	20	355	575	Web Post Buckling
Test 3	20	460	642	Web Post Buckling
Test 3	40	235	419	Vierendeel
Test 3	40	355	584	Vierendeel
Test 3	40	460	650	Web Post Buckling
Test 3	80	235	421	Vierendeel
Test 3	80	355	595	Web Post Buckling
Test 3	80	460	661	Vierendeel
Test 3	without concrete	measured (408/467/488/453)	380	Web Post Buckling
Test 3	without concrete	235	217	Buckling Upper Flange
Test 3	without concrete	355	329	Vierendeel

Table 2-8: Summary of parametric study on material properties – Test 4

Test	Concrete f_{ck} [N/mm ²]	Steel f_{yk} [N/mm ²]	Failure load F [kN]	Failure mechanism
Test 4	pure steel	measured (437/449)	808	Vierendeel
Test 4	pure steel	235	433	Vierendeel
Test 4	pure steel	355	650	Vierendeel
Test 4	pure steel	460	838	Vierendeel

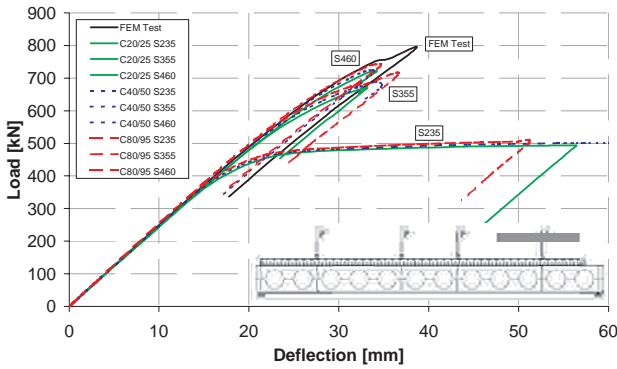


Figure 2-47: Parametric study - Test 1A

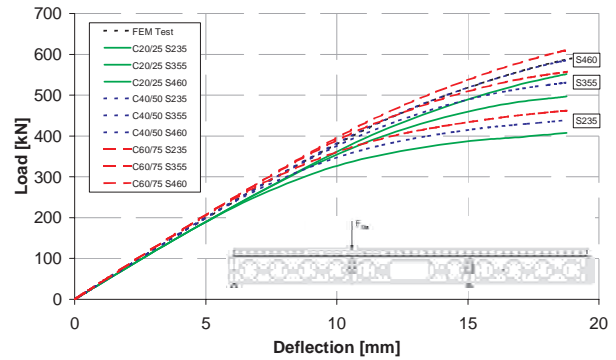


Figure 2-48: Parametric study - Test 2A

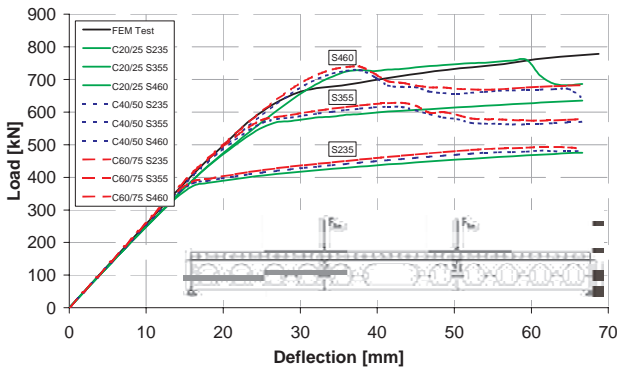


Figure 2-49: Parametric study - Test 2B

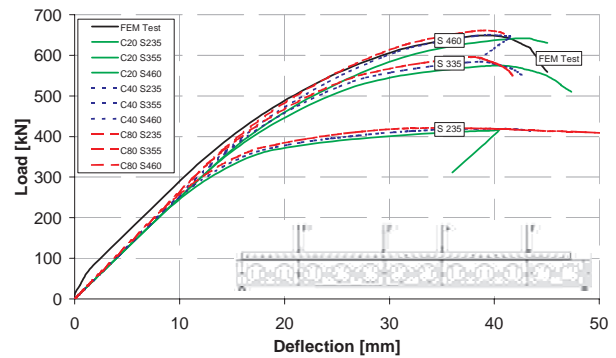


Figure 2-50: Parametric study - Test 3

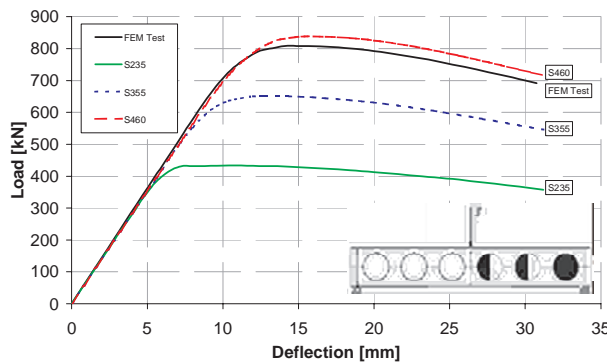


Figure 2-51: Parametric study - Test 4

2.5.4.2 Conclusions of parametric study on material properties

As failure of composite beams with cellular openings occurs due to shear the parametric study verified that the failure load and failure mechanism mainly depends on the steel grade whereas the concrete strength has a minor influence on the behaviour.

In the case of Test 1A a large rotational capacity for a steel S235 could be confirmed until the failure takes place due to web post buckling between the 11th and 12th opening. For the steel S355 and S460 the failure criterion changes into the occurrence of web post buckling between the 11th and 12th opening without any rotational capacity. For Test 1A generally for all steel grades Vierendeel mechanism could be preliminarily identified until failure due to post buckling occurs.

For Test 2A obviously failure due to the Vierendeel mechanism at the elongated opening 6 governs the design as it has been intended for testing. Higher steel grades increase the ultimate failure load.

The parametric study on material properties for test 2B once more shows, that higher strength steels tend to fail by local instability. Therefore the failure mode of Test 2B changes from failure by excessive yielding of the bottom chord to web post buckling for higher grade steels like S460, however with an increased failure load. This change of the failure mode is accompanied by a decreasing moment rotational capacity of the specimen with increasing steel strength. Furthermore it has to be remarked that the rotational capacity is also effected by the concrete strength of the chord.

The results from the analysis of Test 3 analysis is comparative to the results of the FE-simulation for Test 1A. As failure due to shear is clearly governing the failure mode plausibly the steel strength only influences the failure load significantly. Since the failure modes web post buckling and Vierendeel mechanism affect each other the minor influence of the concrete strength causes a change of the failure mode of Test 3.

All numerical analyses of Test 4 failed by local failure at the 4th opening.

2.5.4.3 Influence of the geometry

2.5.4.3.1 Test 1 - End Cell

The scope of Test 1 has also been to study the composite action in the end cell. Therefore FE-analyses have been performed considering a composite beam with and without the end cell concreted, see Table 2-9.

Table 2-9: Summary of parametric study - Test 1A

Configuration	Concrete f_{ck} [N/mm ²]	Steel f_{yk} [N/mm ²]	Failure Load F [kN]	Failure Mechanism
end cell non-concreted	42	measured	794	Web Post Buckling
end cell concreted	42	measured	640	Web Post Buckling

According to the FE-analysis the non-concreted end cell is beneficial for the ultimate limit state behaviour of the beam. The beam possesses more ductile behaviour for shear load transformation and Vierendeel mechanism can largely locally develop until failure by web post buckling. Else the concreted end cell induces the shear directly into the web post and large deformations are prevented by the concrete chord on top. Therefore earlier buckling of the web post is occurring.

2.5.4.3.2 Test 4 - Stiffening

Since the purpose of Test 4 has been to investigate the influence of stiffening concepts 3 further geometries have additionally been modelled. In the following study Geometry 1 represents the

original configuration tested. Geometry 2 is compatible to Geometry 1 leaving away all stiffening configurations. Geometry 3 corresponds to Geometry 1 but with closed openings 3 to 6. It focuses on the effect of ring stiffening. Finally Geometry 4 is related to geometry 1 having all openings closed to compare the effect of stiffening to a beam with a compact web without any openings. The results of the comparative study are shown in Table 2-10.

Table 2-10: Summary of parametric study - Test 4

Steel f_{yk} [N/mm ²]	Failure Load F [kN]	Configuration	Failure Mechanism
235	433	Geometry 1	Vierendeel
355	650	Geometry 1	Vierendeel
460	838	Geometry 1	Vierendeel
235	395	Geometry 2	Vierendeel
355	573	Geometry 2	Web Post Buckling
460	682	Geometry 2	Web Post Buckling
235	396	Geometry 2 - without imperfection	Vierendeel
355	593	Geometry 2 - without imperfection	Vierendeel
460	763	Geometry 2 - without imperfection	Vierendeel
235	468	Geometry 3	Vierendeel
355	701	Geometry 3	Vierendeel
460	903	Geometry 3	Vierendeel
235	573	Geometry 4	M_{pl}
355	861	Geometry 4	M_{pl}
460	1109	Geometry 4	M_{pl}

Generally the stiffening arrangements should shift the failure mode to achieve an increase of the failure load level and strengthen the specimen.

Comparing the stiffened beam tested to a beam with the same geometry but non-stiffened openings clearly the stiffening configuration increases the failure load and stiffness, see Figure 2-52. No stiffening results into an early failure by web post buckling. The non-stiffened geometry 2 without considering an initial imperfection excludes web post buckling. Nevertheless the failure load is lower than for the stiffened specimen. Therefore the use of half moon stiffeners is an efficient way to increase the failure load significantly.

According to the parametric study comparing the ways of stiffening, see Figure 2-53, the appliance of ring stiffeners is the most effective way to strengthen the openings.

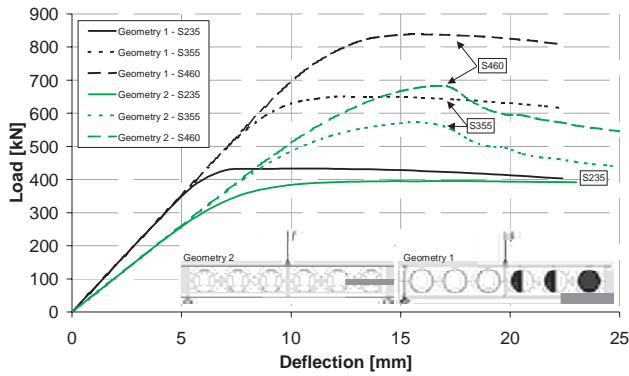


Figure 2-52: Parametric study on geometry (1) - Test 4

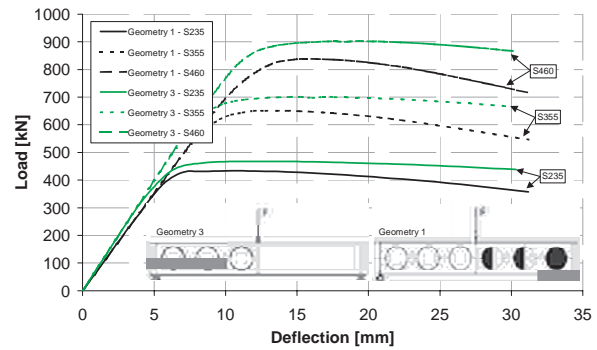


Figure 2-53: Parametric study on geometry (3) - Test 4

Comparing the failure load of beams with ring-stiffened openings to the failure load of beams with a compact web with no openings a reduction of the failure load of 81% with a corresponding loss of stiffness of 7% has been identified by the numerical studies. Therefore it has to be stated that it is not possible to reach the load capacity of a beam with a compact web by the stiffening methods investigated.

2.5.4.3.3 Influence of load introduction

According to the FE-simulations the appliance of stiffeners at the location of the load introduction slightly increases the failure loads and does not change the failure mode of Test 1A. The stiffeners were mainly provided to avoid early buckling under concentrated load introduction for the fire test (see section 3.3) but they are not necessary for cold design. In addition studies varying the load introduction show that the chosen test setup using 4 point loads instead of a uniformly distributed load does not influence the outcome of the tests significantly.

The aim of Test 2B has been to identify the influence of load introduction via secondary beams on the overall behaviour of the test specimen. In accordance to the parametrical study by numerical simulations no major influence of the load introduction could be detected and the failure mode is not concerned.

2.6 Summary and conclusion

The objectives of work package 1 “Tests on Composite Beams with Web Openings” has been to analyse the behaviour of composite beams with multiple regular web openings under “normal” conditions.

The test programme comprehended 3 tests on composite beams with multiple regular web openings and 1 test on a pure steel beam with stiffened multiple regular web openings as follows:

- Test 1 - Composite action in the end cell
- Test 2A - Elongated openings
- Test 2B - Load introduction
- Test 3 - Asymmetric design
- Test 4 - Stiffening of web openings

Therefore experimental investigations accompanied by numerical studies have been performed.

ad Test 1

The scope of Test 1 has been to study a basic test with multiple regular web openings. Additionally the composite slab has been left away at one of the supports to investigate the composite action in the end cell.

Uplifting of the concrete chord during testing shows that Vierendeel mechanism tends to develop starting at low load levels due to the cellular geometry of the specimen. Finally the beam fails by flexural web post buckling at the non-concreted opening. An unequal slippage of both sides has been identified. After closing the failed opening the test specimen has been reloaded and failed due to web post buckling at the concreted end cell on a significantly higher load level. The composite action in the end cell therefore is contributing to the ultimate limit state behaviour.

The examination of Test 1 clearly reveals the dependency of failure modes on the steel grade. The concrete strength hardly affects web post buckling whereas an influence of the concrete strength is detected for the Vierendeel mechanism. Additionally it has been identified that the rotational capacity of composite beams with cellular openings and higher steel grades is limited as instability of the web post is governing the design. The non-concreted end cell is beneficial for the ultimate limit state behaviour of the beam as the beam possesses more ductility for shear load transformation. Vierendeel mechanism can largely develop. Else the concreted end cell is inducing the shear directly into the web post and earlier buckling of the web post occurs.

ad Test 2A

The scope of Test 2A was to study the behaviour of an elongated opening. The opening is situated in the area of moment and shear interaction.

The failure mode of Test 2A has clearly been the Vierendeel mechanism as expected. Comparing the ultimate load of Test 2A to the one of Test 2B the bearing capacity in the area of moment and shear interaction is reduced to approximately 40% due to the elongated opening.

ad Test 2B

The scope of Test 2B was to study the influence of the load introduction via secondary beams on composite beams with regular web openings.

Test 2B shows that the load introduction via secondary beams is neglectable for the design, if minimum requirements, e.g. for reinforcement, the strength of secondary beams and its connection, etc. are met. The failure mode is not affected.

ad Test 3

The scope of Test 3 was to study the behaviour of an highly asymmetrical steel section with web openings as a composite beam. The same beam has also been tested under fire conditions, see section 3.3.

The test revealed, that Vierendeel mechanism tends to develop at low load levels due to the cellular geometry of the specimen. Finally the beam fails by flexural web post buckling at the non-concreted opening. The buckling mode of the post has obviously been influenced by the stronger and thus strengthening web part of the lower flange. An unequal slippage of both sides has been identified.

As failure due to web post buckling is clearly governing the design of Test 3 the parametric study plausibly shows that only the steel strength influences the failure load significantly. Since the failure modes web post buckling and Vierendeel mechanism affect each other the minor influence of the concrete strength may causes a change of the failure mode.

As the outcome of the Test 3 analysis is comparative to the results of Test 1 it is possible to state that the limitation for the design of hybrid sections according to ENV 1994-1-1: 1992 to the ratio

$A_{f,b} / A_{f,t} < 3$ is too conservative for composite beams. The concrete chord is sufficiently linked to the upper flange to marginally strengthen the section and avoid local buckling of the compression chord. Additionally the safety against web post buckling seems to be increased since the upper web part is strengthened by the lower part due to different web thicknesses evoking a change in the buckling mode.

ad Test 4

The scope of Test 4 is to check the behaviour of ring-stiffened, half-closed or closed circular web openings.

Test 4 fails due to Vierendeel mechanism evoking buckling of the half moon stiffener. The upper flange is extremely deformed.

Comparing the stiffened beam tested to a beam with the same geometry but non-stiffened openings clearly the stiffening configuration increases the failure load and stiffness. The parametric study comparing 2 ways of stiffening shows that stiffening by ring stiffeners is the most effective way to strengthen the openings. The appliance of half moon stiffeners is also an efficient way to stiffen openings to increase the failure load. Generally the stiffening arrangements should shift the failure mode to achieve an increase of the failure load level and strengthen the specimen. In general it has to be stated that it is not possible to reach the load capacity and stiffness of a beam with a compact web by the stiffening methods investigated.

2.7 Design recommendations

As general design recommendation it should be stated that web post buckling, i.e. local instability, should not govern the design. If necessary ring stiffeners or equal measures increase the web post buckling resistance.

Furthermore the effect of the shifted plastic neutral axis due to the concrete chord or asymmetry of the cross section of the beam is not notably affecting the buckling resistance as far as examined.

Further on different web thicknesses are not critical in terms of instability of the web post. Buckling of the upper and thinner web part is stabilised by the stronger lower part of the web.

As web post buckling is very sensitive to imperfections buckling curve c should be applied for design.

As beams with large web openings tend to fail by Vierendeel mechanism it is essential to chose an adequate location of the large openings, i.e. in areas of low shear, so that the resistance of the beam is not limited by local failure of the opening.

Additionally the interaction between Vierendeel mechanism and web post buckling should be checked.

More over the stiffness of the beams is largely influenced by regular web openings leading to larger deflections. Therefore serviceability is often governing the design of cellular beams.

The shear connection between the concrete chord and the upper flange of the steel beam is influenced due to large deflections and local Vierendeel effects. These effects have to be considered when designing an adequate shear connection for the composite beam.

2.8 Literature

[1] MSC.Marc Mentat 2003

[2] H. Bode. Euro-Verbundbau, 2. Auflage. Werner Verlag GmbH & Co. KG, Düsseldorf. 1998.

3 Contribution from CTICM

3.1 General

This section summarises the activities of the Centre Technique Industriel de la Construction Métallique (CTICM), St Rémy lès Chevreuse, in the ECSC Project "Large Web Openings for Service Integration in Composite Floors" for the period between 1st July 2001 and 31st December 2003 as well as the main results obtained.

In the frame of this project, CTICM has focused its work especially on the two following topics :

- 1) Predesign tools for steel and composite cellular beams. The result consists in a specific document including hypertext links to edit graphs and tables.
- 2) Fire behaviour of cellular beams. Two tests have been performed by CTICM in Maizières-lès-Metz.

Moreover CTICM has participated to all the meetings of the project and has been involved in the discussions concerning the various works performed by the partners in the frame of this research.

The main actions achieved during the research period have been :

- 1) Predesign tools
 - definition of the technical specifications
 - development of a specific software module for the calculation of loading capacity of steel and composite cellular beams
 - elaboration of the loading tables for steel cellular beams
 - elaboration of the loading tables for composite beams
 - elaboration of graphs
 - guidance for the predesign of cellular beams
- 2) Fire behaviour of cellular beams
 - definition of the tests
 - numerical simulations to estimate the behaviour
 - performing the tests at the testing laboratory of CTICM
 - treating on-site measurements and issuing test report
- 3) Tests on the programme developed by the Steel Construction Institute

Some calculation tests have been performed by CTICM and remarks were sent to the SCI.

The progress of the work during the research period has been in satisfactory accordance with the provisions.

3.2 Predesign tools for cellular beams

3.2.1 Introduction

The aim of this topic is to develop simple tools for the predesign of cellular beams fabricated from European I-rolled profiles.

These tools mainly consist in tables giving the loading capacity for a wide range of span lengths, but they also consist in tables of geometric properties. Graphs have also been plotted in order to facilitate the predesign.

The loading capacity of cellular beams have been determined by using the software **ARCELOR Cellular Beams** (ACB) developed outside of the project, by CTICM for ARCELOR. This software allows the designer to check a steel or composite cellular beam. The verifications are based on the Eurocodes 3 [1] and 4 [3], and more particularly the specific rules for cellular beams are those from Annex N of Eurocode 3 [2]. Some calculation aspects are not in the field of application of the Annex N, that is why the ACB software also refers to the SCI Publication n°100 [4].

However a specific software module has been developed as an interface between the Excel spreadsheet and the ACB Software. This module includes an iterative process based on a dichotomy method for the estimation of the loading capacity. For this purpose, several ultimate limit states are considered such as :

- bending resistance,
- shear resistance,
- local bending with Vierendeel effect,
- M-N-V interactions,
- web post buckling,
- ...

and a deflection condition for the serviceability limit state.

Finally more than 50000 cases of steel cellular beams have been studied (different geometries, different steel grades, different span lengths...). This leads to a great number of tables and it has been proposed to make them available on a CD ROM only. Therefore only examples of these tables are given in this final report.

3.2.2 Steel cellular beams

3.2.2.1 Basic assumptions

The main assumptions concerning the predesign tables are given hereafter for steel cellular beams.

For steel cellular beams, only doubly symmetric cross-sections are considered : same basic profile for the upper chord and the lower chord of the cellular beam, with the same steel grade.

For a given basic profile, an infinite number of geometrical possibilities (diameter a_0 and width w of intermediate posts) exist even if some geometrical requirements must be fulfilled. Therefore some specific limits have been proposed.

a) *Geometrical conditions*

The diameter a_0 and the width w of the posts are chosen in such a way that :

$$a_0 \geq 100 \text{ mm}$$

$$w \geq 70 \text{ mm}$$

$$0.2 \leq w/a_0 \leq 0.5$$

$$H_t/a_0 \leq 2.5$$

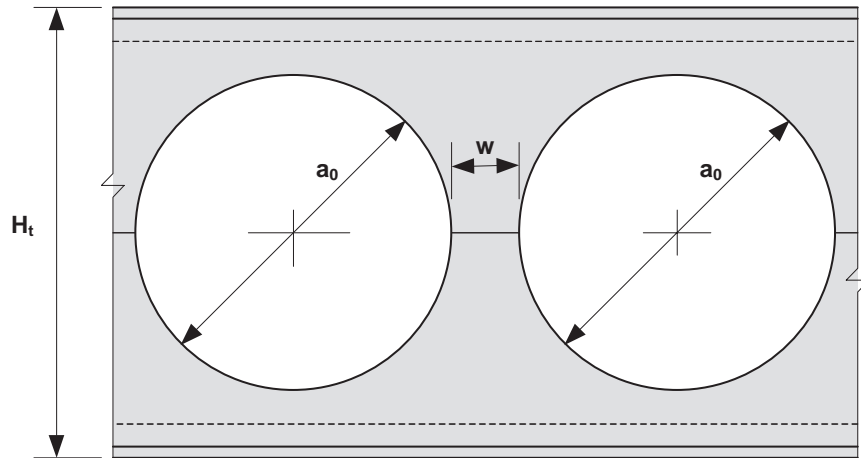


Figure 3-1: Geometry of the openings

In the tables, the diameter varies from the minimal diameter to the maximal diameter with a pitch of 50 mm. For each diameter, the width of the web posts is taken equal to 70 mm, 100 mm, 150 mm, 200 mm... up to the maximal value w_{max} .

The basic profiles with a total depth lower than 190 mm are excluded.

b) *Basic profiles and steel grades*

The following basic profiles are considered : IPE, HEA, HEB, HEM

The following steel grades are considered : S235, S275, S355, S420, S460

c) *Span length*

The span length varies from 5 m to 10 m with an increment of 1 m and from 12 m to 24 m with an increment of 2 m. In order to propose realistic solutions, it has been decided to keep the solutions which approximately fulfil the following conditions :

$$5 \leq L/H_t \leq 50$$

However the solutions which do not fulfil :

$$10 \leq L/H_t \leq 30$$

are presented with a grey background colour.

d) *Supports and lateral restraints*

The beam is assumed to be simply supported and fully restrained against lateral displacement. Therefore no lateral torsional buckling verification is performed.

e) *Load combinations*

Combination for ULS checks : $\gamma_G G + \gamma_Q Q$

Combination for SLS check : $G + Q$

where : $\gamma_G = 1.35$

$\gamma_Q = 1.50$

G is only the self-weight of the cellular beam

Q is the variable load (uniformly distributed)

The predesign tables supply the load capacity Q. This is conservative because the user may include other permanent loads in the load capacity Q. These permanent loads are then assumed to be factored by 1.50 instead of 1.35. This may be considered as acceptable at a predesign stage.

f) *Limit states*

Under the ULS combination, one of the following limit states may be determinant for the load capacity of a cellular beam :

- 1 Resistance to axial force (N)
- 2 Resistance to shear force (V)
- 3 Resistance to bending moment (M)
- 4 N-V interaction
- 5 M-N interaction
- 6 M-V interaction
- 7 M-N-V interaction
- 8 Horizontal shear resistance of a post
- 9 Buckling resistance of a post
- 10 Section resistance
- 11 SLS deflection limit

Items 1 to 7 are related to the resistance of each chord. These limit states include Vierendeel effects. All the verifications are performed according to Eurocode 3 part 1-1 "General rules and rules for buildings" and according to the specific rules from Annex N "Openings in webs".

The partial safety factors are taken from the ENV version of Eurocode 3 :

$$\gamma_{M0} = 1,10$$

$$\gamma_{M1} = 1,10$$

Item 11 is related to the maximal deflection of the beam under the SLS combination :

$$v_{\max} \leq L/250$$

where : v_{\max} is the maximal deflection,

L is the span length of the beam.

3.2.2.2 Examples of predesign tables for steel cellular beams

The Table 3-1 is an example of predesign table for steel cellular beams. For various solutions (basic profile, opening diameter and intermediate post width) and for various span lengths, it gives :

- the number n of openings along the beam
- the width we in mm of the end posts
- the loading capacity q in kN/m (uniformly distributed)
- a code for the determinant limit state as above mentioned

Table 3-1: Predesign tables for steel cellular beams

Steel grade S235			7 m				8 m				9 m				10 m			
Basic Profile	a0 mm	w mm	n	we mm	q kN/m	L. S.	n	we mm	q kN/m	L. S.	n	we mm	q kN/m	L. S.	n	we mm	q kN/m	L. S.
IPE 330	300	100	17	150	16,8	9	19	250	14,8	9	22	150	12,5	9	24	250	11,2	7
IPE 330	350	70	16	175	10,6	9	18	255	9,3	9	21	125	7,7	9	23	205	7,0	9
IPE 330	350	100	15	175	15,4	9	17	225	13,2	9	19	275	11,6	9	22	100	9,8	9
IPE 330	350	150	13	325	19,9	7	15	325	15,8	7	17	325	12,8	7	19	325	10,5	7
IPE 330	400	100	13	300	14,6	9	15	300	12,3	9	17	300	10,6	9	19	300	9,3	9
IPE 330	400	150	12	275	17,8	7	14	225	14,5	7	16	175	11,9	7	17	400	9,9	7
IPE 360	200	70	25	160	18,1	9	29	120	15,3	9	33	80	13,3	9	36	175	12,1	9
IPE 360	250	70	21	175	15,5	9	24	195	13,3	9	27	215	11,7	9	31	75	10,0	9
IPE 360	250	100	19	225	22,0	9	22	200	18,6	9	25	175	16,1	9	28	150	14,0	7
IPE 360	300	70	18	205	13,7	9	21	150	11,5	9	24	95	9,8	9	26	225	9,0	9
IPE 360	300	100	17	150	19,2	9	19	250	16,9	9	22	150	14,3	9	24	250	13,0	9
IPE 360	350	70	16	175	12,1	9	18	255	10,5	9	21	125	8,8	9	23	205	7,9	9
IPE 360	350	100	15	175	17,6	9	17	225	15,1	9	19	275	13,3	9	22	100	11,2	9
IPE 360	350	150	13	325	25,5	9	15	325	20,5	7	17	325	16,5	7	19	325	13,5	7
IPE 360	400	100	13	300	16,7	9	15	300	14,1	9	17	300	12,1	9	19	300	10,7	9
IPE 360	400	150	12	275	23,6	9	14	225	19,3	7	16	175	15,8	7	17	400	13,1	7
IPE 360	450	100	12	250	15,0	9	14	200	12,5	9	16	150	10,6	9	18	100	9,2	9
IPE 360	450	150	11	275	21,0	5	13	175	17,3	7	14	375	14,5	7	16	275	12,1	7
IPE 400	200	70	25	160	21,1	9	29	120	17,9	9	33	80	15,5	9	36	175	14,1	9
IPE 400	250	70	21	175	18,0	9	24	195	15,5	9	27	215	13,5	9	31	75	11,6	9
IPE 400	250	100	19	225	25,7	9	22	200	21,8	9	25	175	18,9	9	28	150	16,6	9
IPE 400	300	70	18	205	15,9	9	21	150	13,3	9	24	95	11,4	9	26	225	10,4	9
IPE 400	300	100	17	150	22,5	9	19	250	19,8	9	22	150	16,7	9	24	250	15,1	9

The Figure 3-2 is an example of graph for the predesign of steel cellular beams. The Table 3-2 gives the main section properties of the cellular beams contained in the predesign table.

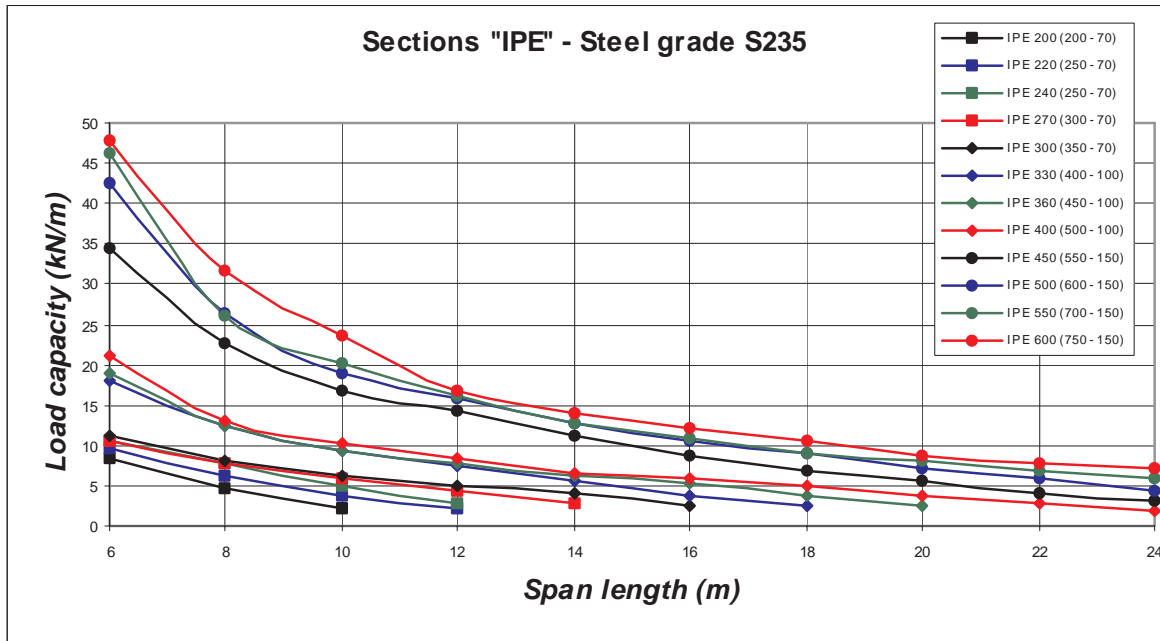


Figure 3-2: Predesign of Steel Cellular Beams (IPE – S235)

Table 3-2: Section properties

IPE Basic Profile	Ratios					Gross Section		Net Section		Mass kg/m	Tee Section		
	a_0 mm	w mm	H_t mm	w/a_0	H_t/a_0	A cm ²	I_y cm ⁴	A_{net} cm ²	$I_{y.net}$ cm ⁴		A_m cm ²	$Z_{G,m}$ mm	$I_{y,m}$ cm ⁴
IPE 330	300	100	462,90	0,333	1,54	72,57	25368	50,07	23681	46,57	25,04	66,63	91,30
IPE 330	350	70	493,29	0,200	1,41	74,85	29346	48,60	26667	45,27	24,30	58,69	62,37
IPE 330	350	100	489,33	0,286	1,40	74,56	28810	48,31	26130	45,94	24,15	57,07	57,41
IPE 330	350	150	479,21	0,429	1,37	73,80	27461	47,55	24781	46,60	23,77	52,87	45,92
IPE 330	400	100	515,37	0,250	1,29	76,51	32454	46,51	28454	45,26	23,25	47,06	32,95
IPE 330	400	150	506,74	0,375	1,27	75,86	31218	45,86	27218	46,10	22,93	43,38	26,33
IPE 360	200	70	445,08	0,350	2,23	79,54	26294	63,54	25761	55,13	31,77	98,79	326,59
IPE 360	250	70	471,64	0,280	1,89	81,66	30003	61,66	28961	54,47	30,83	89,90	243,05
IPE 360	250	100	465,77	0,400	1,86	81,19	29159	61,19	28118	54,93	30,60	87,64	224,56
IPE 360	300	70	497,61	0,233	1,66	83,74	33908	59,74	32108	53,74	29,87	80,58	173,13
IPE 360	300	100	492,90	0,333	1,64	83,36	33179	59,36	31379	54,34	29,68	78,73	161,17
IPE 360	350	70	523,29	0,200	1,50	85,79	38046	57,79	35187	52,96	28,90	70,93	117,18
IPE 360	350	100	519,33	0,286	1,48	85,48	37391	57,48	34532	53,67	28,74	69,34	109,40
IPE 360	350	150	509,21	0,429	1,45	84,67	35742	56,67	32884	54,38	28,33	65,23	91,06
IPE 360	400	100	545,37	0,250	1,36	87,56	41831	55,56	37564	52,95	27,78	59,54	69,50
IPE 360	400	150	536,74	0,375	1,34	86,87	40327	54,87	36060	53,84	27,43	55,95	57,98
IPE 360	450	100	571,16	0,222	1,27	89,62	46521	53,62	40446	52,19	26,81	49,37	40,67
IPE 360	450	150	563,62	0,333	1,25	89,02	45120	53,02	39045	53,23	26,51	46,14	33,80
IPE 400	200	70	485,08	0,350	2,43	91,78	35823	74,58	35249	64,19	37,29	114,00	547,09
IPE 400	250	70	511,64	0,280	2,05	94,06	40453	72,56	39333	63,48	36,28	105,28	425,83
IPE 400	250	100	505,77	0,400	2,02	93,56	39403	72,06	38283	63,98	36,03	103,08	398,46
IPE 400	300	70	537,61	0,233	1,79	96,30	45303	70,50	43368	62,70	35,25	96,18	320,90
IPE 400	300	100	532,90	0,333	1,78	95,89	44399	70,09	42464	63,35	35,05	94,38	302,51

3.2.3 Composite cellular beams

3.2.3.1 Basic assumptions

The number of basic parameters for composite cellular beams is far greater than for pure steel cellular beams. So it has not been possible to deal with the whole field of possibilities including various classes of concrete, various types of slab (plain slabs, slabs with profiled steel sheeting...), various steel grades... Moreover it is more efficient for composite cellular beams, to use a mono-symmetric steel section (lower chord and upper chord are cut from different I-rolled profiles). This leads to a greater number of solutions.

So it has been decided with the partners to limit the number of loading tables to some very common solutions. The main assumptions for these solutions are presented hereafter.

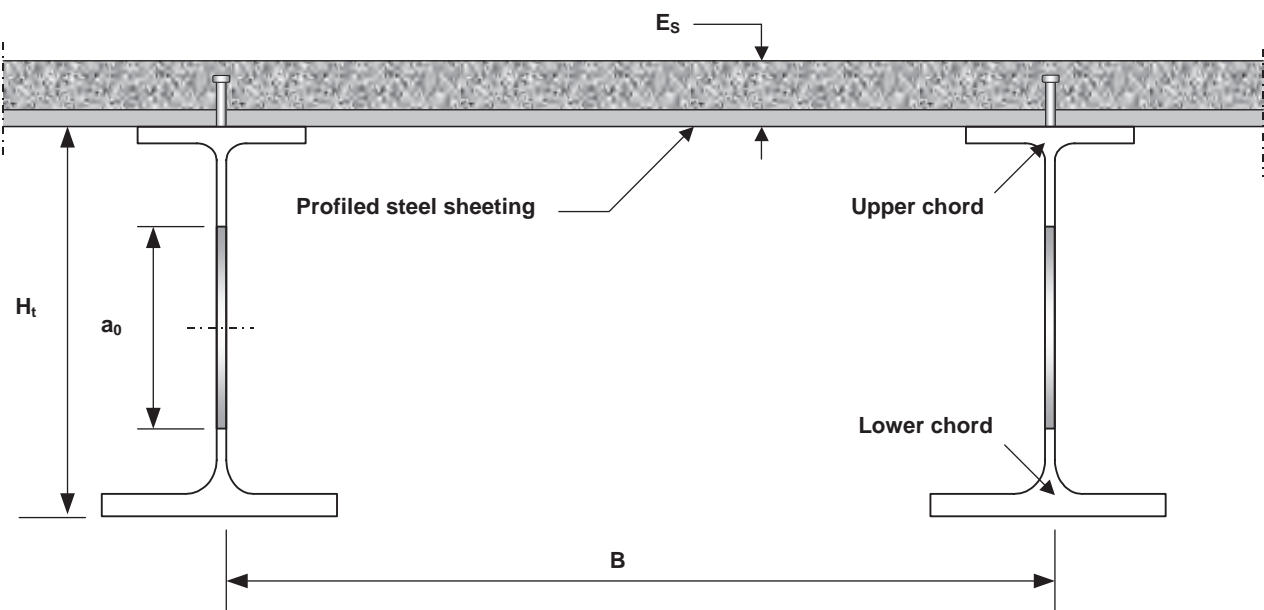


Figure 3-3: Composite cross-section

The basic assumptions are the following :

- Slab with profiled steel sheeting perpendicular to the beam
- Total depth of the slab 12 cm
- Participating width of the slab : $2 \times L/8$
- Concrete class : C25/30
- The beam is assumed to be fully propped during concreting
(no check at this stage)
- Profiled steel sheeting : PAB Cofradal 60 (open profile)
- Connector : Welded stud 100x19 mm

The calculations are similar to those performed for steel cellular beams, except that the composite effect significantly improves the loading capacity of the beam. The self weight of the slab is automatically included in the permanent loads, factored by 1.35 for the ULS verifications.

3.2.3.2 Examples of predesign tables for composite cellular beams

Tables are available for 2 cases of association of basic profiles :

- IPE serial for upper chord and HEA for lower chord,
- IPE serial for upper chord and HEB for lower chord,

for 3 steel grades : S235, S355 and S460,

and for 2 ratios : $w/a_0 = 0.2$ and $w/a_0 = 0.4$.

Table 3-3: Predesign tables for composite cellular beams

Steel Grade S235					6 m				7 m				8 m			
Upper Chord	Lower Chord	a0 mm	w mm	Ht mm	n	we mm	q kN/m	L. S.	n	we mm	q kN/m	L. S.	n	we mm	q kN/m	L. S.
IPE 300	HEA 260	240	50	384	20	125	5,9	9	24	45	3,3	9	27	110	2,6	9
IPE 330	HEA 280	270	54	424	18	111	6,8	9	21	125	4,9	9	24	139	3,4	9
IPE 360	HEA 300	300	60	464	16	150	8,8	9	19	110	6,3	9	22	70	4,4	9
IPE 400	HEA 340	350	70	528	14	95	11,6	9	16	175	9,2	9	19	45	6,3	9
IPE 450	HEA 400	400	80	608	12	160	16,9	9	14	180	13,0	9	16	200	10,3	9
IPE 500	HEA 450	450	90	682	11	75	20,8	9	12	305	18,3	9	14	265	14,3	9
IPE 550	HEA 550	500	100	782	10	50	26,2	9	11	250	22,7	9	13	150	17,3	9
IPE 600	HEA 700	600	120	931	8	180	39,0	9	9	320	32,4	9	11	100	23,7	9
IPE 300	HEB 240	240	50	379	20	125	5,7	9	24	45	3,1	9	27	110	2,4	9
IPE 330	HEB 260	270	54	419	18	111	6,6	9	21	125	4,6	9	24	139	3,2	9
IPE 360	HEB 300	300	60	469	16	150	8,8	9	19	110	6,3	9	22	70	4,4	9
IPE 400	HEB 320	350	70	523	14	95	11,4	9	16	175	9,1	9	19	45	6,1	9
IPE 450	HEB 360	400	80	593	12	160	16,2	9	14	180	12,5	9	16	200	9,8	9
IPE 500	HEB 450	450	90	687	11	75	21,0	9	12	305	18,5	9	14	265	14,5	9
IPE 550	HEB 600	500	100	812	10	50	27,8	9	11	250	24,2	9	13	150	18,5	9
IPE 600	HEB 800	600	120	986	8	180	42,7	9	9	320	35,6	9	11	100	26,1	9
IPE 300	HEA 260	240	96	376	17	192	16,2	9	20	188	12,5	9	23	184	9,9	9
IPE 330	HEA 280	270	108	415	15	219	20,2	9	18	152	15,1	9	21	85	11,6	9
IPE 360	HEA 300	300	120	454	14	120	22,4	9	16	200	18,7	9	19	70	13,9	9
IPE 400	HEA 340	350	140	517	12	130	28,4	9	14	140	22,7	9	16	150	18,5	9
IPE 450	HEA 400	400	160	595	10	280	40,8	9	12	220	31,2	9	14	160	24,9	9
IPE 500	HEA 450	450	180	667	9	255	50,5	9	11	125	37,1	9	12	310	33,1	9
IPE 550	HEA 550	500	200	765	8	300	63,2	9	10	100	45,5	9	11	250	39,9	9
IPE 600	HEA 700	600	240	911	7	180	78,8	9	8	260	64,5	9	9	340	54,4	9
IPE 300	HEB 240	240	96	371	17	192	15,9	9	20	188	12,2	9	23	184	9,6	9
IPE 330	HEB 260	270	108	410	15	219	19,9	9	18	152	14,8	9	21	85	11,3	9
IPE 360	HEB 300	300	120	459	14	120	22,7	9	16	200	18,9	9	19	70	14,1	9
IPE 400	HEB 320	350	140	512	12	130	28,0	9	14	140	22,3	9	16	150	18,3	9
IPE 450	HEB 360	400	160	580	10	280	39,8	9	12	220	30,4	9	14	160	24,1	9
IPE 500	HEB 450	450	180	672	9	255	51,2	9	11	125	37,7	9	12	310	33,6	9
IPE 550	HEB 600	500	200	795	8	300	66,9	9	10	100	48,0	9	11	250	42,3	9
IPE 600	HEB 800	600	240	966	7	180	85,9	9	8	260	70,4	9	9	340	59,5	9

Série "IPE-HEA" - Steel Grade S235
w/a0 = 0,2

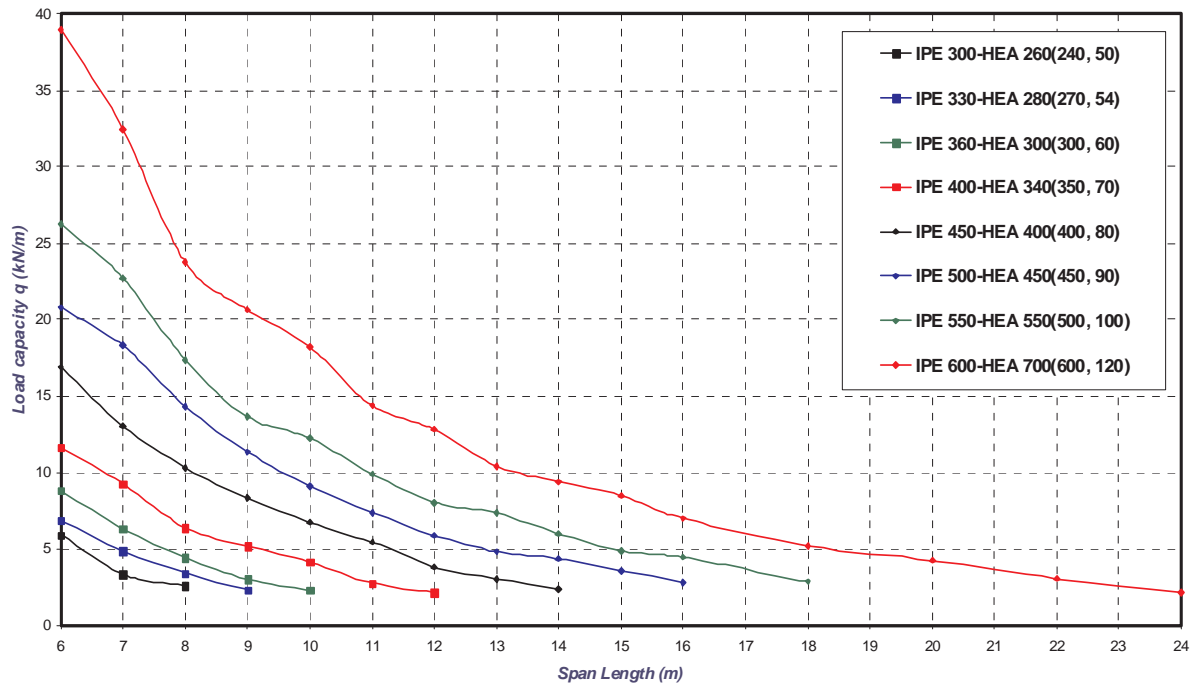


Figure 3-4: Predesign of composite cellular beams (IPE-HEA – S235)

3.3 Fire behaviour of cellular beams

A test on cellular beams exposed to fire was performed in the CTICM Test Station (at Maizières-Metz) on Friday 4th October 2002.

The testing elements were composed of two beams:

P1 : a loaded protected cellular beams of 7.20m span, same as the Test 3 beam tested at cold temperature

The beam is composite. It is composed of a steel profile, based on HEB 340 for the lower flange and IPE 300 for the upper flange, and a 130 mm thick concrete slab.

The beam length is 7200 mm and it is composed of 12 openings of 570 mm length. The 1st and the 12th cell are full. The distance between supports is 6840 mm. There are 3 stiffeners. The slab includes a HI-BOND 55 steel deck. The slab is connected to the steel profile with one file of ϕ 19 connectors, spaced out each 150 mm. The yield stress of steel was measured on different points and is resumed in the Table 3-4.

Table 3-4: Yield stress of steel (MPa)

Lower flange	Web		Upper flange
	Lower part	Upper part	
484	390	456	400

The yield stress in compression of concrete is 40 MPa. The load is distributed on 3 times 100 kN, at the level of the 3 central stiffeners (see Figure 3-5).

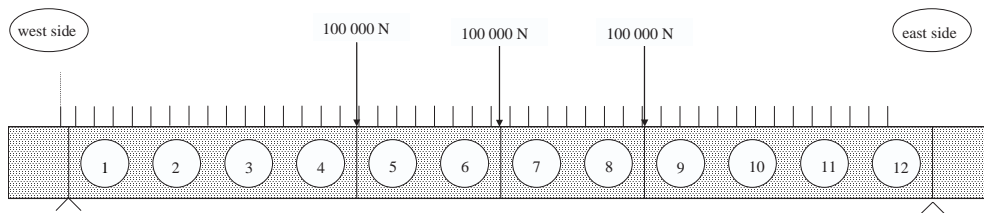


Figure 3-5: Loading

P2 : a cellular beam based on IPE 400, with some openings are filled, same as Test 1 beam tested at cold temperature, protected with some unprotected edges of opening

The beam P2 was unloaded with three different part for which the details are given in the following figure.

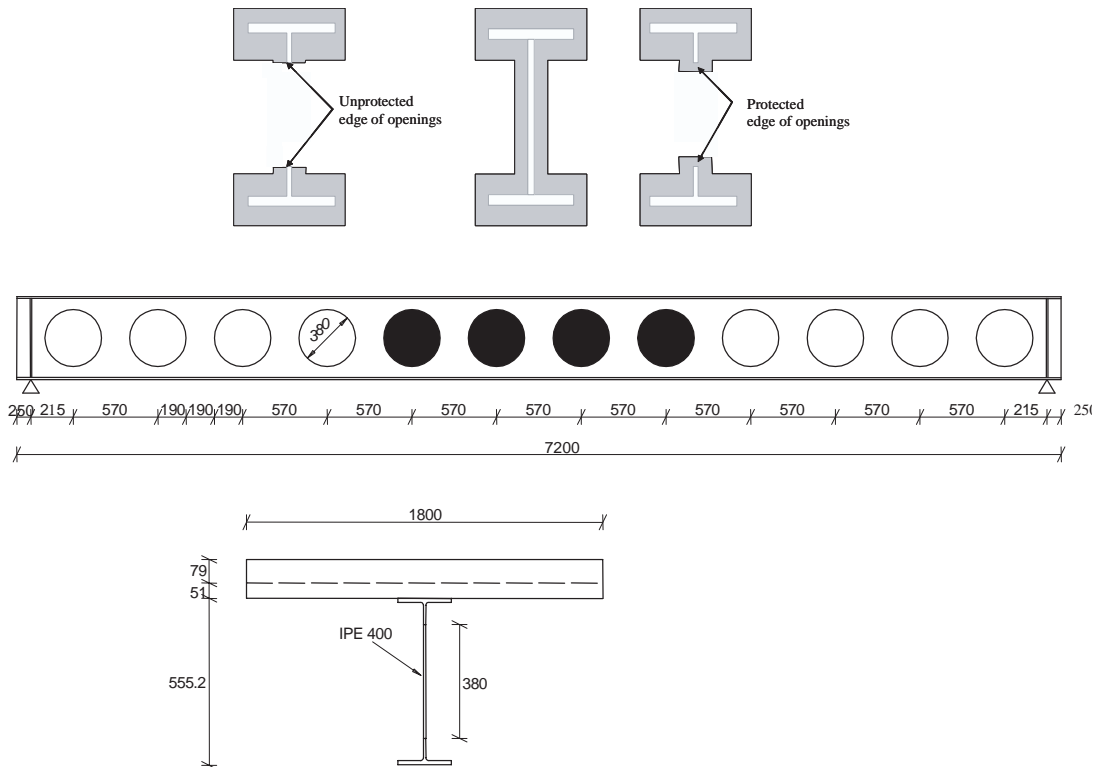


Figure 3-6: View of the beam P2

More details about the numerical and testing conditions and results are given in the plenary report.

3.3.1 Experimental results on the unloaded beam

For the unloaded beam P2, the protection thickness was applied with the following conditions :

Table 3-5: Protection thickness

Position	Measured thickness (mm)			
	Min	Average	Max	Variation
total	10	21	28	3
Opening edge	10	18	25	6

The temperature was recorded on different sections that correspond to the following conditions :

- Sections S1, S2 and S3 : sections with openings but without protection on the opening edges
- Sections S4 and S5 : sections without opening
- Sections S6, S7 and S8 : sections with openings and with protection on the opening edges

In that respect, the effect of the opening and the effect of the protection on the opening edge can be studied by comparison of the measurements on the three types of sections.

The following figures show the comparison of the average temperatures on the three types of sections at the centre of the web, near the opening in the web, at the lower flange and at the upper flange. For more details, one can refer to the test report.

After about 90 minutes, a part of the protection localised on the ‘no opening’ part (mid span of the beam) on the lower face of the lower flange (a length of about 50 cm) has fallen down, leading to higher temperature of this part (Sections S4 and S5).

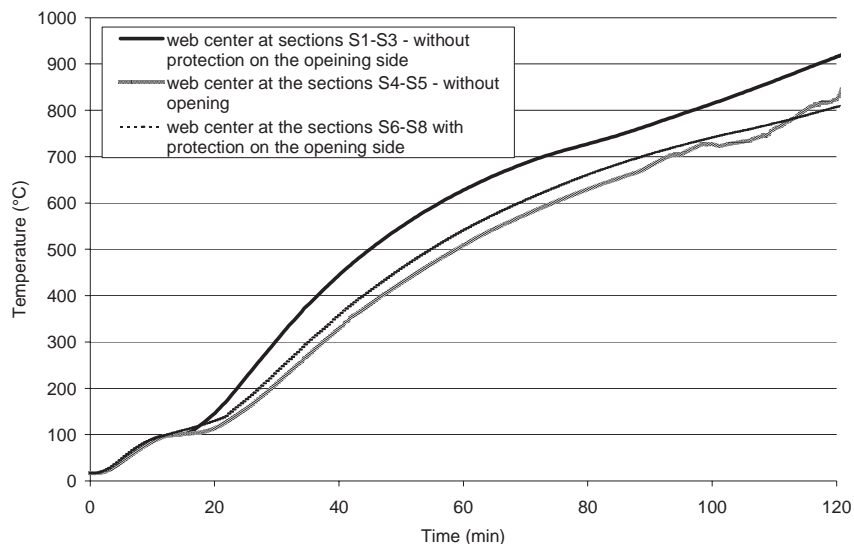


Figure 3-7: Average temperature in the centre of the web at mid height

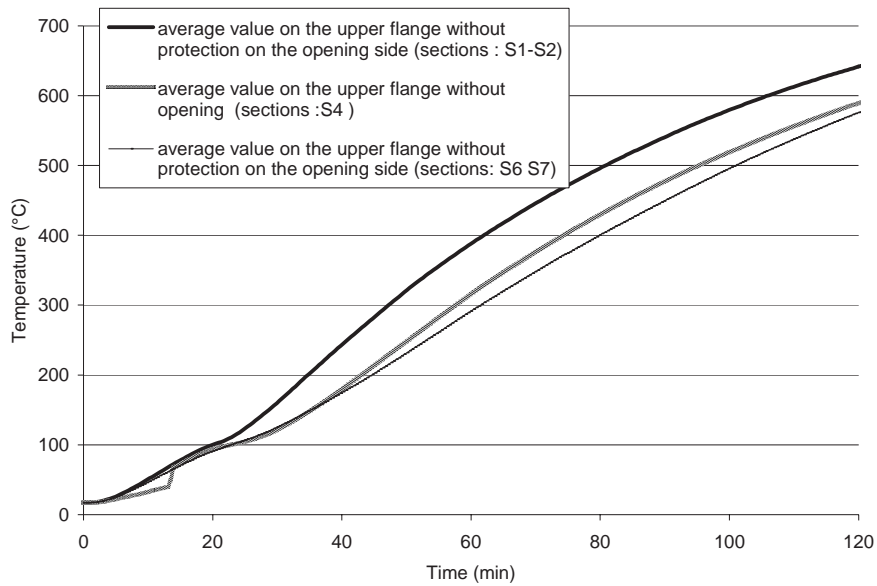


Figure 3-8: Average temperature in the upper flange

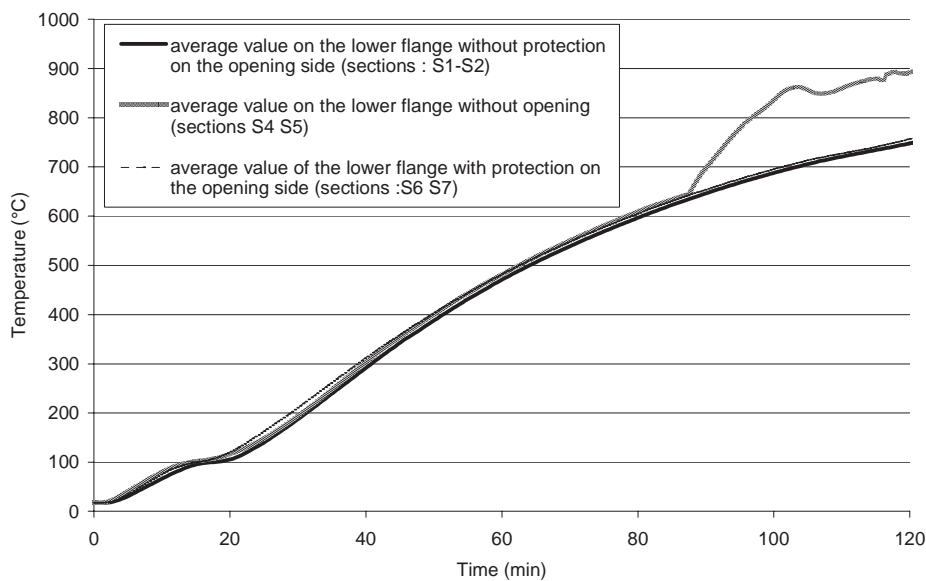


Figure 3-9: Average temperature in the lower flange

These results show that :

- the lower flange temperature is not modified by the opening (with or without opening, or with or without protection on the opening edge) – Figure 3-9
- for the upper flange temperature, the non protection of the opening edge leads, after 20 minutes of fire exposition, to higher temperature, that can be more than 100°C compared to the case with protection on the opening edge or more than 80°C compared to the case without opening. The opening with protection on the opening edge, leads to lower temperature than the case without opening. This can be explained by the heat flux from the web to the flange that is reduced due to the reduction of the width of the web – Figure 3-8.

- For the web, the average or localised temperatures lead to the same analysis : the opening increases a little bit the temperature on the web when all is protected, of about 30°C, but this temperature increase is higher without protection on the opening edge of more than 100°C – Figure 3-7.

In conclusion, it is clear that if there is no protection on the opening edges of cellular beams, specific assessment of the temperature field in the cellular beams has to be made in order to study the fire stability of the cellular beam. When protection is applied on the opening edge, compared to the temperature without opening, higher temperature (about 30°C) is recorded. This needs to be taken into account in the methodology to be developed for calculating the fire stability duration of cellular beams. Generally, the simple approach of massivity factor differentiating lower flange, upper flange and web part leads to safe approach of temperature distribution in cellular beams, when protection is applied on the opening edges.

3.3.2 Experimental results on the loaded beam

The loaded beam has been protected by an average thickness, of Newspray insulation Product, given by the manufacturer Projiso that is thanks for its contribution to the present research, of 24 mm. Displacements, rotation and many temperatures were measured in some locations. The fire stability was 108 minutes.

3.3.2.1 Displacements

The deflection was measured at $\frac{1}{4}$, $\frac{1}{2}$ and $\frac{3}{4}$ of the beam length. The recorded measurements are shown in the following figure.

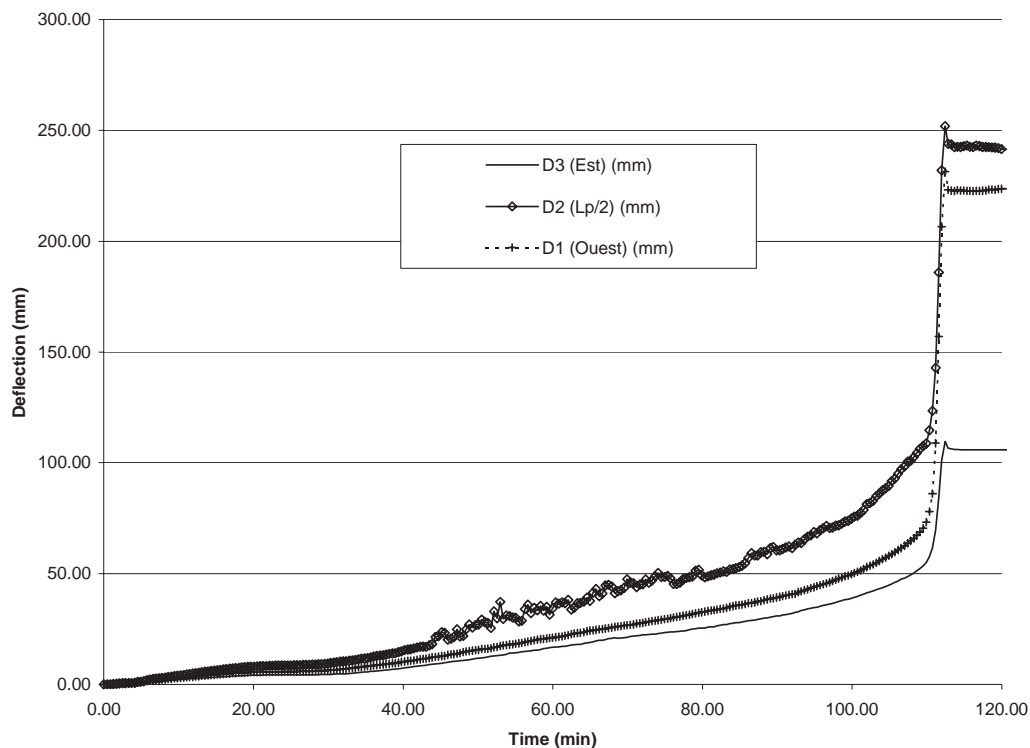


Figure 3-10: Deflection of the beam

3.3.2.2 Temperature measurements

About 172 Thermocouples recorded the temperature on the steel sections as a function of time.

In order to show that the temperature distribution along the beam length was not constant, the following figure shows the temperature at three same point on the web position but at $\frac{1}{4}$, $\frac{1}{2}$ and $\frac{3}{4}$ of the beam length.

The temperature reached at the failure time is given in the following table.

Table 3-6: Temperature at the failure time

	Temperature (°C)		
	Min	Average	Max
Web	286	545	663
Lower Flange	326	517	590
Upper Flange	263	317	374

The global analysis of the test results for the two beams by numerical simulations describes the fire behaviour of the beam. Finite element calculations were made for comparison and understanding of the thermo-mechanical behaviour of these beams.

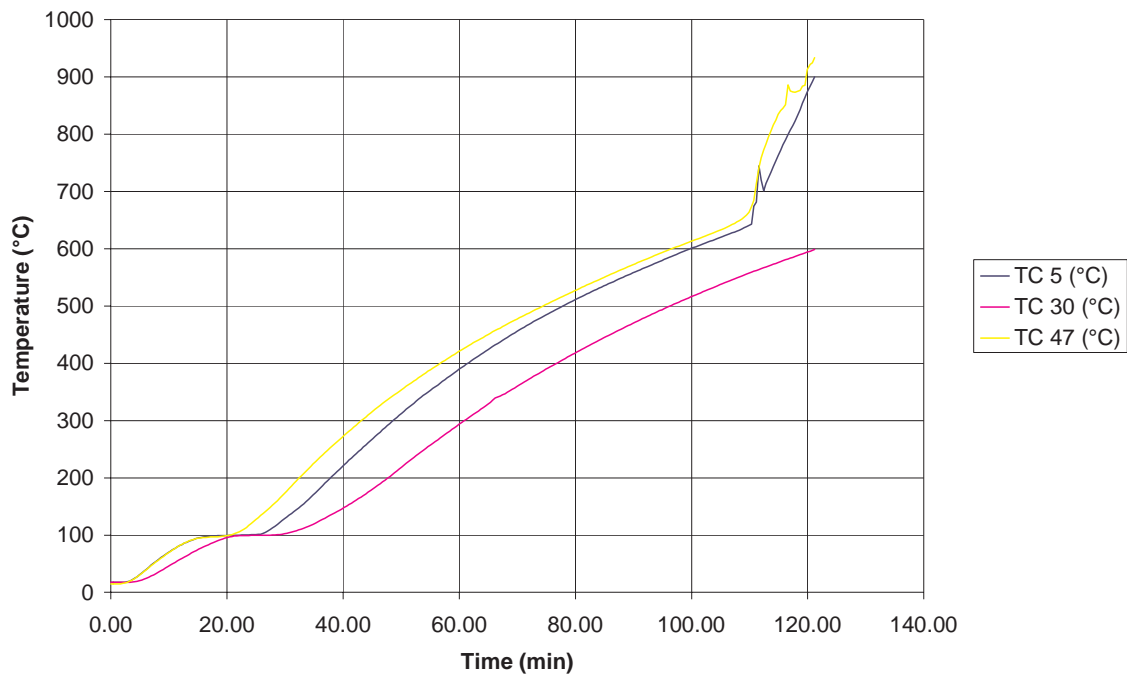


Figure 3-11: Web temperature along the beam versus time

3.3.2.3 Observations

During the tests, no fall or degradation of the insulation was observed up to failure time.

The following photo shows the state of the beam after the tests.



Figure 3-12: View of the failed part of beam in the furnace after the test

The results of the test of the loaded beam have shown that the failure had occurred firstly by web instability at the first exposed web element (between opening 2 and opening 3), but we can observe the effect of failure by the instability of the second web post (between opening 3 and opening 4). The numbering of openings is given in Figure 3-5.

3.3.3 Numerical mechanical behaviour of the loaded beam

3.3.3.1 At ambient temperature

The test has been performed taken into account as a reference the Test 3 of the test campaign realised at ambient temperature. Nevertheless, in order to adapt the beam to the furnace of CTICM, the beam tested at high temperature has been modified reducing a few the length, but closing the two extreme opening on the web, decreasing the number of openings from 12 openings to 10 openings. The test 3 has led to failure load of 656 kN.

The maximum load level reached by the FEA has been 628.2 kN with a corresponding deflection of 43.73 mm. The load-deflection curve is displayed in Figure 3-13.

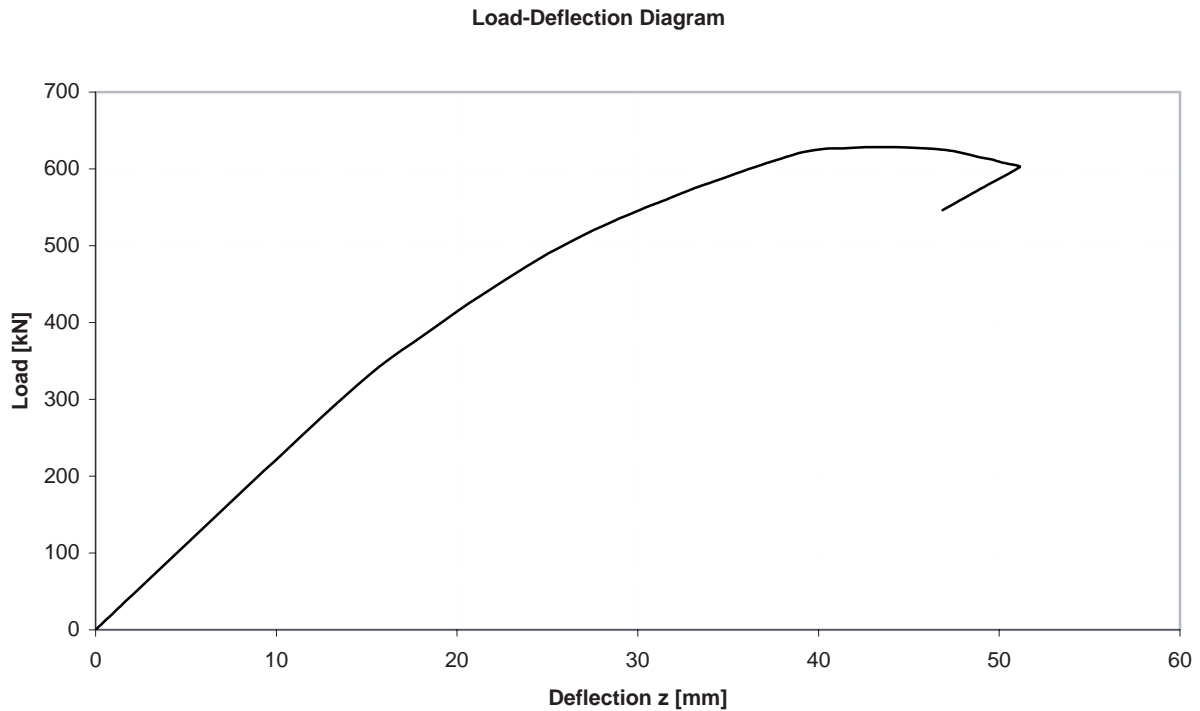


Figure 3-13: Load-Deflection Curve of the FEA

The indicated failure mechanism has been web post buckling occurring between the 9th and 10th opening.

3.3.3.2 At high temperature

The tested beam is not totally symmetric, at the level of the slab and the connectors, as shown on the Figure 3-5. However only half the beam was modelled, in order to minimize the calculation time. The modelled side is the east side, which is the weakest.

3.3.3.2.1 Heating up

The heating up of the beam used in the calculation comes from the measured temperature. For each point, an average was done on the 3 sections. This average was used in the calculation. Also the temperature field used in the calculation is uniform on the length. During test, the part of beam which is at the extremity, after the support, is outside the oven. This part of beam remains cold.

The Figure 3-14 shows the heating up of the beam used in the calculation.

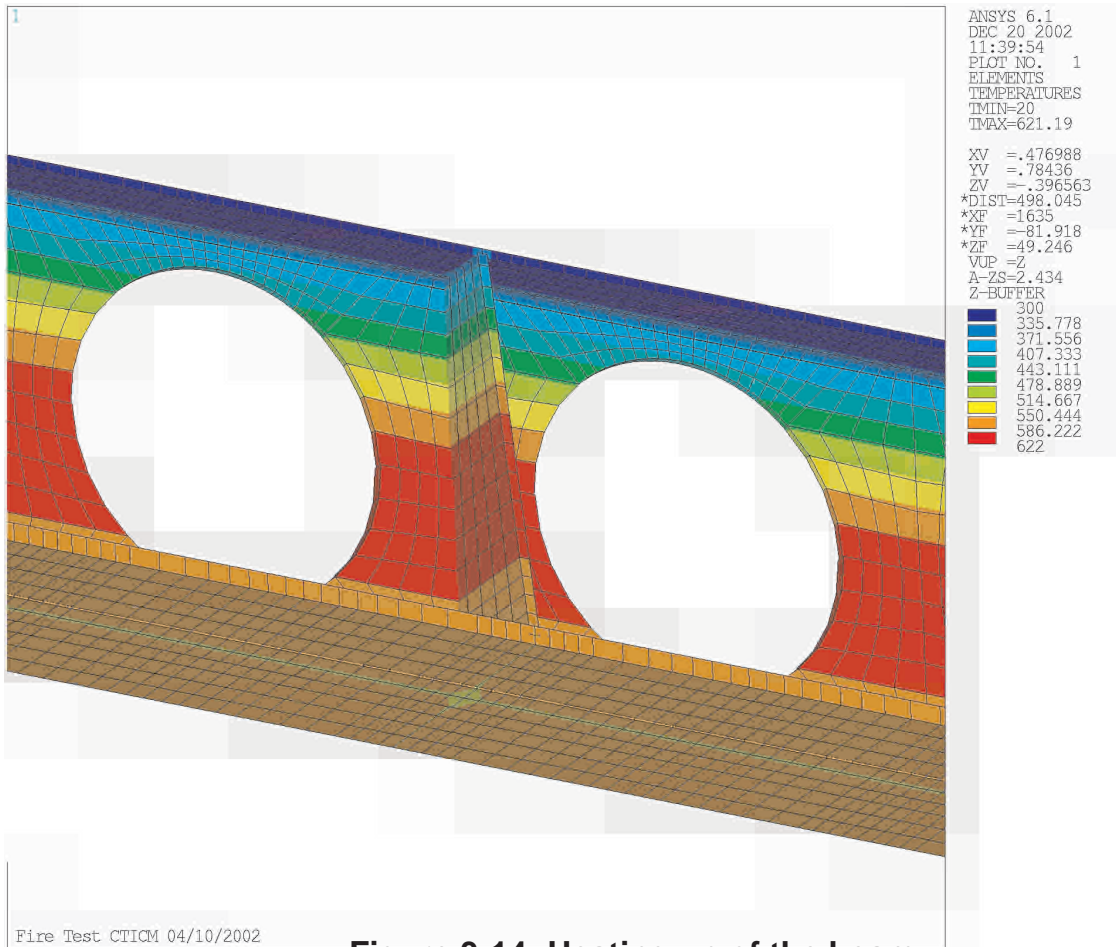


Figure 3-14: Heating up of the beam

3.3.3.2.2 Results

The failure mode of the beam, observed during test, is web post buckling, between openings 2 and 3, and then between openings 3 and 4. The calculation allows to find this failure mode and gives the horizontal displacement of web. As the simulation used a symmetrical beam, the numerical failure occurs in a same way between openings 2 and 3 or openings 10 and 11. During test, the vertical displacement was measured at quarter of span, at mid-span and at three quarters of span. The rotation on the supports was measured too. The Figure 3-15 shows the comparison between test and calculation for these results.

The Figure 3-15 shows a very good correlation between calculation and test. Indeed the displacement value before collapse, as the instant value of collapse, are very well found by calculation.

The simulation, as it has been observed during the test, leads to the conclusion of a weak impact of the reduction of connection between the beam and the slab at the extremity of the beam. The term “weak” is used in order to show that the small difference between the failure time (2 minutes) may be due to that, but this should be shown only by simulation of the global beam. It appears also that temperature during the test was not exactly symmetrical, and adaptation for simulation may lead to small differences between test and numerical results.

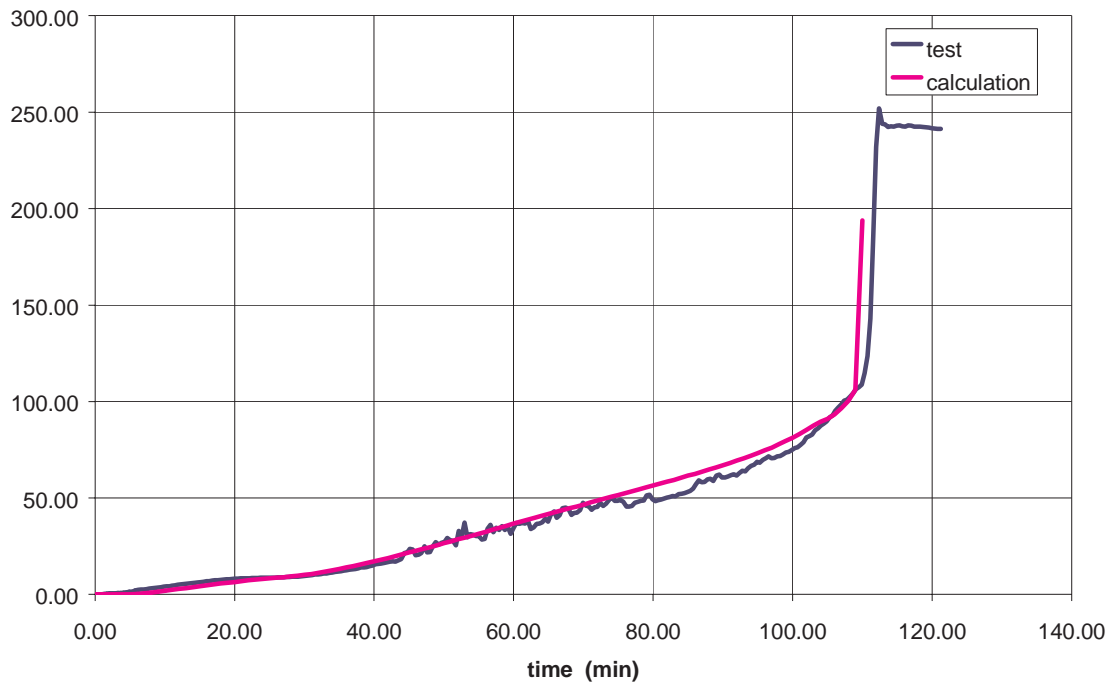


Figure 3-15: Numerical and experimental vertical displacement at mid-span

3.3.4 Analysis

The numerical model leads to a very good correlation with the main experimental results :

- the failure mode (web post buckling)
- the time of failure
- the vertical displacement at mid-span.

3.3.4.1 Thermal analysis

The thickness of the protection applied on the beam varied from 11 to 45 mm, with an average value of 24 mm.

This leads to very difficult comparison between calculations and measurements for the thermal transfer. So it has decided to not compare calculated temperature with measurements.

A simple calculations considering a 3 different part of the beam with massivity factors protected by the average value of Newspray of 24 mm, leads to a high temperature compared to measured one :

Table 3-7: Comparison of measured and calculated temperatures

	Thickness (mm)	Massivity factor	Mean measured temperature (°C)	Calculated temperature (°C)
Web HEB 240	10	200	576	694
Flange HEB 240	17.5	114.285714	517	570
Web IPE 300	7.1	281.690141	521	750
Flange IPE 300	10.7	93.4579439	317	514

It can be observed the effect of the slab by a lower temperature on the IPE 300 upper flange, and on the web IPE 300 that are lower than the calculated one. This leads to a large safety factor when using simple calculation model. A large effect is also shown on the lower part of the web (web of HEB 240), but a weak effect on the lower flange of the HEB 240 part.

The temperature distribution on the unloaded beam should lead to better understanding of the thermal behaviour of such a beam.

3.3.4.2 Mechanical behaviour

The numerical thermo-mechanical analysis of the tested loaded beams leads to a very good correlation with the test. The failure occurs numerically and experimentally at about 108 min, by web buckling.

At this time, the average temperature of the web was 545°C, with maximum localised temperature of 663°C. The calculations have shown, without horizontal gradients in the beam, that the maximum temperature in the web (near the centre) was 600°C at the failure time. This confirms the global failure temperature of the web.

Due to similar failure mode at high temperature and at ambient temperature, the mechanical load factor is determined from mechanical behaviour at ambient temperature. The failure load is 628.2 kN. So a load factor of 0.477 has been applied at high temperature. The maximum web temperature at the failure time, so 600°C, leads to a reduction of effective yield strength to 47% according to the Eurocode 3 part 1.2.

So it can be thought that a simple approach considering the reduction of the effective yield strength reduction from the load factor could be used for the determining the critical temperature of the beam.

Nevertheless, a single test may not generalised this simple approach to design of protection thickness to all cellular beams.

3.3.5 Conclusion

First, the experimental study of the fire behaviour of the cellular beams has allowed to give referenced value for the scientific world in the structural fire resistance world, that did not exist previously.

The analysis has been performed in the two domains :

- thermal transfer
- mechanical behaviour at high temperature

Thermal transfer :

Concerning the thermal transfer, the temperature measurements on the unloaded beam leads to the following conclusions :

- if there is no protection on the opening edges of cellular beams, specific assessment of the temperature field in the cellular beams has to be made in order to study the fire stability of the cellular, because of higher temperature can be encountered.
- When protection is applied on the opening edge, compared to the temperature without opening, higher temperature (about 30°C) is recorded. This needs to be taken into account in the methodology to be developed for calculating the fire stability duration of cellular beams. Generally, the simple approach of massivity factor differentiating lower flange, upper flange and web part leads to safe approach of temperature distribution in cellular beams, when protection is applied on the opening edges.

This last conclusion about the simplified model considering the massivity factor if the flanges and the web has been confirmed by the temperature measurement in the loaded beam.

Mechanical behaviour :

First the numerical thermo-mechanical analysis of the tested loaded beams leads to a very good correlation with the test, confirming the ability of such FEM codes with Eurocode 4 part 1.2 materials properties at high temperature to determine the fire behaviour of cellular beams.

The mode of failure of the cellular beam was the buckling of the web, similarly to the failure mode at ambient temperature.

The load factor from the failure load at ambient temperature is about 0.48 that is equal to the reduction of the effective yield strength at the maximum web temperature calculated (600°C). So it can be thought that a simple approach considering the reduction of the effective yield strength reduction from the load factor could be used for the determining the critical temperature of the beam.

Nevertheless, a single test may not be generalised this simple approach to design of protection thickness to all cellular beams. Developments by calculations and verification on additional tests are necessary to develop a simplified thermal and mechanical model for design of protection thickness of cellular beams.

General :

The development of a more specific simplified method for the design of protection thickness of cellular beams needs more work. This future work should be based in a large part on numerical tools for which the present calculations have again shown their ability to model thermo-mechanical behaviour of steel beams, even if the particular situations (cellular beams) or with specific failure mode (buckling of the web). But it will need additional test to validate it.

3.4 References

- [1] **Eurocode 3 : Design of steel structures - Part 1.1** : General rules and rules for buildings. ENV 1993-1-1. European Committee for Standardisation.
- [2] **Eurocode 3 : Design of steel structures - Annexe N** : Openings in webs. ENV 1993-1-1 : 1992/A2. European Committee for Standardisation.
- [3] **Eurocode 4 : Design of composite steel and concrete structures – Part 1.1** : General rules and rules for buildings. ENV 1994-1-1. European Committee for Standardisation.
- [4] **J. K. Ward**. Design of composite and non-composite cellular beams. SCI Publication n°100.
- [5] **Catalogue ProfilARBED** : Programme de vente, poutrelles, profilés U et cornières. Edition octobre 1995.
- [6] **ARCELOR Cellular Beams** Version 1.33. User's manual. February 2003.

4 Contribution from PROFILARBED-RESEARCH

4.1 Summary

The tasks of PROFILARBED-Research were mainly focused on the WP2 "Improved manufacture of beams with web openings". Nevertheless cellular beams as well as built up sections have been realised in the scope of the different working packages. The 3 different steps can be pointed out:

- ACB ARCELOR Cellular Beams fabrication ;
- Fabrication of the test specimen for the different universities ;
- Improvement of the welding procedures for cellular beams.

4.2 ACB ARCELOR Cellular Beams fabrication

ARCELOR Cellular Beams are rolled reconstituted beams with circular periodic web openings. These beams are produced by oxycutting the web in two passes (one pass consists in a repetitive series of a continuous horizontal line and a half circle line (see Figure 4-1). After having separated them the two half beams are shifted until the 2 straight parts are lined up (see Figure 4-2). The webs between two openings are then welded together.



Figure 4-1: ACB oxycutting



Figure 4-2: ACB reassembling

4.3 Fabrication of the test specimen

During the second project meeting that was held in Paris in February 2002, the final configuration of the beams to test at the University of Luleå in the scope of WP5, at the University of Kaiserslautern for RWTH in the scope of WP1 and at CTICM in the scope of WP3 has been discussed. The final drafts have been sent after this meeting by the different partners to PROFILARBED-Research by March 2002. The beams have been ordered and characterisation tests have been performed in order to know the real steel properties. The beams have been analysed at following specific points (see Figure 4-3).

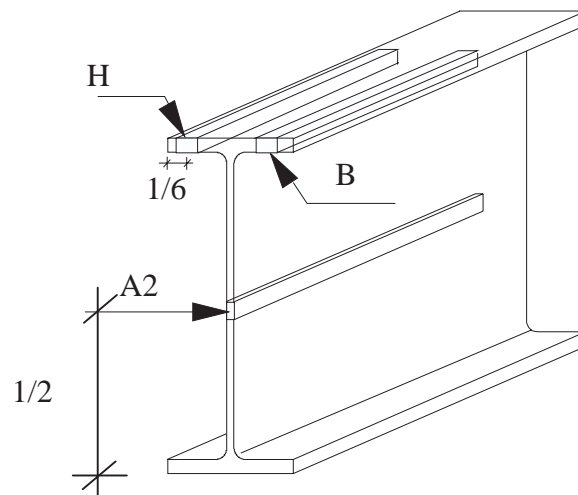


Figure 4-3: Outcut for characterisation

After confirmation of the characterisation results, the beams have been assembled and sent with their certifications to the different partners.

The next figure shows a fabricated specimen for the University of Luleå.

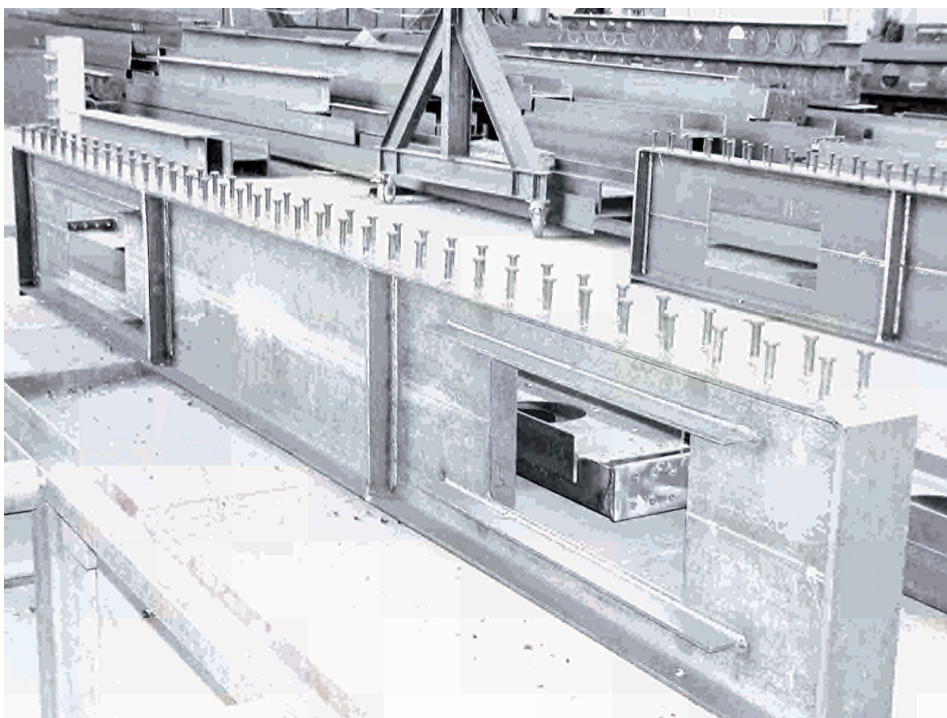


Figure 4-4: Test specimen for the University of Luleå

4.4 Improvement of the welding procedures for cellular beams

4.4.1 Actual assembling procedure for cellular beams

Following the shifting step in chapter 4.2, two configurations are then possible; if the weld throat thickness to apply is less than two times six millimetres $a \leq 2 \times 6\text{mm}$, the chamfering of the two parts to weld isn't necessary. This value represents the upper weld throat thickness limit that can be achieved without chamfering. In case that the weld to apply is more important than two times six millimetres, $a > 2 \times 6\text{mm}$, a chamfering of the two parts to weld isn't avoidable.

In order to simplify the welding procedure, every web post is foreseen with a gap of two millimetres (see Figure 4-5). This allows to start welding without any kind of grinding.

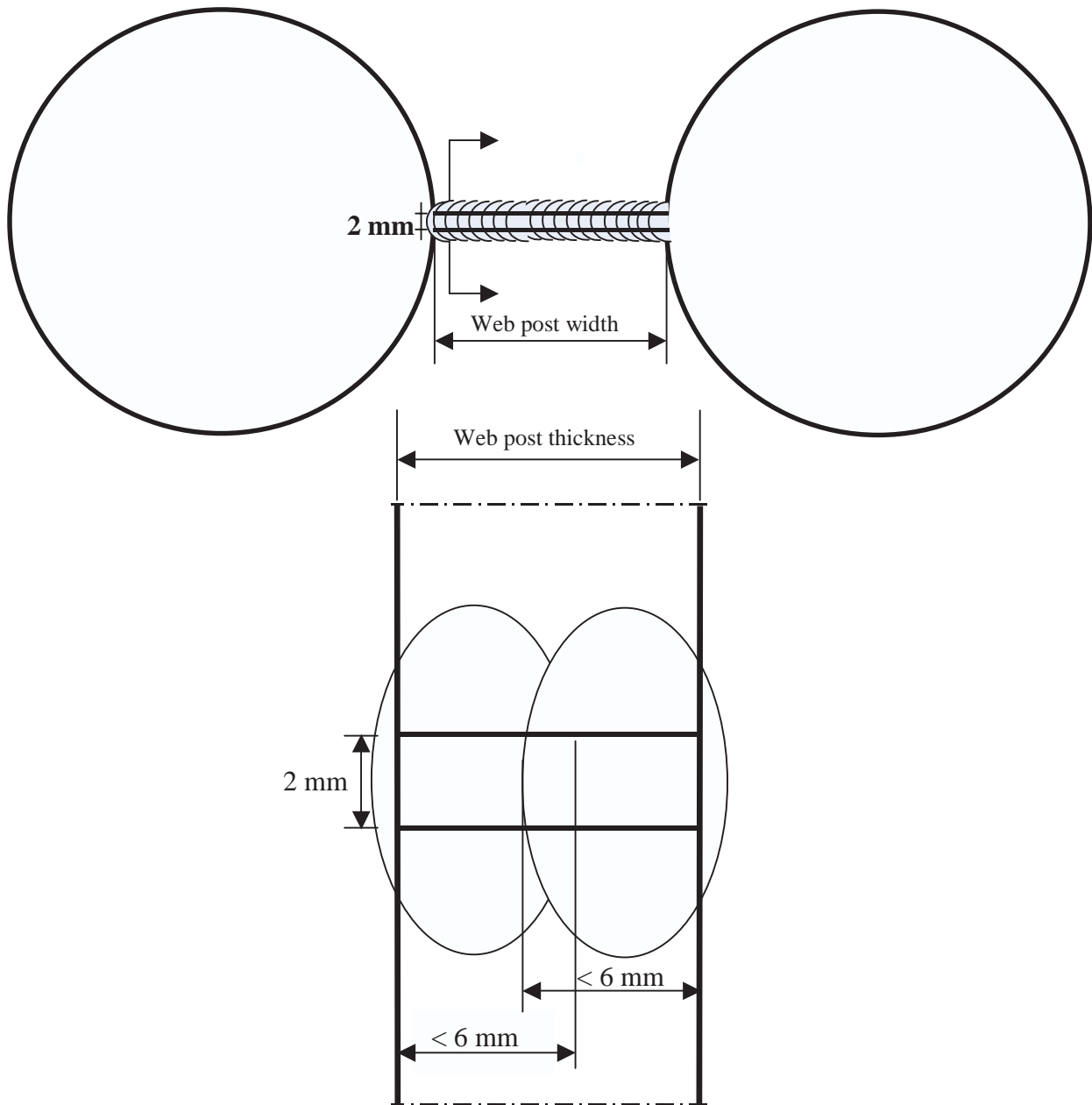


Figure 4-5: Welding of the web post

4.4.2 Small scale tests

4.4.2.1 General

In order to improve the welding procedures for cellular beams, it has been decided to compare the actual welding configurations with new possibilities. The aim is as required into the WP2 to achieve an improved welding procedure for the rewelding of oxycutted beams.

At the beginning only the welds were to be analysed. As real scale prototypes are very expensive, small scale tests have been performed. These tests are resumed in welding two plates together. These plates are supposed to represent the web post.

Different welding procedures, configurations and parameters have been analysed. The goal was to determine the deformation in case of a one side welding after taking away of the restraints.

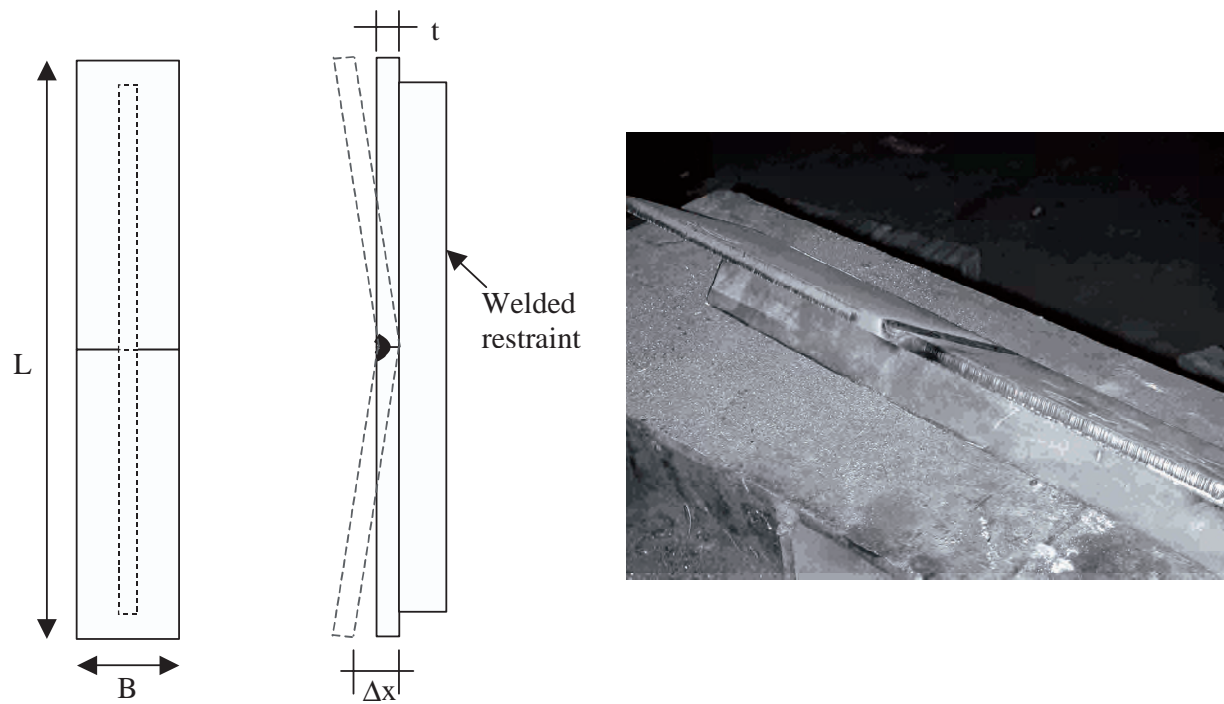


Figure 4-6: Plates with supposed deformation after taking away of the restraint

4.4.2.2 Test configuration and observations

The whole set of the tests had total length of 600mm, a width varying from 60mm to 150mm and a thickness from 8mm to 20mm. These parameters represent the general geometrical web values of cellular beams.

13 specimens have been tested, the deformation Δx (see Figure 4-6) has been measured and a comparison in the welding configuration has been made. A small space between the two plates is foreseen for the specimens, in order to consider the effective oxycutting method for cellular beams as shown in chapter 4.2.

The following shows only a few tested configurations. The results obtained for the whole configuration can be found into the large report under chapter "Small scale tests".

Specimen 2



B x L x t

Dimensions: 150x600x12

Welding on one side **with** chamfering

Welding thickness a = 8mm (3 passes)

$\Delta x = 0$



Specimen 3



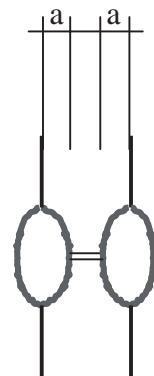
B x L x t

Dimensions: 150x600x12

Welding on two sides **without** chamfering

Welding thickness = 4+4mm (1 pass each)

$\Delta x = 0$



The specimens 2 and 3 which have exactly the same configuration achieving a total weld thickness of 8mm. Two execution configurations are possible:

- a one side welding of 8mm with chamfering avoiding to turn the beam upside down
- two weldings of 4mm (1 pass for each side) avoiding the chamfering which is an annoying step, but with a supplementary manipulation step. The comparison for the welding passes number is increased from 2 to 3 in case of a one side welding. The measured deformation Δx is in both cases equal to 0.

Specimen 9



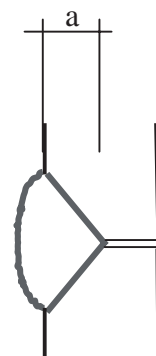
B x L x t

Dimensions: 150x600x20

Welding on one side **with** chamfering

Welding thickness = 10mm (5 passes)

$\Delta x = 2.0\text{mm}$



Specimen 10



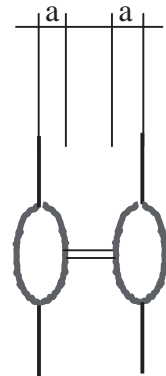
B x L x t

Dimensions: 150x600x20

Welding on two sides **without** chamfering

Welding thickness = 5+5mm (1 pass each)

$\Delta x = 0\text{mm}$



The specimens 9 and 10 have again exactly the same configuration as for specimens 2 and 3. Here again the comparison for the welding passes number is increased from 2 to 5 in case of a one side welding. In this case, a small deformation has been highlighted; a 2.0mm deformation over a length of 300mm corresponding to a slope of 0.67%.

Specimen 11



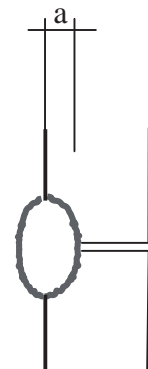
B x L x t

Dimensions: 150x600x20

Welding on one side **without** chamfering

Welding thickness = 5mm (1 pass)

$\Delta x = 3\text{mm}$



For the specimen number 11, a deformation of 3mm has been measured over a length of 300mm corresponding to a slope of 1.0%, which is the maximum highlighted deformation (see Figure 4-7).

Specimen 12



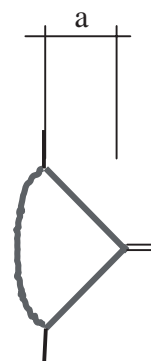
B x L x t

Dimensions: 150x600x20

Welding on one side **with** chamfering

Welding thickness = 16mm (6 passes)

$\Delta x = 1.5\text{mm}$



Specimen 13



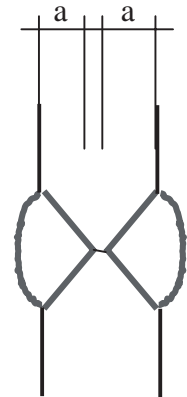
B x L x t

Dimensions: 150x600x20

Welding on two sides **with** chamfering

Welding thickness = 8+8mm (5 passes each)

$\Delta x = 0$



The specimens 12 and 13 have again exactly the same configuration. In this case the comparison of the welding passes number is increased from 6 to 10 in case of a two side welding. The reason is that in both cases, a chamfering has been necessary as the welding thickness is more important than 6mm. A deformation Δx of 1.5mm for specimen 12 corresponding to a slope of 0.5% has been highlighted.

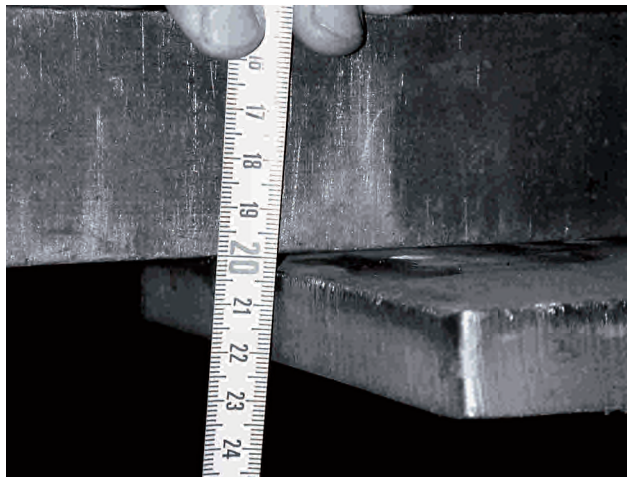


Figure 4-7: Deformation (3mm) after taking away of the restraint for the specimen 11

4.4.2.3 Conclusions

The results show that a deformation occurred for the one side welding specimens only in some cases. The most important deformation has been highlighted for test specimen 11 with 3mm deformation giving a slope of 1.0%. This can be accepted and the conclusion is that a one side welding applied for cellular beams is possible without important deformations.

The esthetical aspect isn't considered until now. Due to the small space that will remain in case of a one side welding on the not welded side (see specimen 11), the fact is that an oxidation could be possible in this zone. The second aspect is: would a person feel insecure in case of standing under a cellular beam that hasn't been welded on one side?

The second goal of this analyse was to have a direct comparison between

- a one side welding with chamfering,
- and a standard 2 sides welding without chamfering but with a supplementary manipulation of the beam.

The first observation is that the chamfering step is to be avoided as it is a very annoying and tiring step for the welder. In second, the welding passes generally increase for a one side welding as the chamfer shape becomes wider with an increasing in depth. This means that more weld material has to be deposited for a one side welding, for example a throat depth of 10mm has a bigger surface compared to a two sides welding with a throat depth of 2 times 5mm.

By the other hand a manipulation step, this means turning the beam upside down one more time, is necessary in case of a two sides welding.

The conclusion is that a two sides welding will be more efficient in case that the welding configuration allows to avoid the chamfering step. This is possible until the welding thickness doesn't exceed 12mm as a two times 6mm weld is possible without chamfer (see specimens 5 and 6). In case that a two sides chamfering is necessary ($a > 6\text{mm}$ for both sides) as it was done for the specimens 12 and 13, a one side welding is usable.

The next step will consist on performing real scale tests with welding thicknesses lower than 2 times 6mm subjected to horizontal shear failure mechanism. The goal will be to prove that there is no failure into the weld itself.

4.4.3 Large scale tests

4.4.3.1 Summary

Following the previous realised small scale welding tests during the year 2002 and according to the explanation of the technical report N°3, it has been decided to perform real scale tests on cellular beams and test different welding configurations in order to optimise the actual procedure. As PROFILARBED itself isn't able to perform such tests, a subcontracting has been requested to the COMMISSION. Here the University of Kaiserslautern has been chosen, as PROF. FELDMANN and his staff have already performed cellular beam tests in the scope of this project for WP1.

The report presents the results of short steel beams with large web openings gained from experimental and numerical investigations. The results were evaluated in terms of load deformation behaviour, failure modes and strain development. The comparison to the available prediction model shows the large safety of the model.

4.4.3.2 Objectives

As explained in the conclusions of the small scale tests (see chapter 4.4.2.3), a two sides welding without weld preparation is more efficient if the welding configuration allows to avoid the chamfering step. This is possible until the welding thickness doesn't exceed 12mm resulting from the consideration that a 2 x 6mm – weld is feasible without chamfer. The objective is to demonstrate that a full penetration should only then be necessary if the calculation method requires it for the throat thickness. A more realistic and economic design approach is to provide a partial penetrated weld being determined to be fully exploited.

In observing the load deformation behaviour, the stress capacity and the reserves of the welds while loading the beam up to failure the task is to validate the method.

4.4.3.3 Background

Although normal practice in the industry has been to require full penetration welds at the web posts, it has been recognised that this full penetration is often not necessary. A consistent standard minimum thickness required by the loading and design is often satisfactory. The requirement for full penetration butt welds can increase significantly the costs of production, thus it should be avoided.

Following the previous performed calculations of the project it has been confirmed that for many geometries, the standard design procedures indicate that other modes of failure intervene before fully penetrated butt welds of the web post fail by horizontal shear. The weld requirements for butt welds are defined by the magnitude of the horizontal shear forces in the web posts.

The minimum throat thickness is calculated considering two continuous welds on a web post with a width w . The minimum throat thickness is calculated as follows:

$$a = \frac{|V_{h,Sd}| \beta_w \sqrt{3}}{2 w f_u / \gamma_{Mw}} \quad (4-1)$$

with

$V_{h,Sd}$ = the acting horizontal solicitation into the web post

β_w and f_u defined as follows:

Table 4-1: Weld throat thickness parameters

Steel grade	S235	S275	S355	S420	S460
f_u (N/mm ²)	340	370	470	520	550
β_w	0,80	0,85	0,90	1,00	1,00

$\gamma_{Mw} = 1.25$ following EC3 Part1.1

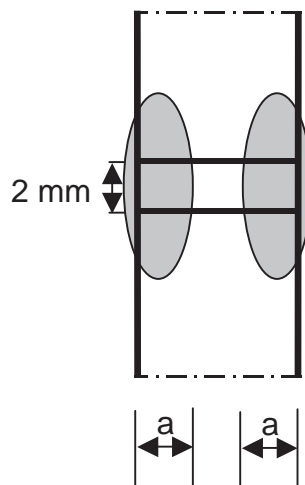


Figure 4-8: Weld throat thickness definition

It is important to recognise however that failure may occur by other mechanisms and limit states before the limiting condition for horizontal shear in the web post is reached.

4.4.3.4 Testing

4.4.3.4.1 Test specimen

Following the different communications that took place between the fabrication shop, the University of Aachen, PROFILARBED-RECHERCHES and the University of Kaiserslautern, a configuration for 10 tests has been defined; the idea is to cover the whole web thickness' range of all available PROFILARBED profiles for cellular beams. Therefore the following solutions have been retained (nominal values). The nominal steel grade is S235 for the whole sections.

The detailed view of the test specimen configuration is given in Annex A of the contribution to Part 2 of this report.

Table 4-2: List of specimens for testing

Specimen n°	Upper profile	Lower profile	Web thick.	Beam depth	Span length	Web post width	Diameter a ₀	w/a ₀ ratio
			[mm]	[mm]	[mm]	[mm]	[mm]	[-]
1-ss	IPE 400	IPE 400	8.6	558,0	1910	122	360	0.34
2-hs	HE 300 A	HE 300 M	8.5/21	477,0	1800	95	350	0.27
3-ss	HE 400 B	HE 400 B	13.5	599,0	1990	63	425	0.15
4-ss	IPE 400	IPE 400	8.6	600,0	1990	55	430	0.13
5-hs	IPE 300	HE 300 M	7.1/21	482,0	1690	55	355	0.15
6-ss	HE 300 M	HE 300 M	21	495,0	1590	50	335	0.15
7-hs	HE 300 B	HE 300 M	11/21	482,0	1870	123	350	0.35
8-hs	HE 300 A	HE 300 B	8.5/11	415,0	1800	147	300	0.49
9-ss	HE 400 B	HE 400 B	13.5	524,0	1846	150	310	0.48
10-ss	HE 300 M	HE 300 M	21	462,0	1800	147	300	0.49

ss corresponds to symmetric section; hs corresponds to hybrid section

To ensure proper load introduction for supports and centre-load, introduction stiffeners are applied across the total depth of the beam.

As mentioned two failure modes can occur: web post buckling and shear failure in weld. These failure modes occur to different load levels and at different locations. For this reason one half of the beam was stiffened such that the web post should not buckle any more and thus failure due to excessive plastic strains can develop (see Figure 4-9 that shows a photo of a specimen during testing).

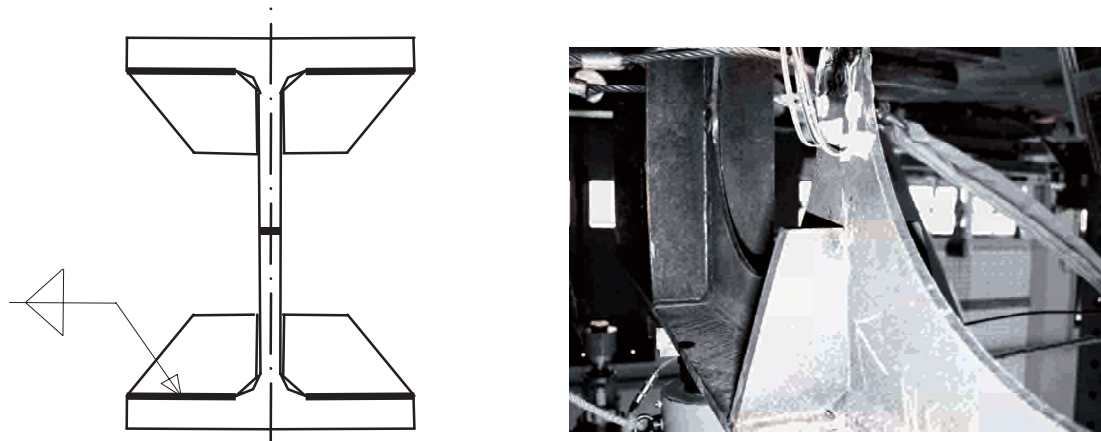


Figure 4-9: Web post stiffeners

The dimensions of the stiffeners depend on the prevailing profile. The thickness of all stiffeners is constant with 20mm. The stiffeners are only welded at the flange (and not at the web) such that a lateral support of the web will be created without having an in-plane constraint in the web.

4.4.3.4.2 Test setup and test procedure

The statical system was a single-span beam under three point bending, both ends were simply supported so that the system was statically determinated, (see Figure 4-10). A concentrated load was introduced by a hydraulic jack onto the top flange in the middle of the beam.

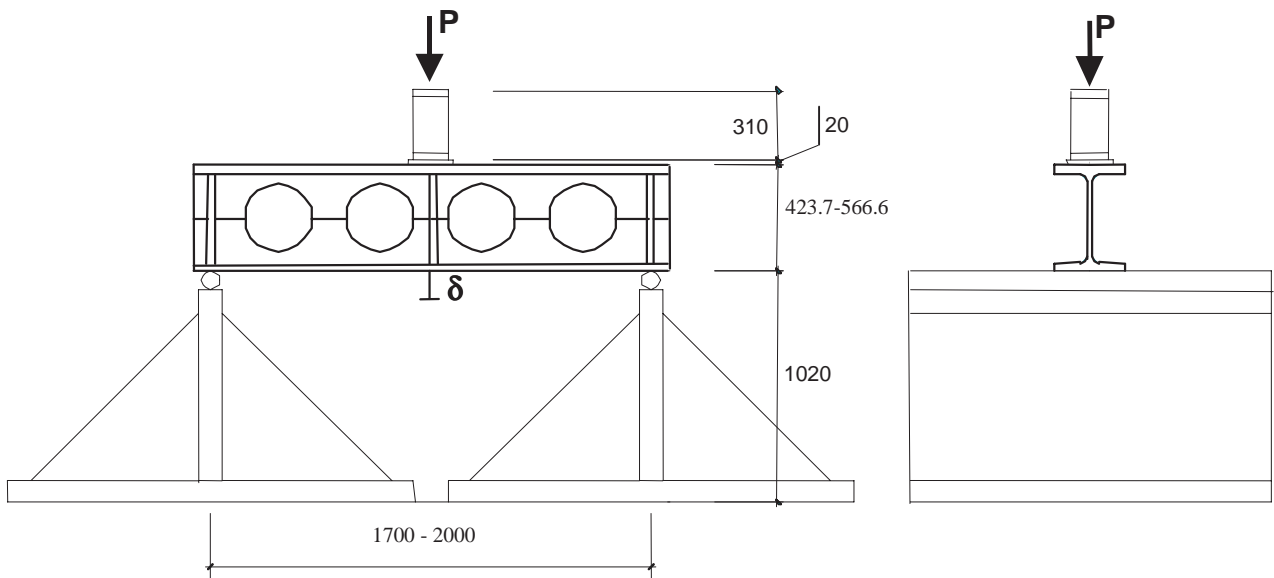


Figure 4-10: Test arrangement

The load application was deformation – controlled by a low displacement rate. Furtheron the load was applied stepwise by holding the displacement at these steps to record the load relaxation – effects. The tests were performed until not only the maximum load has been reached but also a sufficient branch of the descending load deformation curve has been recorded.

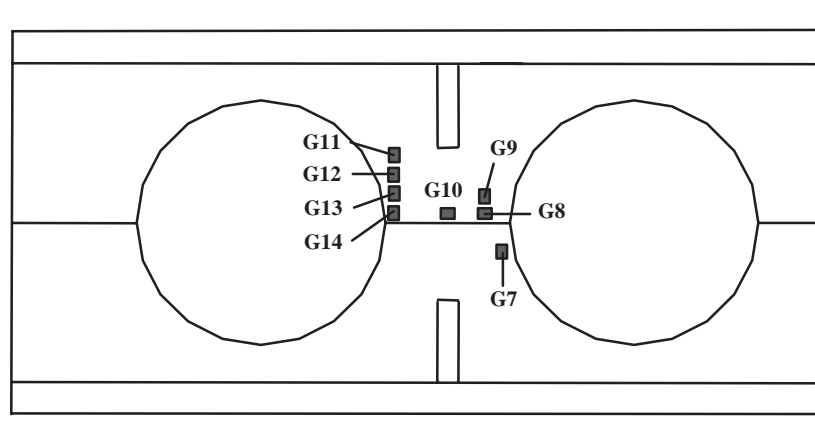
The complete test arrangement and loading data are given in Annex A of the contribution to Part 2 of this report.

4.4.3.5 Measurement Devices

4.4.3.5.1 Strain Gauges

Strain gauges are located on both halves of the beam and on both sides of the web. It was intended to gain most exact overview of the strain distribution in the web post. The exact position can be taken from the following drawings.

Forefront



Back-side

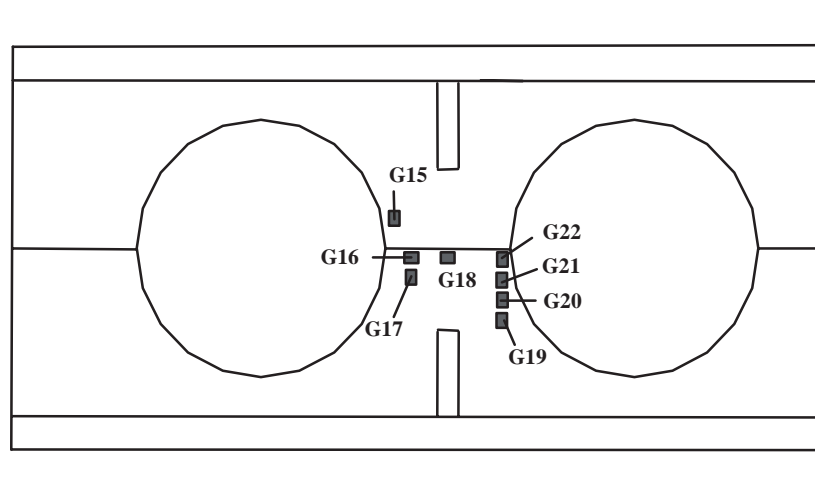


Figure 4-11: Strain gauge distribution

The four vertical gauges in vertical line are arranged to observe the influence of the weld geometry on the stress distribution. The gauges G7 and G21 as well as G13 and G15 are at the same position from the weld to control the results of the gauges of the other side of the weld. By means of the rosettes G10 and G18 the two – dimensional stress-state can be fully recorded and thus the shear stress can be determined.

4.4.3.5.2 Displacement Transducers

To measure the vertical deflection of the beams three inductive displacement transducers have been used. They are positioned underneath each web post in the middle of the lower flange. The range of each transducer was $\pm 50\text{mm}$, see Figure 4-12.

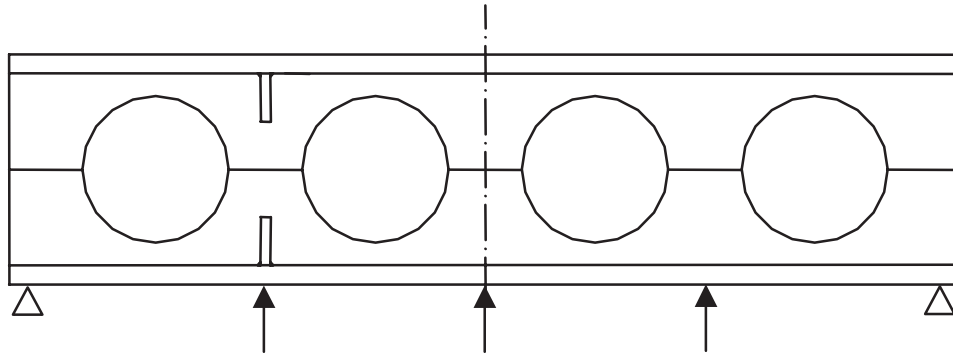


Figure 4-12: Displacement Transducers

4.4.3.6 Test results

As agreed between both parts only eight specimen were carried out including all hybrid beams. Instead of both tests, not foreseen F.E. simulations were carried out for the whole configuration. In the following the plain data obtained from the experiments are given.

4.4.3.6.1 Actual dimensions

In Table 4-3 the actual measured dimensions of the test specimen are given.

Table 4-3: Actual dimensions of specimen

Specimen n°	Upper Profile	Lower Profile	Span Length [mm]	Total Depth [mm]	Web post width [mm]	Opening Diameter [mm]
1-ss	IPE 400	IPE 400	1897	558	122	358
2-hs	HEA 300	HEM 300	1800	475	95	350
3-ss	HEB 400	HEB 400	1940	599	63	422
4-ss	IPE 400	IPE 400	1944	600	55	430
5-hs	IPE 300	HEM 300	1644	482	55	354
6-ss	HEM 300	HEM 300	1559	495	50	334
7-hs	HEB 300	HEM 300	1866	472	123	350
8-hs	HEA 300	HEB 300	1800	415	147	300

4.4.3.6.2 ACB design results with actual dimensions

Following the design calculations performed with ACB, although considering the real geometrical and mechanical properties, the failure load as well as the weld throat thickness have been determined for the different configurations. The theoretical failure occurs by web post buckling for all cases, except for test 8 where a Vierendeel mechanism should occur. The theoretical second failure mechanism is the horizontal shear failure. Following the 1st failure mode, the minimum throat thickness has been calculated according to equation (4-1), see Table 4-4.

Table 4-4: Theoretical failure load and throat thickness values

Specimen n ^o	Upper part of the profile	Lower part of the profile	Theoretical web post buckling failure load [*] [kN]	Theoretical Horizontal shear failure load [*] [kN]	Calculated minimum weld throat thickness for the 1 st failure mode [mm]	Theoretical applied weld throat thickness a [mm]	Measured average weld throat thickness a [mm]
1-ss	IPE400	IPE400	357	465	2.8 ^{**}	3.0	3.3
2-hs	HE300A	HE300M	245	320	2.7 ^{**}	3.0	4.2
3-ss	HE400B	HE400B	260	390	3.7	4.0	4.5
4-ss	IPE400	IPE400	138	227	2.2 ^{**}	3.0	3.2
5-hs	IPE300	HE300M	110	169	1.9 ^{**}	3.0	3.9
6-ss	HE300M	HE300M	331	486	5.9	6.0	6.0
7-hs	HE300B	HE300M	417	507	3.7	4.0	4.8
8-hs	HE300A	HE300B	249 ^{Vierendeel}	436	2.0 ^{**}	3.0	4.1

* According to ACB-software

** According to EC3, a minimum throat thickness of 3.0mm has been retained

4.4.3.6.3 Macrography

After having performed the tests, small pieces of the web post have been cut out in order to perform macrographies and determine the real weld throat thickness. Both welds have been measured and the average value has been retained.

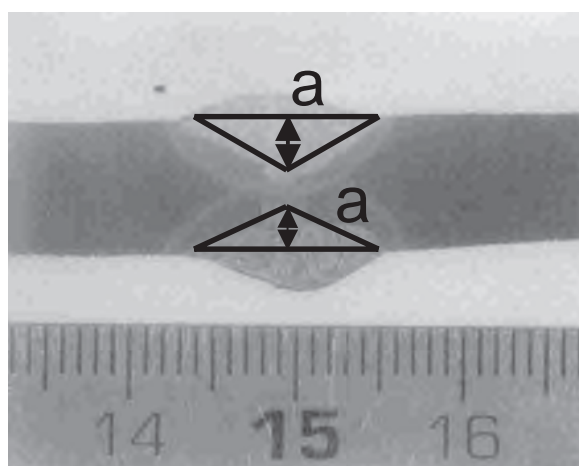


Figure 4-13: Specimen 1

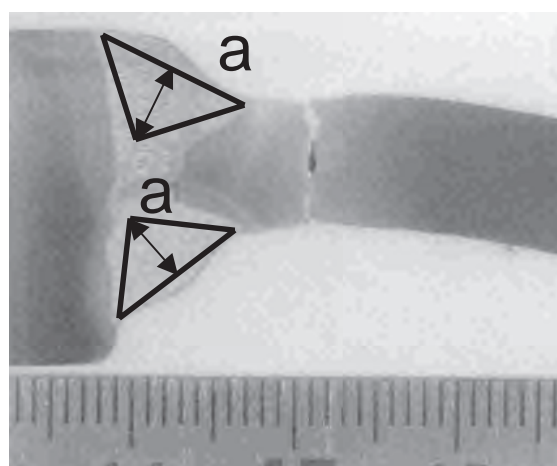


Figure 4-14: Specimen 2

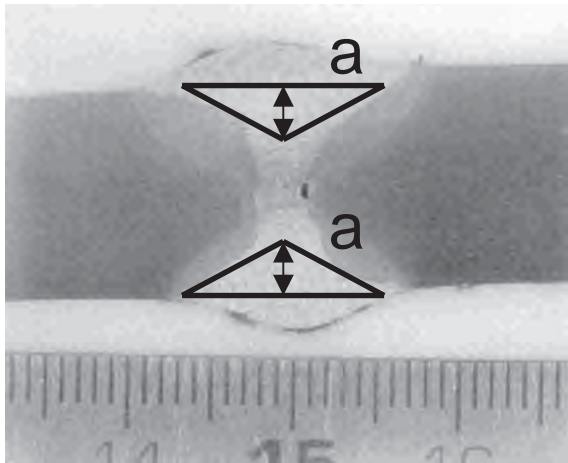


Figure 4-15: Specimen 3

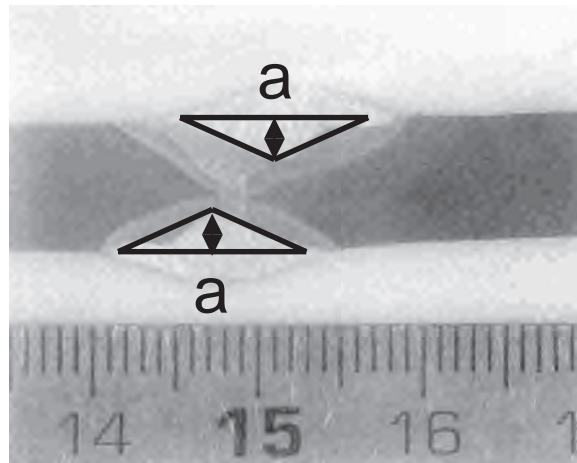


Figure 4-16: Specimen 4

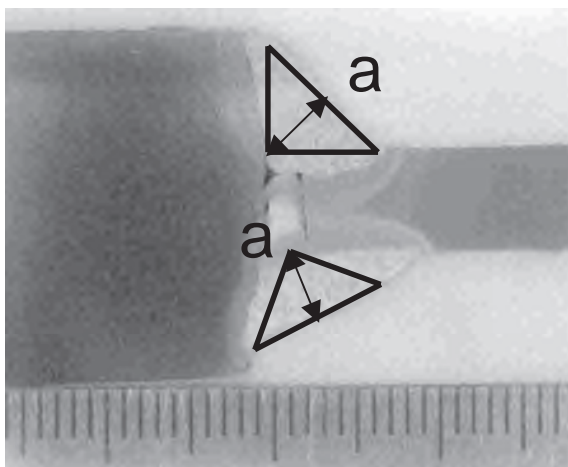


Figure 4-17: Specimen 5

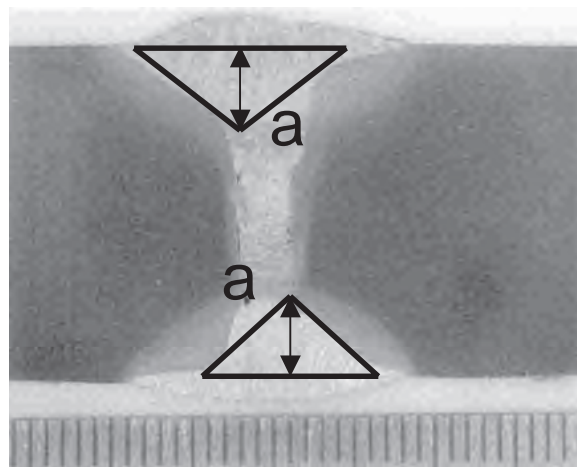


Figure 4-18: Specimen 6

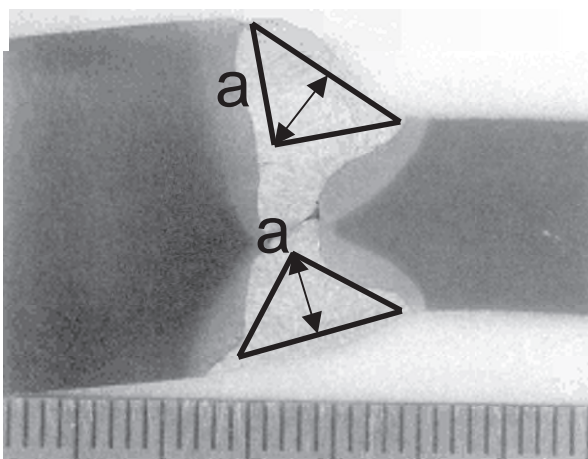


Figure 4-19: Specimen 7

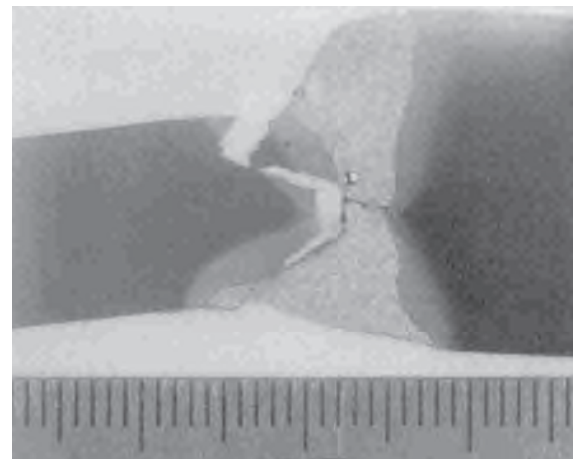


Figure 4-20: Specimen 7 with weld failure

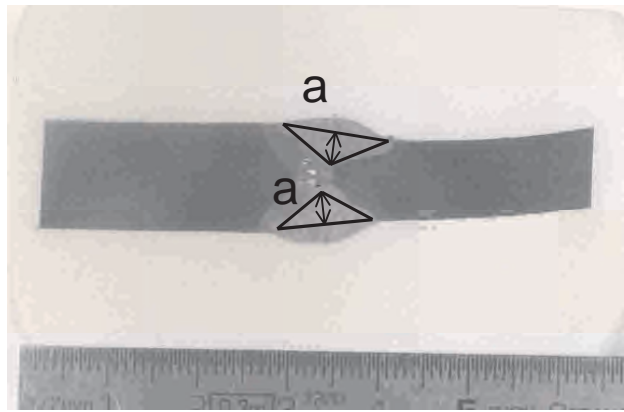


Figure 4-21: Specimen 8

4.4.3.6.4 Failure loads and mechanisms

In the following Table 4.5 the designed (= theoretical by ACB-software) limit loads and the measured limit loads are given.

Table 4.5: Failure loads and mechanisms

Specimen n°	as designed (= theoretical, see Table 4-4):		as observed:				$F_{u,i,ex} / F_{u,i,th}$
	$F_{u,1,th}$ [kN]	$F_{u,2,th}$ [kN]	$F_{u,1,ex}$ [kN]	1. Failure Mechanism	$F_{u,2,ex}$ [kN]	2. Failure Mechanism	
1-ss	357	465	500	WPB of the unstiffened post	537	WPB of the stiffened post	1.50
2-hs	245	320	660 ¹⁾	LSF at the unstiffened side	-	-	2.06
3-ss	260	390	627	WPB of the stiffened post	-	-	2.41
4-ss	138	227	252	WPB of the unstiffened post	264	WPB of the stiffened post	1.91
5-hs	110	169	393	WPB of the stiffened post	-	-	3.57
6-ss	331	486	971	Stop of the test due to reaching of the limit load of the dynamometer → no failure			-
7-hs	417	507	905 ²⁾	LSF at the stiffened side	-	-	1.78
8-hs	249	436	685	WPB of the stiffened post	-	-	2.75

¹⁾The maximum load was reached at 660 kN, the failure occurred in the descending load deformation curve at 606 kN.

²⁾The maximum load was reached at 905 kN, the failure occurred in the descending load deformation curve at 880 kN.

With $F_{u,1,th}$ = designed limit load for web post buckling (WPB)

$F_{u,2,th}$ = designed limit load for longitudinal shear failure (LSF)

$F_{u,1,ex}$ = Load at which the first failure mechanism in the test occurred

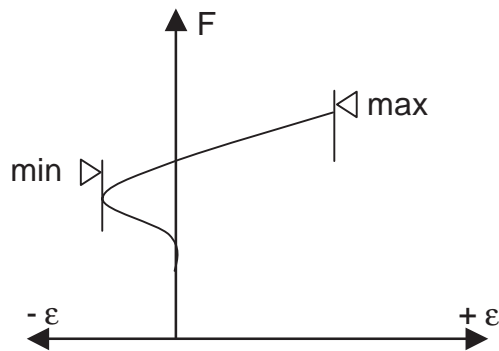
$F_{u,2,ex}$ = Load at which the second failure mechanism in the test occurred

Some explanations and the reasons for the big (safe-sided) differences of the theoretical and experimental loads are indicated under chapter 4.4.3.8 “Conclusions”.

4.4.3.6.5 Strains

4.4.3.6.5.1 Strains in the midpoint of the web post

The characteristic (typical) load-strain development in the centre of the web post is given in Figure 4-22.



Three phases can be distinguished:

1. linear load strain behaviour within a range of +/- 100 $\mu\text{m}/\text{m}$
2. increasing negative strains
3. reversal and increasing positive strains

Figure 4-22: Characteristic load-strain development

Rough interpretation of this behaviour can be the following:

Phase 1: linear elastic behaviour according to theory, no normal strains occur

Phase 2: change to plasticity and in-plane membrane effects lead to a developing of normal strains

Phase 3: Overlaying of instability effects such as local buckling and change of sign of the strains can finally occur.

Vertical strains

The results of the gauges G2 and G5 on the unstiffened half and gauges G10 and G18 (vertical part of the rosette) on the stiffened half are given in Table 4-6 (in [$\mu\text{m}/\text{m}$]).

Table 4-6: Vertical strains in the midpoint of the web

Specimen n°	G2 (upper profile)		G5 (lower profile)		G10 (upper profile)		G18 (lower profile)	
	min ϵ	max ϵ	min ϵ	max ϵ	min ϵ	max ϵ	min ϵ	max ϵ
1-ss	0	2781	-202	1303	-1724	0	0	1343
2-hs	-112	5413	defect		0	6576	defect	
3-ss	-479	4835	-690	886	-1044	7409	0	7984
4-ss	-1278	0	-189	0	-506	379	0	649
5-hs	0	5292	0	896	-2133	1580	0	397
6-ss	-2641	6611	-2239	4816	-1677	6259	-1379	3024
8-hs	0	5524	-538	4094	-1746	1639	-211	8065

Horizontal strains

The measured strains of the gauges G1 and G4 on the unstiffened half and gauges G10 and G18 (horizontal part of the rosette) on the stiffened half are given in Table 4-7 (in [$\mu\text{m}/\text{m}$]).

Table 4-7: Horizontal strains in the midpoint of the web

Specimen n°	G1 (upper profile)		G4 (lower profile)		G10 (upper profile)		G18 (lower profile)	
	min ϵ	max ϵ	min ϵ	max ϵ	min ϵ	max ϵ	min ϵ	max ϵ
1-ss	-914	0	-689	1085	-1421	0	-854	0
2-hs	-1728	1829	-582	0	defect		-2098	434
3-ss	-376	1442	-435	674	-359	675	-1269	470
4-ss	-544	297	0	635	0	1402	-816	156
5-hs	-218	2887	-521	0	0	5164	-770	0
6-ss	0	2494	-427	3351	0	5813	0	2779
8-hs	-1928	1047	-1254	434	0	4869	-2301	0

The corresponding load strain diagrams are given in Annex B of the contribution to Part 2 of this report.

Some explanations of the strain development are given in chapter 4.4.3.8.

4.4.3.6.5.2 Strains at the edge of the web post

The strain development at the edge of the web post is characterised by a slow linear increase over 50-70 per cent of the limit load, a sharp bend with a following excessive strain increase.

Vertical strains

The results of the gauges G3 and G6 on the unstiffened half and gauges G14 and G22 on the stiffened half are given in Table 4-8 (in [$\mu\text{m}/\text{m}$]).

Table 4-8: Vertical strains at the edge of the web

Specimen n°	G3 (lower profile)		G6 (upper profile)		G14 (upper profile)		G22 (lower profile)	
	max $ \epsilon $		max $ \epsilon $		max $ \epsilon $		max $ \epsilon $	
1-ss	7151		6820		17578		21537	
2-hs	-1699		6351		10087		15989	
3-ss	defect		7636		4477		5217	
4-ss	1926		1828		3057		1625	
5-hs	3762		-4041		2028		1513	
6-ss	defect		-5307		-		-	
7-hs	-		-		19397		19798	
8-hs	-2128		3564		9878		19463	

The corresponding load strain diagrams are given in Annex B of the contribution to Part 2 of this report.

Some explanations of the strain development are given in chapter 4.4.3.8 .

4.4.3.7 Finite Element Analysis (FEA)

For the verification of the test results and for clarifying the internal forces (in particular in the horizontal weld) a finite element analysis was carried out using the FE-program ANSYS, version 7.0. Meshing and particular parameters can be taken from Annex D of the contribution to Part 2 of this report.

In the following figure (Figure 4-23) the stresses due to a unit load according to the first critical mode are given as a representative for the imperfection model of the FEA. It becomes clear that the buckling behaviour of the web post can be simulated fairly exact.

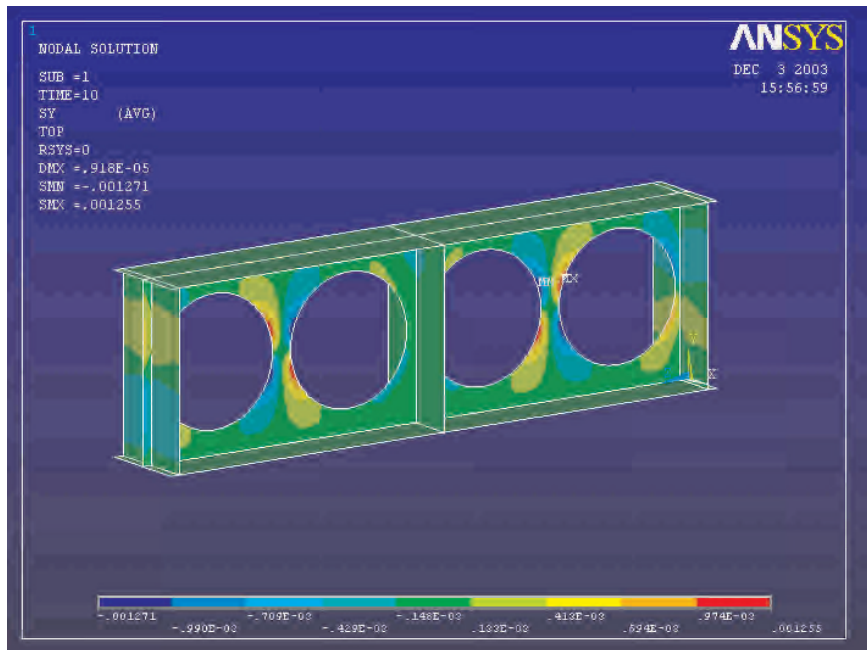


Figure 4-23: Imperfection acc. to first critical mode

The nonlinear buckling analysis was carried out using the following assumptions:

- Use of 4 nodes shell element with quadratic deformation approach.
- Big distortion approach.
- Geometrically as well as materially non-linear calculation.
- Solver by iterations according to Newton-Raphson.
- Ideal elasto-plastic material behaviour using actual (measured) values.
- The full (real) stress – strain curve was not included. The error that was induced by this simplification however is negligible.
- The beam geometry is based on the measured dimensions of tested beams.
- The little stiffeners at the outer web post are not considered.
- The imperfection of the web is based on the first critical mode (eigenvalue) that was obtained from a linear buckling analysis in a first step, see Figure 4-23.
- The load is applied stepwise on one node in the middle of the upper flange.
- The influence of meshing and its refinement has been tested out in advance, such that the presented FE-results can be regarded as consolidated.

Table 4-9: Results of the FEA

Specimen n°	Limit load [kN]			Max shear force in the weld V_h [kN]			Failure mode
	ACB	Test	ANSYS	ACB*	ANSYS	ANSYS**	
1-ss	357	500	480	195	184	157	Web post buckling
2-hs	245	606	565	193	242	145	Web post buckling
3-ss	260	627	623	137	120	98	Web post buckling
4-ss	138	252	261	85	61	51	Web post buckling
5-hs	110	393	340	104	114	62	Web post buckling
6-ss	331	971	1072	145	147	105	Web post buckling
7-hs	417	905	815	285	363	249	Web post buckling
8-hs	249	685	601	291	321	144	Web post buckling

* according to the first failure mode for ACB, according to eq.(4-1) and using actual dimensions (see Table 4-4), and material properties

** at the ACB limit load

To show the good congruence of the global beam behaviour between the FEA and the real tests one of the load-deflection-curve is compared in the following.

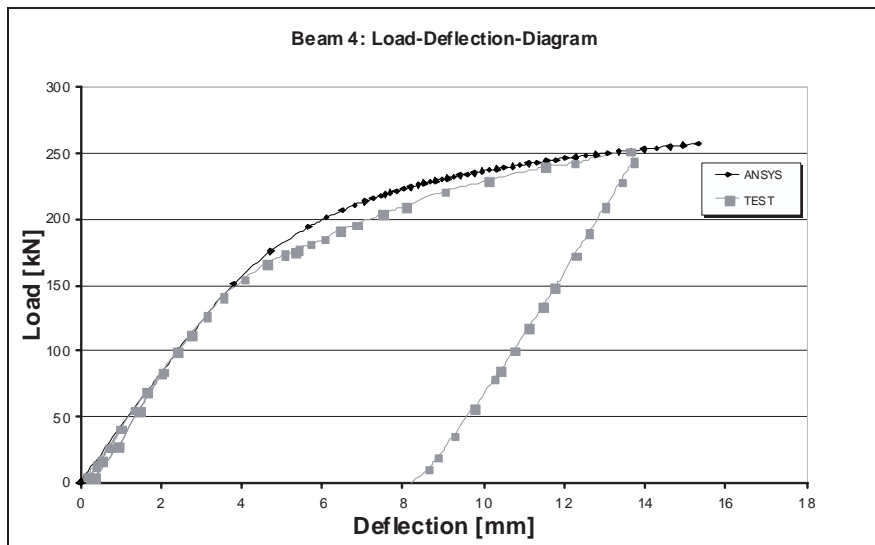


Figure 4-24: Load-Deflection Diagram (Beam 4)

Further FE-results are given in Annex D of the contribution to Part 2 of this report.

From the comparison between the maximum shear force in the weld at ACB load level obtained by FE-calculations and the design shear force at the first instability mode obtained by ACB-software it can be seen that the horizontal acting loads predicted are greater than in the simulated reality.

Therefore the resulting weld-dimensions will be overestimated. Consequently the welds can be minimized and performed mostly without chamfering if the weld throat thickness to apply is less than two times six millimetres $a \leq 2 \times 6\text{mm}$.

4.4.3.8 Conclusions

The load-deformation behaviour of short beams with large web openings has been investigated. In particular the welds of the web posts along the neutral axis have been thoroughly considered by means of experiments and Finite Element simulations. The research results have been compared to the results from the ACB-software. Furthermore very important conclusions for the preparation, design and dimension of the welds could be drawn.

From the experiments it came out, that in all cases the obtained experimental ultimate load exceeded the predicted loads. This shows the safe sided approach of cellular beams behaviour and the reserves into the welds that are available before failure occurs. Although having reached the horizontal plateau into the load deflection curve (see Annex B of the contribution to Part 2 of this report and chapter 4.4.3.7), meaning that all redistribution mechanism has been activated and that the welding thickness corresponding to the 1st redistribution mechanism has been exceeded by far, only one horizontal shear failure into the weld itself (test 7) could be provoked, in test 2, a failure into the base material occurred .

As far as the welds are concerned it can be noted that predicted shear stress values by ACB-software are safe sided higher as the calculated ones from the simulations. Together with the experiments it can be considered, that the theoretical shear stresses and as result of the calculated weld throat thicknesses are overestimated, taking into account the whole stress state at the weld in longitudinal direction and perpendicular to the weld. So the model used in the ACB software for the prediction of the weld throat thickness is on the safe side and it reproduces the behaviour with an acceptable reliability. In many cases a full penetration weld is not necessary. Even chamfering can be avoided in a lot of cases.

It should be pointed out again that the weld throat thicknesses determined by the means of ACB correspond to the stress level at the first theoretical instability mode. Therefore the effects of the further developing redistribution mechanism and their complexity are not considered for the determination of the theoretical weld throat thickness by ACB.

5 Contribution from SCI

This section summarises the activities of the Steel Construction Institute (SCI) in the ECSC project 7210-PR-315 entitled “Large Web Openings for Service Integration in Composite Floors” for the period 1 July 2001 to 31 December 2003.

In the framework of this project, SCI has focused its efforts in developing design guidance and software. An overview of the work is given below, which describes the following:

1. A summary of the results of a series of Finite Element Analyses (FEA) of cellular beams comprising regular circular openings in which the openings were placed non-centrally in the beam depth, and unequal web areas for the top and bottom Tees.
2. A generalised design method that may be applied to hot rolled and fabricated steel sections, and to beams with discrete and regular circular openings.
3. The back-analyses of eight Arcelor tests on cellular beams for both symmetric and asymmetric cross-sections, which demonstrate the level of accuracy inherent within the proposed design guidance.
4. A full account of the engineering logic used in the design software for the purpose of representing and testing the proposed design guidance.

5.1 Finite Element analysis of web post buckling

The results of a series of Finite Element Analyses (FEA) were collated for a cellular beam with equally spaced circular openings. The beam was analysed as a cantilever in order to examine the shear transfer around the opening and through the web-post between the openings. The FEA was carried out using ANSYS, a generalised FEA program. The openings were 60% of the depth of the beam and were placed at 1.25 , 1.5 and $1.8 \times$ opening diameter (centre-centre) along the beam.

Three cases of asymmetry were considered:

- Centrally placed openings in the beam depth.
- Non-centrally placed openings (ratio of depth of Tees of 3 : 1).
- As the cases above, but with different web thicknesses of the top and bottom Tees (ratio of thicknesses of 2 : 1).

The FEA considered plasticity, buckling of the web-post, and other failure modes, dependent on the geometry of the cross section and opening. The following conclusions were drawn from this study:

- The effect of asymmetry of opening position makes a small effect on the failure load (by 2 to 10%).
- The effect of differential web thickness is beneficial and increases the failure load when compared to a section of uniform thickness. The level of shear utilisation is similar in all cases of the same web-post width.
- The level of horizontal shear utilisation exceeds 1.0 for some asymmetric openings with differential web thickness indicating a highly complex stress state. The current design approach is conservative for asymmetric sections.
- Web-posts of width of $0.8 \times$ opening diameter do not fail by web-post buckling or horizontal shear.
- Ring stiffened openings increase the buckling resistance of the web-post, but the effect diminishes for alternate ring stiffened openings with wider web-posts.

Based on these FEA results, a simplified theory of web-post bending has been proposed, which may be combined with horizontal shear to assess the buckling resistance of the web-post. An alternative

compression field or ‘strut’ model is also proposed, in which compression and bending in the web-post may be combined.

It is concluded that the effect of asymmetry in opening position and web thickness is not as critical as first thought, and the tendency for web-post buckling is not increased significantly.

5.2 Design guidance for composite beams with large openings for services

The design of composite beams with large rectangular or circular openings is a practical problem which is caused by the need to pass service ducts through the structural zone of the beams. Careful sizing and positioning of these openings can minimise their adverse effects on the shear and bending resistances of composite beams. The design guidance extends that given in SCI P068 [1] and P100 [2], and presents a generalised design method that may be applied to hot rolled and fabricated steel sections, and to beams with discrete and regular circular openings.

The new aspects of the design approach that are covered in detail are: bending and tension interaction effects in the bottom ‘Tee’ of the section; treatment of highly asymmetric sections; and local composite effects at large openings. A step-by-step design procedure is presented, which is consistent with BS 5950-1 and -3 and with Eurocodes 3-1 and 4-1.

General guidance on positioning of openings is presented. The same general principles may also be extended to notched beams and to tapered beams.

Large openings cause a significant reduction in the shear resistance of beams, due to the loss of a major proportion of the web but a smaller reduction in bending resistance. Therefore, the shear transfer across large openings is the most important design requirement, and it is good practice to locate large openings remote from the high shear zones of a beam in order to minimise their effect.

Shear transfer occurs by Vierendeel or ‘four corner’ bending in the web flange ‘Tee’ sections, which leads to a complex interaction of forces at the corners of the opening. Horizontal stiffeners improve the transfer of shear by this local bending action.

Fabricated beams may also have slender webs, which may require stiffening to prevent buckling of the web close to the opening. However, the use of stiffening should be minimised by choosing a thicker web to avoid vertical stiffeners, or by careful positioning of the openings away from point loads.

5.2.1 Existing publications

SCI Publication 068 ‘Design of openings in the webs’[1] was prepared in 1988 to present a design method for discrete openings in hot rolled steel beams in composite construction. The methodology was calibrated against tests on a 10 m span composite beams carried out at the University of Warwick. These tests used $533 \times 210 \times 82$ kg/m UB sections ($d/t \approx 50$) with a range of opening sizes of 700×350 , 600×200 and 450×250 , and 350 mm square.

SCI Publication 100 ‘Design of composite and non composite cellular beams’[2] was prepared in 1990 to extend the design methodology to cover beams with regular circular openings. The new aspect of SCI P100 was the design method for the interaction of forces between adjacent openings and its effect on the stability of the web post.

Modern design and construction of composite beams with web openings differs in important respects from the scope of SCI P068 and P100, and from the data base of existing tests:

- The steel sections are often highly asymmetric in terms of their flange area.
- The webs are often relatively slender, so that the effect of buckling is increased.
- Openings are relatively long in terms of their aspect ratio (length : depth).
- Openings may be asymmetric in the depth of the section and are often close to the flanges.

- Elongated openings can be formed by removing the web post between adjacent circular openings.
- Deep beams may be used as ‘transfer’ structures supporting columns or heavy loads, and can be perforated for doors or large ducts from plant rooms.

These changes in practice have necessitated a re appraisal of these existing publications, so that they can be extended to cover a greater range of applications to both hot rolled and fabricated steel sections. However, general structural design principles should be observed for unusual design cases, and it is not possible to give definitive guidance for all cases. This is particularly true for fabricated sections, where some stiffening is generally required to resist local forces and to control the effects of buckling.

5.2.2 Scope of publication

The guidance offered in SCI P068 and P100 has been extended for both hot rolled and fabricated sections. The design method is common to all these applications and differs only in:

- The depth of web that is used in the definition of the shear area to BS 5950-1.
- The classification of the cross section for local buckling.
- The control of web buckling by use of stiffeners.

SCI P068 is still valid for hot rolled steel beams with discrete openings, and SCI P100 is still valid for cellular beams of approximately symmetric cross section. However, the scope of new design guidance has been generalised to cover the cases of:

- Highly asymmetric sections.
- Openings placed non centrally in the depth of the section.
- Slender webs.
- Narrow web posts.
- Fabricated sections.
- Notched beams.

The publication does not cover:

- Tapered fabricated sections.
- Fire engineering design.

A worked example, is provided which illustrates the use of these methods.

5.2.3 Design codes

This guidance is prepared in general analysis terms and cross refers to BS 5950-1 and -3, and Eurocode 3-1-1 and Eurocode 4-1-1, as appropriate. The principal difference between these design codes is in terms of the partial factors for loads and materials. However, some other limits exist regarding partial shear connection and shear connection resistances.

Both codes are expressed in terms of limit state principles.

5.2.4 Material strengths

The strength of steel is expressed in terms of its yield strength in N/mm^2 (f_y to EC3 1-1 or p_y to BS 5950-1). Standard grades are S275 and S355. A partial factor of 1.0 applies to steel.

The strength of concrete is expressed in terms of its cube strength, f_{cu} , to BS 5950-3, or its cylinder strength, f_{ck} , to EC4 1-1. The design strength of concrete is given by $0.45 f_{cu}$ or $0.85 f_{ck} / \gamma_c$, respectively according to the two codes γ_c is the partial strength for concrete ($\gamma_c = 1.5$). The highest concrete grade that may be used in composite design is C40/50.

The shear resistance of the shear connectors is dependant also on the concrete grade. The design resistance is taken as $0.8 \times$ characteristic resistance (the 0.8 factor representing the inverse of a partial safety factor of 1.25). A further reduction in resistance may be required due to the shape of the deck profile and for the use of lightweight concrete (LWAC).

For cases when LWAC is used, the stud strength should be multiplied by 0.9 in accordance with BS 5950-3. Whereas for EC4-1-1 the secant modulus, E_{cM} should be multiplied by $(\rho/2200)^2$ in accordance with EC2-1-1 (where ρ is the dry density of concrete in kg/m^3).

5.3 ARCELOR web post buckling tests

The following tables present the analysis of eight Arcelor tests on Cellular beams for both symmetric and asymmetric cross-sections. Most beams failed by web-post buckling or Vierendeel bending often at large displacements. The web-post buckling analysis is based on the models in the Design Guide. The Model Factor defines the conservatism that exists in the analysis model. *.pdf documents from software analysis of Tests 1, 3 & 4 have been created, see contribution to Part 2 of this report.

5.3.1 Symmetric Beams

Tests 1, 3 and 4 failed by web-post buckling. The model factor for these tests exceeds 1.0 by a significant margin, indicating that the design model is conservative; particularly for narrow web-posts. Test 6 failure by plastic deformation, involving some 'tension field' action in the web-posts.

Table 5-1: Model factors for symmetric beams

Test	Beam	$\bar{\lambda}$	V_{test} kN	V_h kN	$V_{h,Rd}$ kN	Model factor	Failure mode
1	IPE 400	0.95	268	240	197	1.23	Web-post buckling
3	HEB 400	0.72	313	269	172 [×]	1.73	Web-post buckling
4	IPE 400	1.14	132	110	77	1.54	Web-post buckling
6	HEM 300	0.38	350 [*]	311	233 [*]	1.33	Web-post shear/rotation

Assumed yield strength = $350 N/mm^2$

$\bar{\lambda}$ effective slenderness of web-post

V_h is horizontal shear in web-post

$V_{h,Rd}$ is web-post shear or buckling resistance

* failure load taken at point of plasticity in test

× failure based on pure shear of web post

5.3.2 Asymmetric Beams

Tests 2, 5 and 7 failed by Vierendeel bending of the top Tee at the opening together with web-post buckling or shear. The distribution of shear between the top and bottom Tees is unknown, and the difference between the shear forces in the Tees determines the moment developed in the web-post for equilibrium between the Tees.

An upper bound to the shear force in the top Tee is its Vierendeel bending resistance or its shear resistance. The Vierendeel bending resistance is calculated for an effective opening width of $0.45 d_o$ and opening height of $0.9 d_o$ (d_o = opening diameter). The remaining shear force is resisted by the bottom Tee. The web-post moment M_h is calculated from equilibrium, and is generally higher than the elastic bending resistance of the web-post $M_{h,el}$. This indicates that plasticity or tension yielding develops in the web-post, and so the use of its elastic bending resistance is conservative.

The effective horizontal shear force $V_{h,eff}$ acting on the web-post takes into account the combined effect of shear and moment (which reduces the effective shear in the top Tee but which increases the effective shear in the bottom (heavier) Tee). The model factor in tests 7 and 8 was reasonable, but was very high for radically different Tee sizes (e.g. IPE300/HEM300) and a narrow web-post, indicating that the method is very conservative for this case. Test 8 failed more by vertical and horizontal shear with a model factor of 1.19.

Table 5-2: Model factors for asymmetric beams

Test	Beam (top/bottom)	$\bar{\lambda}$	V_{test} kN	V_h kN	$V_{h,Rd}$ kN	M_h kNm	$M_{h,el}$ kNm	$V_{h,eff}$ kN	Model factor	Failure mode
2	HEA300 HEM300	0.97	303	303	158 403	3.0	4.5 11.1	285 320	1.80	Vierendeel bending and web-post buckling
5	IPE300 HEM300	1.14	196	174	63 233	9.4	1.3 3.9	120 226	1.90	Vierendeel bending and web-post buckling
7	HEB300 HEM300	0.76	452	485	273 522	15.6	9.8 18.7	401 568	1.47	Vierendeel bending and web-post shear
8	HEA300 HEB300	0.89	392	372	262 322	8.8	10.7 13.8	313 430	1.19	Vertical shear and web post shear

Assumed yield strength = 350 N/mm^2

Notes to table:

Failure occurs by buckling or yielding in the top part of web-post or by Vierendeel bending in the top chord.

M_h is the moment in the web-post which is calculated assuming shear is resisted by the top Tee according to its maximum shear or Vierendeel bending resistance and the remaining shear is resisted by the bottom Tee. M_h is allowed to exceed $M_{h,el}$ in this analysis.

$M_{h,el}$ is the elastic bending resistance of the web post

Effective horizontal shear force: $V_{h,eff} = V_h - 2 M_h/d_o$ (top) or $V_{h,eff} = V_h + 2 M_h/d_o$ (bottom)

5.3.3 Conclusions

The average model factor for the symmetric beams was 1.46, whereas for the asymmetric beams this was 1.59; indicating that the proposed design method for web-post buckling is conservative, and becomes increasingly conservative when the relative sizes of the Tee increases. This is probably because of tensile yielding effects in the web leading to additional post-buckling resistance. This effect was apparent in some tests on beams with thicker flanges.

5.4 Engineering logic for the analysis and design software

The following application rules are consistent with the principles of Eurocode 4 and Eurocode 3 Annex N, and apply to cellular beams with regular circular openings and beams with isolated openings. The rules apply to composite beams and may be adapted to steel beams (by ignoring the contribution of the concrete slab). They are suitable for hand calculations.

1 *Effective length of opening*

1.1 *Effective length*

For Vierendeel bending, the effective length of the opening is given by:

$$\ell_o = 0.5 d_o \quad - \text{circular openings}$$

$$\ell_o = s + 0.5 d_o \quad - \text{elongated openings}$$

$$\ell_o = \ell_o \quad - \text{rectangular openings}$$

where:

d_o = the opening depth (or diameter).

s = centre-centre spacing of openings

The minimum depth of the tees is used in subsequent checks for circular and elongated openings.

2 *Shear resistance of perforated composite beam*

2.1 *Shear resistance of tees*

For hot rolled steel sections, the shear resistance of the top and bottom tees is given by:

$$V_{t,Rd} = 0.9 [(2r + t_{wt}) t_{ft}/2 + d_t t_{wt}] f_y / \sqrt{3}$$

and:

$$V_{b,Rd} = 0.9 [(2r + t_{wt}) t_{fb}/2 + d_b t_{wb}] f_y / \sqrt{3}$$

For fabricated steel sections:

$$V_{t,Rd} = d_t t_{wt} f_y / \sqrt{3}$$

$$V_{b,Rd} = d_b t_{wb} f_y / \sqrt{3}$$

where:

t_{wt} = thickness of top web

t_{wb} = thickness of bottom web

d_t = depth of web of top Tee (below flange)

d_b = depth of web of bottom Tee (above flange)

t_{ft} = thickness of top flange

t_{fb} = thickness of bottom flange

r = root radius of a rolled section

f_y = design strength of steel

2.2 Shear resistance of concrete

At an opening, the shear resistance of the concrete slab is considered over an effective width of $3 \times$ effective slab depth plus the flange width according to:

$$V_{Rd,c} = (1.5 (h_s + h_p) + b_f) (h_s - h_p) v_{cd}$$

where:

h_s is the slab depth

h_p is the deck profile height

b_f is the width of the steel flange (≤ 300 mm)

v_c is the shear strength of the concrete to EC2-1-1, depending on the percentage reinforcement in the slab

2.3 Pure shear resistance of perforated section

The pure shear resistance of the section at an opening is given by the sum of the shear resistances of the steel section and the slab:

$$V_{Ed} \leq V_{b,Rd} + V_{t,Rd} + V_{Rd,c}$$

However, the shear force that can be transferred by the bottom Tee is reduced due to Vierendeel bending and is given by:

$$V_b = 2 M_{b,red} / \ell_o \leq V_{b,Rd}$$

where:

$M_{b,red}$ is the reduced bending resistance of the bottom Tee due to axial tension (see Step 5)

2.4 Shear resistance of highly asymmetric sections

For design of highly asymmetric composite sections, the shear resistance is based on equilibrium of the top and bottom tees, as influenced by the width of the web post between adjacent openings. For narrow web posts, the ability to re-distribute shear between the tees is limited. As a first approximation for a composite beam, the shear transferred by the bottom Tee controls the overall shear resistance of the beam, as follows:

$$V_{Rd} = 2V_b / (1 + 2e/h_{eff}) + V_{c,Rd} \geq V_{Ed}$$

where:

e is the eccentricity of the centre-line of the openings above the mid-height of the beam (negative below mid-height)

h_{eff} is the distance between the centroids of the tees of the steel section

$V_{Rd,c}$ is the shear resistance of the slab (see 2.3)

and:

V_{Ed} is the applied shear force at the centre line of the opening

For wider web posts, the shear forces can be redistributed from the bottom Tee to the stronger top Tee by development of an in-plane moment in the web-post, M_h . A closed solution for this case is given in Step 6.4:

2.5 Effective web thickness due to shear

The effective web thickness of the tees is reduced due to the presence of high vertical shear according to:

$$t_{w,eff} = t_w [1 - (2p - 1)^2] \quad \text{for } p > 0.5$$

or:

$$t_{w,eff} = t_w \quad \text{for } p \leq 0.5$$

where:

$t_{w,eff}$ = effective web thickness

t_w = actual web thickness

p = utilisation in shear

$$= V_{Ed}/(V_b + V_{t,Rd} + V_{c,Rd})$$

This effective thickness of the web is used in calculating the reduced section properties of the tees for global and Vierendeel bending.

Note: A process of iteration is required if required because V_b depends on p . Conservatively V_b can be first set to zero to calculate p .

3 Section Classification

The section classification of the composite section depends on:

- The top flange, as influenced by its attachment to the slab
- The web in compression, depending on the asymmetry of the section
- The depth of the web of the tees
- The length of the opening

The first two criteria are defined in EC3 and EC4. The third and fourth criteria depend on the proportions of the opening, as follows:

For Class 1 or 2 sections, plastic section properties may be used.

For Class 3 or 4 sections, elastic section properties may be used.

3.1 Classification of flange

The classification of the flanges may be taken as in EC3 1-1 and EC4 1-1. Generally the top flange may be treated as Class 2 because of its attachment to the slab.

3.2 Classification of the web of the Tee (ENV 1993 1-1, Clause N.1.7.2)

The outstand of the web of the Tee may be classified, depending on the ratio of the length of the opening, ℓ_o , to the outstand depth d_t , as follows:

$$\text{Class 2 webs: } d_t \leq \frac{10t_w \varepsilon}{\sqrt{1 - \left(\frac{32t_w \varepsilon}{\ell_o}\right)^2}} \quad \text{if } \ell_o > 32t_e$$

All Class 3 webs may be treated as Class 2 if $\ell_o \leq 32t_w\epsilon$

For a Class 2 section, the plastic properties of the Tee may be used.

Class 3 webs:
$$d_t \leq \frac{14t_w\epsilon}{\sqrt{1 - \left(\frac{36t_w\epsilon}{\ell_o}\right)^2}} \text{ if } \ell_o > 36t_w\epsilon$$

All Class 4 webs may be treated as Class 3 if $\ell_o \leq 36t_w\epsilon$

For a Class 3 section, the elastic properties of the Tee should be used.

Class 4 webs: Calculate the effective section properties using the limiting value of d_t for a Class 3 web.

Webs that satisfy the lower limit on ℓ_o are classified independently of d_t .

The effective length of the opening may be treated as follows for stability of the web above or below the opening:

$\ell_o = \ell_o$ - rectangular openings

$\ell_o = 0.7d_o$ - circular openings

$\ell_o = \ell_o - 0.3d_o$ - elongated openings

where:

ℓ_o is the actual length of the opening.

The $d_t/(t_w\epsilon)$ limits are presented in Table 1 for different proportions of openings. A second check on the length of the opening should also be made, as in Table 2, as the web classification is automatically satisfied for small openings.

Table 1: Limit on maximum $d_t/(t\epsilon)$ for webs above openings

Type of opening	Class limit	ℓ_o/d_t (or d_o/d_t for circular openings)				
		> 10	10	5	3	2
Rectangular	2	10	10.5	11.9	14.6	18.9
Rectangular	3	14	14.9	17.2	21.9	28.8
Circular	2	10	12.1	13.5	18.2	22.8
Circular	3	14	15.7	20.1	27.8	38.6

d_t = depth of web of Tee

Table 2: Lower bound of ℓ_o below which the web class is satisfied for all values of d_t

Type of opening	Class limit	Web class satisfied if:
Rectangular	2	$\ell_o \leq 32t_w\epsilon$
Rectangular	3	$\ell_o \leq 36t_w\epsilon$
Circular	2	$d_o \leq 46t_w\epsilon$
Circular	3	$d_o \leq 51t_w\epsilon$

3.3 Effect of axial tension on section classification

Tension in the bottom Tee modifies the section classification for unstiffened tees.

Class 3 webs may be treated as Class 2 if:

$$\frac{N(x)}{A_b f_y} \geq 1 - \frac{20t_w^2 \epsilon f_y}{A_b f_y}$$

where:

$N(x)$ is the axial tension in the bottom Tee at point x in the span

A_b is the cross sectional area of the bottom Tee

In this case, the plastic stress blocks for a Tee section subject to bending and tension are such that the depth of web in compression does not exceed $10t_w \epsilon$.

and:

All Class 4 webs may be treated as Class 3 when also subject to axial tension, provided:

$$d_b \leq \frac{14t_w \epsilon'}{\sqrt{1 - \left(\frac{36t_w \epsilon'}{\ell_o}\right)^2}} \quad \text{if } \ell_o > 36t_w \epsilon'$$

where:

$$\epsilon' = \epsilon / (1 - N(x)/(A_b p_y))^{0.5}$$

and:

d_b is the depth of the web of the bottom Tee above the flange

4 Global Bending Action

4.1 Compression in slab

The bending resistance of a perforated section of any position x along the beam depends on the degree of shear connection at that position.

Compression force in slab

$$N_c(x) = n_{sc}(x) P_d$$

where:

$n_{sc}(x)$ is the number of shear connectors from the support to point x

P_d is the design resistance of a shear connector

x is the distance from the support to the closer edge of the opening

4.2 Tensile force in bottom Tee

Equilibrium of the cross-section leads to the following tensile force in the bottom Tee due to global bending:

$$N(x) = \frac{M(x) - N_c(x) \left((h_s + h_p) / 2 + y_{et} \right)}{h - y_{et} - y_{eb}}$$

where:

$N(x)$ is the global moment acting at point x

4.3 Force in top Tee

The tension or compression force in the top Tee depends on the difference between $N_c(x)$ and $N(x)$. A further check is required on the absolute value of the tension or compression force in the top Tee, according to:

$$|N(x) - N_c(x)| \leq A_t f_y$$

where :

A_t is the cross-sectional area of the top Tee

4.4 Minimum degree of shear connection

The minimum degree of shear connection that should be achieved is given by $N_c(x) \geq 0.5 T(x)$ at the opening.

Note: No limit on the degree of shear connection is made in the region close to the supports, provided the minimum degree of shear connection is achieved in mid-span. The shear connectors in the last 300 mm should be ignored because of the unknown detailing of the connection at the stage when the beam is designed.

5 Bending Resistances of tees

The bending resistance of the tees depends on the section classification and is given by the following equations:

5.1 Plastic Resistance (Class 2)

$$M_{pl,T} = A_w f_y (d_t/2 + t_f - y_p) + A_f f_y (y_p - t_f/2) + A_s f_y (d_t - d_s + t_f - t_p)$$

where the plastic neutral axis position is given by:

$$y_p = (A_f + A_w + A_s)/(2A_f) \quad \text{for } A_s \leq A_f - A_w$$

5.2 Elastic Resistance (Class 3)

$$M_{el,T} = \frac{A_w f_y (d_t/2 + t_f - y_e)^2 + A_f f_y (y_e - t_f/2)^2 + A_s (h_s - e_s + t_f - y_e)}{d_t + t_f - y_e}$$

where the elastic neutral axis position is given by:

$$y_e = \frac{A_s (d_t - e_s + t_f) + A_w (d_t/2 + t_f) + A_f t_f / 2}{(A_f + A_w + A_s)}$$

where:

A_w = cross sectional area of web of the Tee = $d_t t_{w,eff}$

A_f = cross sectional; area of flange

A_s = cross sectional area of horizontal stiffener (if no stiffener; $A_s = 0$)

d_t = depth of web of Tee excluding the flange

e_s = offset distance of centre of stiffener from tip of web (≤ 10 mm)

t_f = thickness of flange

A further limit is that $A_s \leq 0.5 d_o t$ in order to ensure that the adjacent solid web is strong enough to resist the forced transferred from the stiffener.

5.3 Reduced bending resistance due to axial force

The bending resistances of the tees is reduced due to axial tension, according to the following formula:

Plastic resistance:

No stiffeners: $M_{pl,T,red} = M_{pl,T} (1 - (N/N_{pl})^2)$

With stiffeners: $M_{pl,T,red} = M_{pl,T} (1 - N/N_{pl})$

Elastic resistance:

All cases: $M_{pl,T,red} = M_{el,T} (1 - (N/N_{el})^2)$

where:

$M_{pl,T,red}$ is the reduced plastic resistance of the Tee section

$M_{el,T,red}$ is the reduced elastic resistance of the Tee section corresponding to the Class 3 limit

N_{pl} is the plastic compressive resistance of the Tee including the depth of web corresponding to the Class 2 limit

N_{el} is the elastic compressive resistance of the Tee including the depth of web corresponding to the Class 3 limit

N is the axial compression or tension force due to the global moment action at any position (x)

6 Vierendeel Bending

6.1 Applied Vierendeel moment

The Vierendeel bending moment due to transfer of shear across the opening is given by:

$$M_v = V_{Ed} \ell_o$$

The effective length of the opening is defined in 1.1.

6.2 Local composite action

The Vierendeel bending resistance is due to both local composite action and the reduced bending resistance of the tees. The local bending resistance due to composite action across the opening is given by:

$$M_{vc,Rd} = n_{sc,o} P_d (y_{et} + h_{s,eff})$$

where:

$y_{e,t}$ is the distance of the elastic neutral axis of the top Tee below the top of the flange.

$n_{sc,o}$ is the number over shear connectors over length, ℓ_o .

$h_{s,eff}$ is the effective depth to the centre of compression of the slab.

k_ℓ is a reduction factor due to the length of the opening given by:

$$k_\ell = 1 - \ell_o / (25 h_t) \quad \text{for unstiffened openings}$$

$$k_\ell = 1 - \ell_o / (35 h_t) \quad \text{for stiffened openings}$$

where:

h_t is the depth of the top Tee.

k_ℓ can be taken as 1.0, provided $\ell_o \leq 5 h_t$ for both unstiffened and stiffened openings.

The maximum value of this local composite resistance that may be included is dependent on possible pull out failure of the shear connectors. The upper bound is given by:

$$\begin{aligned} M_{vc,Rd} &\leq \ell_o P_d && \text{for single shear connectors in line} \\ &\leq 1.5 \ell_o P_d && \text{for shear connectors in pairs} \end{aligned}$$

6.3 Total Vierendeel bending resistance

For widely spaced openings, the shear transfer across the opening must satisfy the combination of the Vierendeel bending resistance of the steel sections and local composite action:

$$V_{Ed} \leq (2M_{b,red} + 2M_{t,red} + M_{vc}) / \ell_o$$

6.4 Closed solution – Circular openings

For closely spaced openings, the Vierendeel bending resistance is potentially reduced due to the bending resistance of the adjacent web post.

As a closed solution, the maximum shear transfer across a beam with circular openings controlled by web post bending should satisfy:

$$V_{Ed} \leq \frac{(4M_{b,red} / \ell_o + 2M_{h,e} / s)}{1 + 2e / h_{eff}} + M_{c,s} / s$$

where:

$M_{h,e}$ is the elastic bending resistance of the web post given by:

$$M_{h,e} = s_o^2 t_w f_y / 6$$

$M_{c,s}$ is the moment developed due to local composite action between the top Tee and the slab over a length s , given by:

$$M_{c,s} = n_{sc} P_d (y_{c,t} + h_{s,eff})$$

h_{eff} is the effective depth of the steel section between the centroids of the tees ($= h_s - y_{et} - y_{eb}$)

n_{sc} is the number of shear connectors in length s between the centre of adjacent openings

6.5 Elongated openings

For analysis of elongated openings in beams with otherwise regular circular openings at spacing s , the term $M_{h,e}$ should be reduced by a factor of:

0.67 for adjacent circular and elongated openings

0.5 for adjacent elongated openings.

Note: An elongated opening is formed by cutting away the web between adjacent openings.

6.6 Closed solution – Rectangular openings

For closely spaced rectangular openings, the shear transfer should satisfy the conditions for web post bending at the top of the opening, given by:

$$V_{Ed} \leq \frac{(4M_{b,red} / \ell_o + 2M_{h,e} / s)}{(1 + (2e + d_o) / h_{eff})} + M_{c,s} / s$$

7 Web post resistance

7.1 Horizontal shear force

Web post shear occurs due to the development of longitudinal forces in the bottom Tee necessary to resist global bending. The horizontal shear force acting on the web post is given by:

$$V_h = \Delta N = \frac{V_{Ed} s}{h_{eff}} - \frac{M_{c,s}}{s}$$

where:

ΔN is the increase in tension in the bottom Tee over a length, s

7.2 Horizontal shear resistance

The horizontal shear resistance is obtained by considering a shear area of the web post (A factor may be introduced due to the possible coincident moment acting on the web post).

$$V_{h,Rd} = s_o t_w f_y / \sqrt{3}$$

where:

s_o = edge to edge spacing of openings

and:

$$V_h \leq V_{h,Rd}$$

Note: For asymmetric beams, t_w is the minimum web thickness. Web-post buckling need not be checked if $d_o \leq 20t_w \epsilon$ for circular openings.

7.3 Effective horizontal stress

Web post buckling may be analysed by considering the compressive stress due to an effective horizontal force in the web post given by:

$$V_{h,eff} = V_h - 2M_h / d_o \quad \text{on the bottom Tee}$$

or:

$$V_{h,eff} = V_h + 2M_h / d_o \quad \text{on the top Tee}$$

where:

V_h is the horizontal shear in the web post

and:

M_h is the moment acting on the web post, with a maximum value as in 2.4 (This is positive when moment is transferred from the bottom Tee to the top Tee).

The compressive stress acting on the web post is given by:

$$s_c = V_{h,eff} / (s_o t) \quad \text{for } s_o \leq d_o \quad (\text{circular openings})$$

$$\quad \quad \quad \text{for } s_o \leq \ell_o \quad (\text{rectangular openings})$$

or:

$$s_c = V_{Ed} / (d_o t) \quad \text{for } s_o > d_o \text{ or } \ell_o \quad (\text{widely spaced openings})$$

Generally, it is the shear resistance of the bottom Tee which is critical and therefore t is the thickness of the bottom Tee.

The compressive strength, $\sigma_{c,Rd}$, is established from an effective length of the web post, given by:

$$\ell_e = 0.5 \sqrt{s_o^2 + d_o^2} \leq 0.7d_o \quad \text{for circular openings}$$

$$\ell_e = 0.7 \sqrt{s_o^2 + d_o^2} \leq d_o \quad \text{for rectangular openings}$$

The effective slenderness is $\lambda = \sqrt{12} \ell_e / t$, and the compressive strength $\sigma_{c,Rd}$ is established from buckling curve c of Eurocode 3-1-1.

Web post buckling does not occur if:

$$\sigma_c \leq \sigma_{c,Rd}$$

7.4 *Web post bending for rectangular openings*

The bending resistance at the top or bottom of a rectangular or square opening should also satisfy:

$$V_{h,eff} d_o / 2 \leq M_{h,e}$$

This is satisfied by the linking equation for V_{Ed} in Section 6.4.

No further web post bending check is required for circular or elongated circular openings, provided $M_h \leq M_{h,e}$.

7.5 *Closed solution for web post buckling*

A closed solution for the maximum shear force controlled by web post buckling should satisfy:

$$V_{Ed} \leq \frac{(4M_{b,red} / \ell_o + \sigma_{c,Rd} t_w s_o)}{(1 + (2e + d_o) / h_{eff})} + M_{c,s} / s$$

This applies to rectangular openings and conservatively to circular openings.

8 Serviceability Performance

8.1 Additional deflection

The additional deflection due to a simple opening at position x may be given by:

$$\frac{\delta_{\text{add}}}{\delta_b} = k_o \left(\frac{\ell_o}{L} \right) \left(\frac{d_o}{L} \right) \left(1 - \frac{x}{L} \right) \quad \text{for } x \leq 0.5L$$

where:

δ_b is the pure bending deflection of the beam (steel or composite beam as appropriate)

and

k_o is the coefficient obtained from the following table:

Beam type	Opening type	
	Unstiffened	Stiffened
Composite	1.5	1.0
Steel	2.0	1.5

Coefficient, k_o , used in serviceability calculation

For circular openings: $\ell_o = 0.5d_o$

For multiple similar sized openings: $\frac{\delta_{\text{add}}}{\delta_b} = 0.5N_o k_o \left(\frac{\ell_o}{L} \right) \left(\frac{d_o}{L} \right)$

8.2 Natural frequency

The natural frequency of the beam may be calculated ignoring the influence of the openings.

5.5 Design Software

The engineering logic described above has been implemented within the software provided on a CD with this report. This software designs and analyses composite and non-composite beams, under distributed and/or point loads. It also covers web openings which may be circular, rectangular or elongated oval-shaped. Both internal beams and edge beams in general building construction are covered.

The program covers the use of the following hot rolled I-sections: UB, UC, IPE and HE (HEA, HEB and HEM). The beam is assumed to be single spanning and simply-supported at both ends. Cantilever and continuous construction are not covered in the present version of this program. The program incorporates options for the use of a solid concrete slab or steel decking acting compositely with the beam. The floor slab may span parallel to or perpendicular to the beam on one or both sides. For edge beams ONLY, the beam may also be loaded by a cladding element on the other side. In all cases, the self weight of the beam and the supported floor is automatically calculated by the program from the floor layout and cross-section geometry.

The program performs a design optimisation on all the sections in the program database for the selected section type, and lists (in weight order) the lightest 10 sections that satisfy all design criteria. The software covers:

- a) Composite and non-composite construction
- b) Use of standard deck profiles, user defined decks or a solid slab
- c) Propped and unpropped construction (of both the beam and the decking)
- d) Use as an edge or an internal beam
- e) Circular, rectangular and elongated openings, with or without stiffeners
- f) Additional point loads and additional uniformly distributed loads
- g) Use of normal weight and light weight concrete
- h) Use of headed shear connectors (including Hilti HVB shear connectors)
- i) Groups of shear connectors along the beam

Some selected screen shots from the software are shown in Figures 5-1 to 5-4 inclusive:

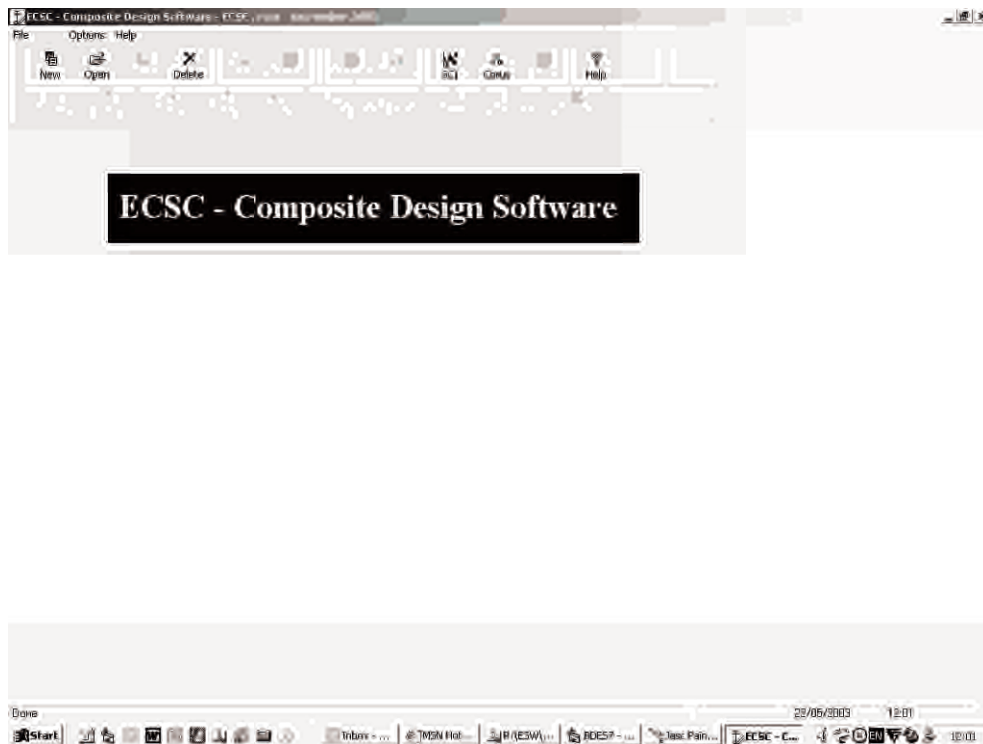


Figure 5-1: Title screen

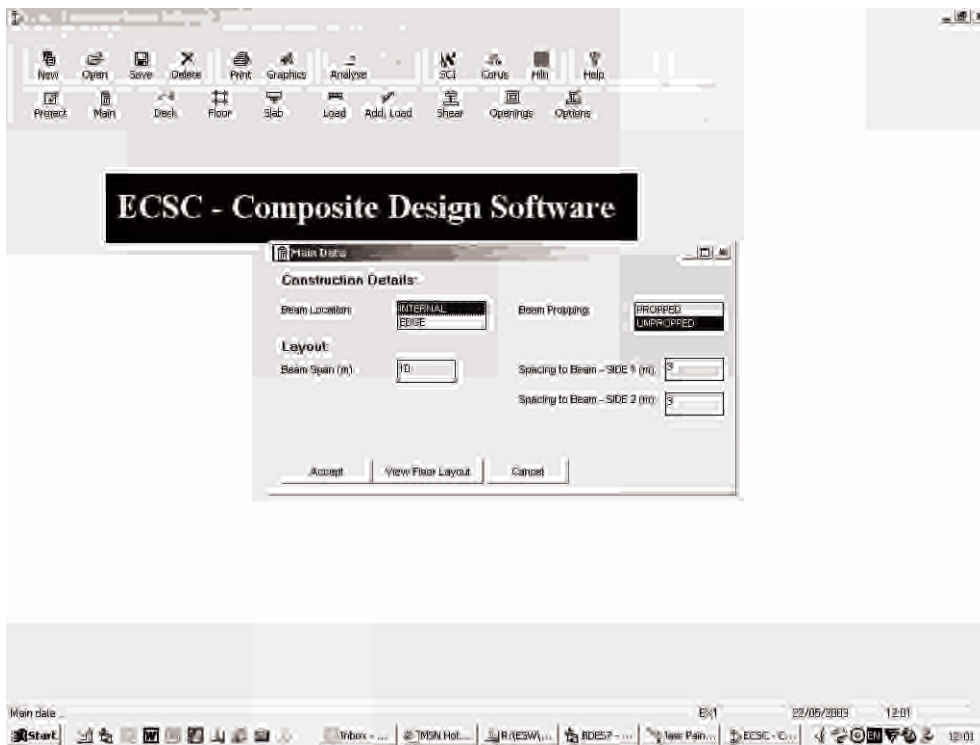


Figure 5-2: Construction details

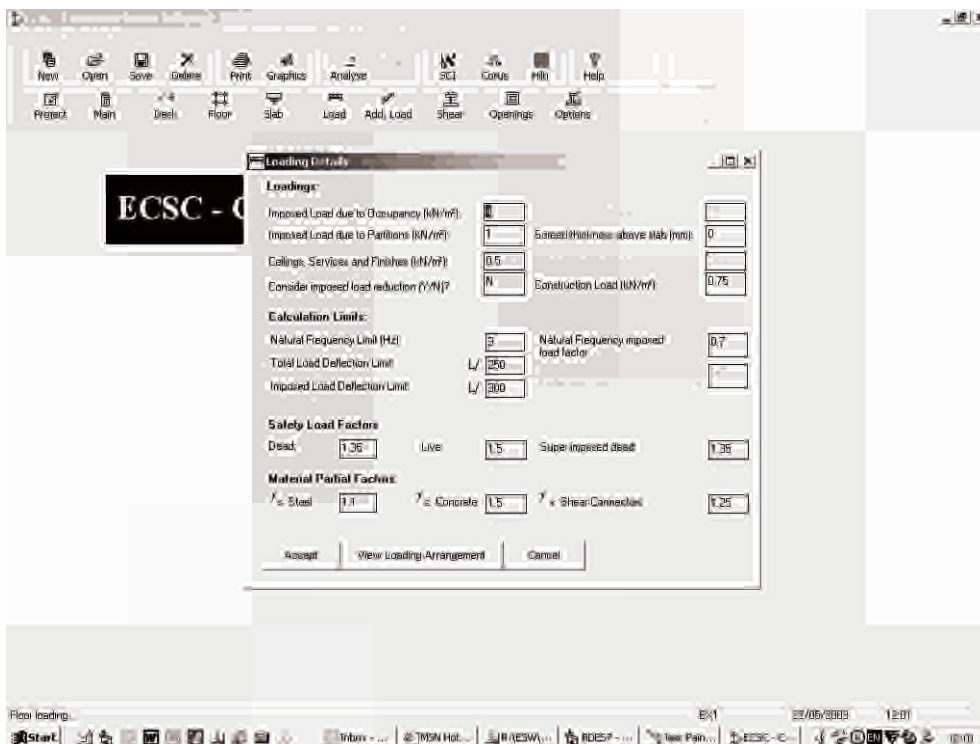


Figure 5-3: Loading data

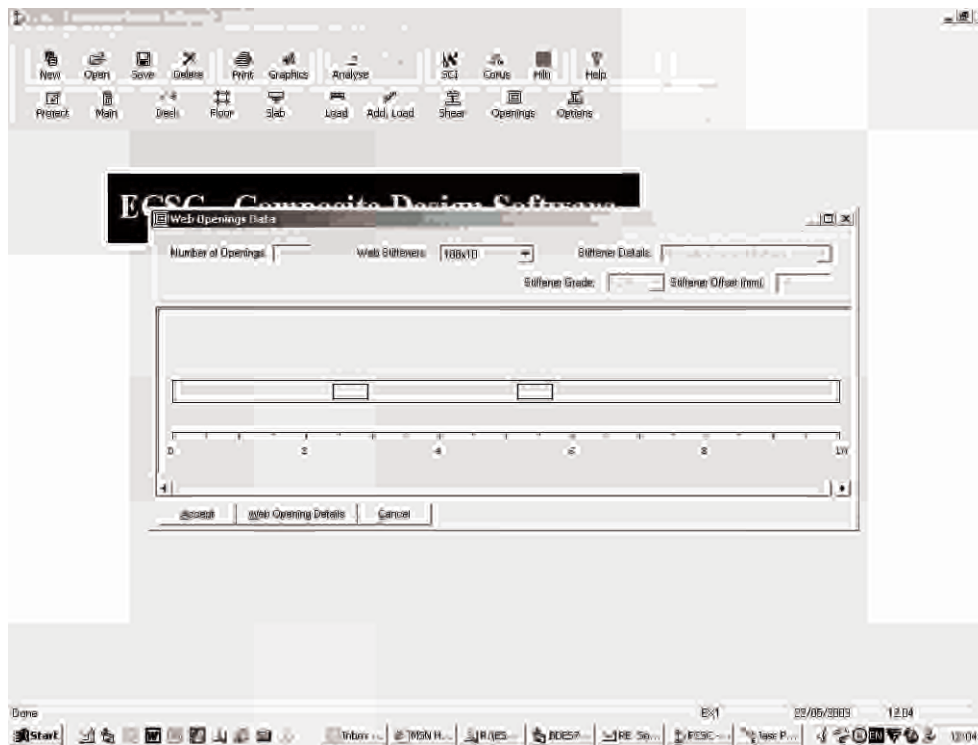


Figure 5-4: Definition of opening positions

5.6 References

1. R M Lawson
 Design for openings in the webs of composite beams (SCI P068)
 The Steel Construction Institute, 1990
2. J K Ward
 Design of composite and non-composite beams (SCI P100)
 The Steel Construction Institute, 1990

6 Contribution from UNIV LULEA

6.1 General

The work at the Division of Steel Structures, Luleå University of Technology (LTU), within this project concerned mainly Work Packages (WP) 1 and 4:

WP 1: Tests on composite beams with web openings.

- Slender web beams with single large web openings subjected to shear.

WP 5: Special cases.

- Design of slender web beams
- Design of elongated circular openings
- Beams in compression including lateral restraints
- Design of semi-continuous joints

6.2 Main objectives

Tests done at LTU constitute the basis for the study of slender web beams subjected to shear. Different sizes of an unstiffened single web opening and the addition of horizontal and vertical stiffeners has been tested at LTU [10].

The expected buckling phenomena for a slender web beam subjected to shear are;

- Local buckling from Vierendeel bending, Figure 6-1A)
- Shear buckling, Figure 6-1B)
- Web-post buckling, Figure 6-1C)

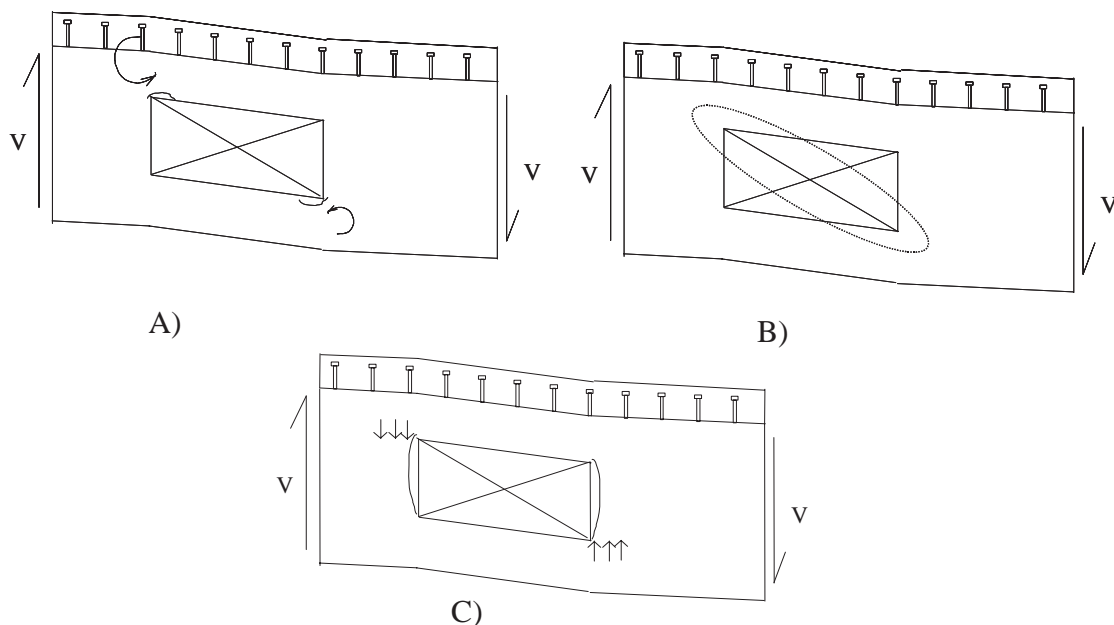


Figure 6-1: Local buckling from Vierendeel bending, B) shear buckling, C) web- post buckling

Several factors effect local buckling due to Vierendeel bending of the outstand of the web, Figure 6-1A). The Vierendeel bending moment has a large gradient over the length of the opening; the flange of the top Tee is connected to the concrete slab and the bottom Tee is subjected to tension from global bending action. The latter assuming a simply supported beam. In design these effects should be included in the classification of the unstiffened web outstands. The phenomenon is prevented by horizontal stiffeners around opening.

Shear buckling, Figure 6-1B), with a web opening is described for bare steel sections in prEN 1993-1-1 (former ENV 1993-1-1, Annex N). This is too conservative for large web openings. The suggestion here is that the concrete adds little to the shear buckling resistance and that the same approach used for bare steel beams should be used for composite cross-sections.

Web-post buckling is a result of Vierendeel bending, Figure 6-1C). The phenomenon is prevented by vertical stiffeners at opening.

When the floor is in place it acts like a bracing of the top flange that prevents lateral deflection. For a simply supported beam this means that lateral buckling cannot occur provided that the supports are sufficiently prevented from rotation. This can normally be assumed to be the case in common frames. For a continuous girder the bottom flange will be in compression close to the supports and hence it may buckle laterally.

Semi-continuous joint are described in EC3 1-8 [9]. The main question is at what distance from the end-plate a large web opening can be placed without interfering with the connection.

6.3 Slender web beams

6.3.1 Test results

Tests 1- 4 consisted of a bare steel section and Vierendeel bending was identified as failure mode for most. Lüder strains were observed at each corner of the openings, i.e. plastic strains suggesting plastic resistance despite a very slender web. As expected the resistance for Test A1-1 was ca twice that for Test A1-2, given Vierendeel bending as failure mode with twice the length for the opening. With horizontal stiffeners the registered resistance increased compared to unstiffened opening but not in correspondence with the area of the stiffener in Vierendeel bending. Shear buckling and web-post buckling was not prevented by horizontal stiffeners only. Adding vertical stiffeners prevented all web buckling.

Tests 5- 8 were composite cross-sections. Tests A2-5 and A2-6 correspond to Tests A1-1 and A1-2 in opening size and steel beam cross-section. Tests B2-7 and B2-8 correspond to Test B1-3 and Test B1-4. Again Lüder strains were observed but also more developed local buckling of the web, shear buckling, local buckling from Vierendeel bending and web-post buckling. Due to the increased resistance from the composite slab these local buckling phenomena developed. Table 6-1 shows the results from the laboratory.

Table 6-1: Results from laboratory test at LTU

Test no.	TEST RESULTS		Shear buckling	Vierendeel $V_{I0}=2M_{vt}+2M_{vb}+M_{vc}$		Web-post buckling
	Applied V (kN)	Observed failure mode	EC3 [4]	Elastic (unreduced)	Plastic (unreduced)	[5]
A1-1	394	Vierendeel	225.2	212	290	225
A2-5	491	Web buckling	275.2 ²⁾	340	455	225
A1-2	206	Vierendeel	40.1	113	179	275 ²⁾
A2-6	302	Vierendeel buckling	90.1 ²⁾	238	308	275 ²⁾
B1-4	393	Web buckling	40.1	338	418	225
B2-8	485	Web buckling	90.1 ²⁾	469	593	275 ²⁾
B1-3	443	Vierendeel	713	338	418	-
B2-7	537	Vierendeel	763 ²⁾	468	588	-

²⁾ Including concrete [5] and [7]

Test B1-4 and B2-8 developed web buckling to the side of the horizontal stiffener. The buckling is clearly not from Vierendeel but rather a mixed shear and web-post buckling. Calculations for shear buckling and web-post buckling resistance for the unstiffened webs are conservative for both bare steel and composite test beams.

Test A2-6 clearly showed local buckling from Vierendeel bending, visible after maximum load was reached. Test A2-5 buckled locally in a mixed shear/ Vierendeel mode.

Plastic Vierendeel resistance of the Tees was reached for several of the tests. This fact is supported by the presence of Lüder strains during testing.

6.3.2 Shear buckling

The resistance to shear of a web with hole according to Annex N of ENV1993-1-1 is based on recommendations in [6], which in turn is a development of design rules in [3]. The reduction factor applied to the shear resistance of the unperforated web

$$\left(1 - \left(\frac{h_0}{h_w} + 0,3 \frac{a_0}{h_w}\right)\right) \quad (6-1)$$

is based on a model that takes Vierendeel action into account as well as shear buckling. Those failure modes are interacting in many cases and it may be hard to identify which one is dominant.

For a composite girder the strength for Vierendeel action is increased by the presence of the concrete slab. This resistance has to be calculated separately and there is accordingly a need for a separate check of the shear buckling resistance. Equation (6-1) would be too conservative for this purpose and computer simulations have been performed in order to identify a more suitable reduction factor that only takes shear buckling into account. As it is only the steel section that is considered for the shear buckling resistance the computer simulations were performed without concrete slab, which makes the calculations much faster. The focus has been on small and medium size holes because very large holes will always be governed by Vierendeel action. The results are

summarized in Table 6-2. V_{cR} denotes the shear resistance according to EN 1993-1-5 for the unperforated web and the resistance considering the hole is given by

$$V_{ocR} = V_{cR} \left(1 - \frac{\sqrt{h_0 a_0}}{h_w}\right) \quad (6-2)$$

This formula has been found by trial and error and it can be seen to give a conservative estimate of the FE-results [10]. The reduction factor depends on the area of the hole but not on its orientation. This seems reasonable considering the disturbance of the rotated stress field in the web caused by the hole. It is clear that the formulae may fail if the size of the hole goes to extremes and the limitations given in [5] should be respected. A recalculation of the test results, where web buckling was identified as failure mode, is presented in Table 6-2.

Table 6-2: Test beams

Test no.	TEST RESULTS		Shear buckling $V_{ocR} = V_{cR} \left(1 - \frac{\sqrt{h_0 a_0}}{h_w}\right)$	Vierendeel $V_{I0} = 2Mvt + 2Mvb + Mvc$		Web-post buckling
	Applied V (kN)	Observed failure mode		Elastic	Plastic	
A2-5	491	Web buckling	410 ²⁾	340	455	225
B1-4	393	Web buckling	155	338	418	225
B2-8	485	Web buckling	205 ²⁾	469	593	275 ²⁾

²⁾ Including concrete [5] and [7]

Further, Table 6-3 gives V_{Vier} which denotes the resistance to Vierendeel action as described in [5]. This clearly depends on the geometry of the hole and it is governing for large holes and also for long holes. The smallest of $V_{o,c,R}$ and V_{Vier} will govern the design and represent the resistance. The last column of Table 6-3 shows the resistance according to FE simulations over the governing resistance. The failure modes indicated in Table 6-3 have been determined from the deformation pattern of the FE-model, see examples in Figure 6-2. The top figure is clear case of Vierendeel failure and the bottom is a clear case of shear buckling. The middle one is deemed as mixed mode. It can be noted in Table 6-3 that the estimated failure mode does not always coincide with the governing design criterion. This is not surprising considering the difficulties to judge the failure mode from the deformation patterns and also the imperfect design models. It should be noted that the error resulting from mistaking the failure mode will be on the conservative side. If for instance a failure in Vierendeel action is taken for a shear failure, the actual shear resistance is higher.

Table 6-3: Results from parametric study

ho x lo (mm)	λw (mm)	V _{Vier} (kN)	EC3 V _{c,R} (kN)	V _{o,c,R} (kN)	V _{FEM} (kN)	$\frac{V_{FEM}}{V_{o,c,Rd}}$	Failure mode
-	1.1	-	909.3	-			Shear buckling ^{c)}
-	1.35	-	610.4	-			Shear buckling ^{c)}
-	2.1	-	265.7	-	358.8		Shear buckling ^{c)}
-	3.16	-	130.0	-	182.9		Shear buckling ^{c)}
300 x 150	1.1	779.5	909.3	619.7	-	-	-
	1.35	588.0	610.4	416.0	455.3	1.09	Shear buckling ^{c)}
	2.1	344.0	265.7	181.1	234.1	1.29	Shear buckling ^{c)}
	3.16	222.7	130.0	88.6	120.0	1.35	Shear buckling ^{c)}
300 x 300	1.1	389.7	909.3	499.7	484.8	1.24	Mixed mode ^{b)}
	1.35	294.0	610.4	335.4	368.7	1.25	Mixed mode ^{b)}
	2.1	172.0	265.7	146.0	193.8	1.32	Shear buckling ^{c)}
	3.16	111.3	130.0	71.4	104.4	1.46	Shear buckling ^{c)}
300 x 450	1.1	259.8	909.3	407.7	397.0	1.52	Mixed mode ^{b)}
	1.35	196.0	610.4	273.7	298.3	1.52	Mixed mode ^{b)}
	2.1	114.7	265.7	119.1	158.8	1.38	Shear buckling ^{c)}
	3.16	74.2	130.0	58.3	88.1	1.5	Shear buckling ^{c)}
300 x 600	1.1	194.9	909.3	330.0	325.6	1.67	Mixed mode ^{b)}
	1.35	147.0	610.4	221.6	243.5	1.65	Mixed mode ^{b)}
	2.1	86.0	265.7	96.4	131.4	1.52	Mixed mode ^{b)}
	3.16	55.7	130.0	47.2	75.1	1.59	Shear buckling ^{c)}
200 x 100	1.1	1617.2	909.3	716.2	-	-	-
	1.35	1258.0	610.4	480.8	-	-	-
	2.1	770.0	265.7	209.3	297.4	1.42	Shear buckling ^{c)}
	3.16	512.0	130.0	102.4	155.2	1.52	Shear buckling ^{c)}
200 x 200	1.1	808.6	909.3	636.2	-	-	-
	1.35	692.0	610.4	427.1	-	-	-
	2.1	385.0	265.7	185.9	268.9	1.44	Shear buckling ^{c)}
	3.16	256.0	130.0	91.0	142.8	1.57	Shear buckling ^{c)}
400 x 200	1.1	406.2	909.3	523.1	461.2	1.14	Mixed mode ^{b)}
	1.35	292.0	610.4	351.2	339.2	1.16	Mixed mode ^{b)}
	2.1	158.0	265.7	152.9	183.8	1.2	Mixed mode ^{b)}
	3.16	99.0	130.0	74.8	93.9	1.26	Shear buckling ^{c)}
400 x 400	1.1	203.0	909.3	363.2	323.0	1.59	Vierendeel ^{a)}
	1.35	146.0	610.4	243.8	234.4	1.6	Shear buckling ^{c)}
	2.1	79.0	265.7	106.1	122.3	1.55	Shear buckling ^{c)}
	3.16	49.5	130.0	51.9	67.2	1.36	Shear buckling ^{c)}

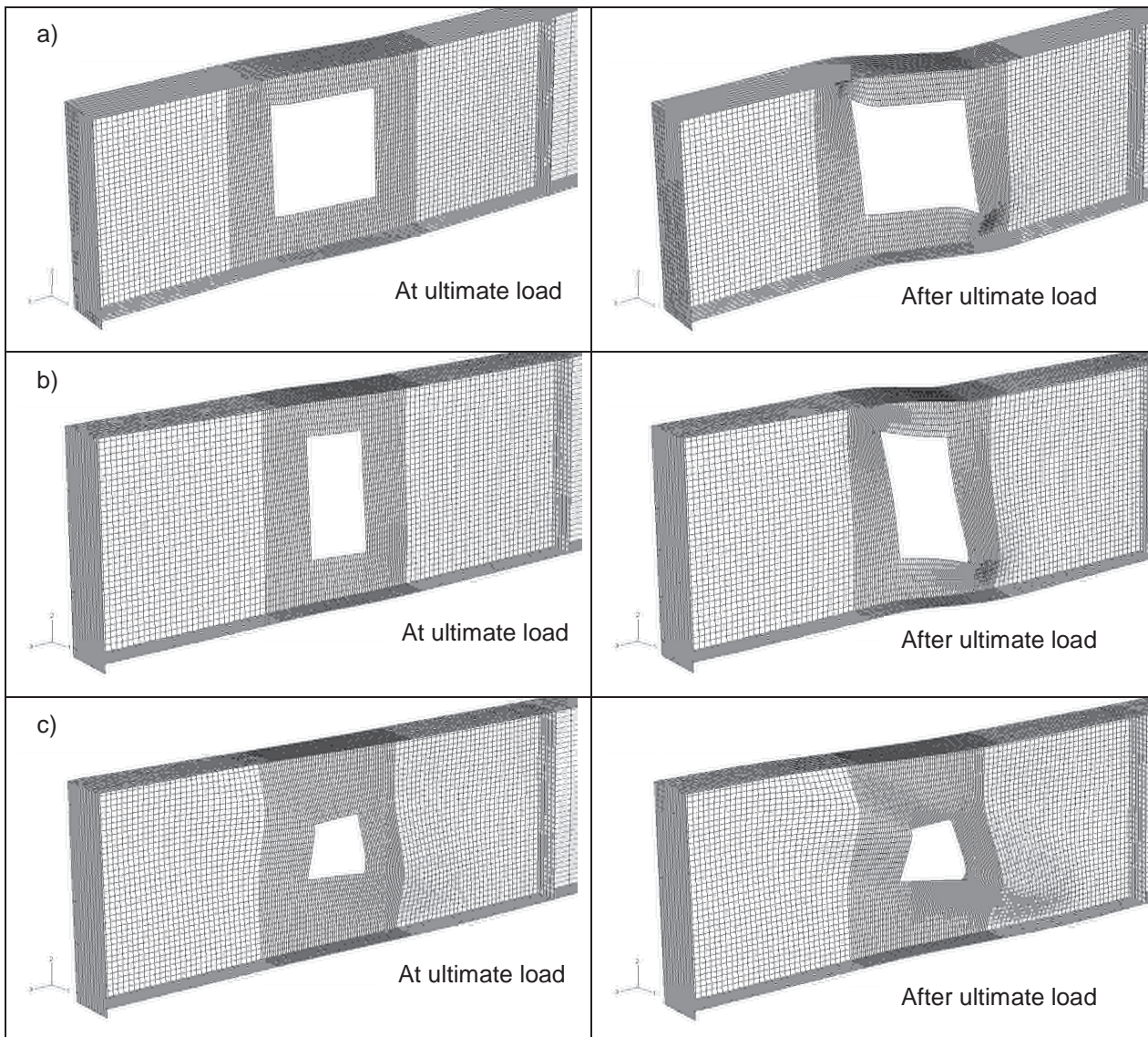


Figure 6-2: Failure modes obtained in the parametric study, the deformations are enlarged three times. a) Vierendeel bending, b) combined Vierendeel bending and shear buckling, c) shear buckling

6.3.3 Vierendeel bending

The classification of the outstand web in [5] is equivalent to EC 3 1-1 [4] outstand flanges:

$d < 10et$ for class 2

$d < 13et$ for class 3

Class 3 and 2 limit originate from buckling factor $k_{\sigma} = 0.425$, i.e uniform compression. The LTU test results show this to be a conservative classification of the Tees. There are three positive effects to consider:

- The effect from global moment, tension in bottom Tee.
- The effect from concrete slab for the top Tee in a composite cross-section
- The effect from a large moment gradient in Tee

The positive effect from tension in the bottom Tee can be considered by calculating the stress distribution from combined Vierendeel and global bending. The compressed portion of the web-tip is then used in the classification [5]. The negative effect from compression in the top Tee can be

done in the same way resulting in a stress distribution where uniform compression in the out stand web is a safe assumption.

The restraint of the web-tip by the concrete slab can be included in classification of the Tee by considering the web as fixed. With this assumption the buckling factor is $k_{\sigma} = 1.25$ for uniform compression. With the same slenderness limits the classification becomes:

$d < 17et$ for class 2

$d < 22et$ for class 3

Whether or not fixed conditions apply depends of course on the flange and number of shear connectors. For the tests here with pairs of connectors in each rib this is clearly the case.

There is also the moment gradient, which is quite large for Vierendeel bending of the Tees. This gives a positive effect but is not included in the classification.

For the LTU composite beams the classification of the Tees becomes class 3 instead of class 4.

6.3.4 Web-post buckling

From test results it is clear that the buckling curve for resistance is conservative with the approach described in [5]. Using plate buckling curve on the other hand shows too optimistic results using the same effective width of the web. Another interesting approach could be to treat the phenomenon as end patch loading but the effective width of the web needs in this case further studying.

An observation from the parametric study, described for shear buckling, is that the web-post failure mode does not occur in the computer simulations. Also in [3] this failure mode was not considered as separate failure mode. It seems likely that this failure can be ignored for isolated holes in thin webs. In this context isolated may be taken as a minimum distance of $1,5h_w$ between adjacent edges of two nearby holes [3]. However, if the hole is provided with longitudinal stiffeners, the web post failure mode should be checked because of the increased shear resistance.

There is an effect from asymmetry for a composite beam with respect to applied loads on the web-post.

6.4 Elongated circular openings

For the design of elongated circular openings in slender web beams the same methods as for rectangular openings is studied using an effective length, l_o . Simulations of steel beams with elongated circular openings are compared to simulations with rectangular openings with the expression for the effective length described in Figure 6-3 [5].

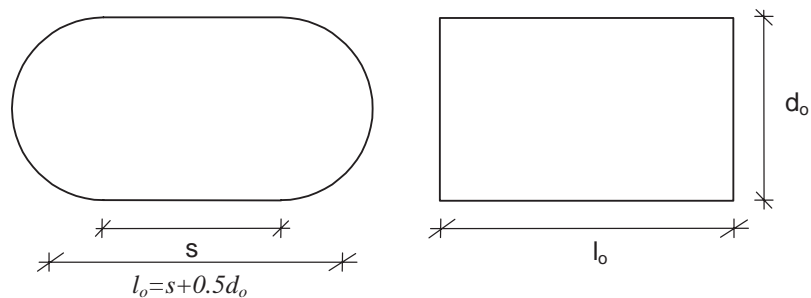


Figure 6-3: Effective length l_o of elongated circular openings

The simulations show very good agreement between rectangular and circular openings using this approach [10].

6.5 Beams in compression including lateral restraints - Lateral torsional buckling of composite beams with web openings

The bottom flange in a continuous girder will be in compression close to the supports and hence it may buckle laterally. Rules for checking LTB of such beams are found in Eurocode 4-1-1[1] called the inverted U-frame model. This model includes the favourable effect of rotational restraint of the top flange. The rules are referred in the text below and modified such that they are applicable also to webs with openings. Limitations of the applicability of the rules are given in Eurocode 4-1-1 but in most practical cases they are fulfilled. In the unlikely case of a long opening close to a support the bottom flange may buckle vertically. This can be checked with the conservative assumption of buckling length equal the length of the opening.

In checks for lateral stability of beams built unpropped, the bending moment at a composite cross-section in Class 1 or 2 is the sum of the moment applied to the composite member and the moment applied to its structural steel component. For cross sections in Class 3 and 4 effects of sequence of construction should be taken into account. For such beams it is simplest to compare the maximum compression stress at support caused by the design loads with $\chi_{LT} f_y / \gamma_{M0}$. The compression stress at support should be calculated considering sequence of construction and for Class 4 sections also effective areas according to Eurocode 3-1-5. In Eurocode 4-1-1 the rules are given for Class 1-3 but they may be applied also for Class 4 as described here.

The design buckling resistance moment of a uniform composite beam with Class 1 or 2 cross-sections is given by

$$M_{b,Rd} = \chi_{LT} M_{Rd} \quad (6-3)$$

where :

χ_{LT} is the reduction factor for lateral-torsional buckling depending on the relative slenderness $\bar{\lambda}_{LT}$ according to Eurocode 3-1-1. There are two sets of reduction curves at it is a national decision which to use.

M_{Rd} is the design resistance moment under hogging bending determined according to Eurocode 4-1-1, 6.2.1.2 for a beam with full shear connection, or 6.2.1.3 for a beam with partial shear connection.

The relative slenderness $\bar{\lambda}_{LT}$ may be calculated by :

$$\bar{\lambda}_{LT} = \sqrt{\frac{M_{Rk}}{M_{cr}}} = \sqrt{\frac{f_y}{\sigma_{cr}}} \quad (6-4)$$

where :

M_{Rk} is the resistance moment of the composite section using the characteristic material properties;

M_{cr} is the elastic critical moment of the composite section for lateral-torsional buckling. For a composite beam assumed continuous at one or both ends, M_{cr} should be determined at the internal support where the hogging bending moment is maximum;

σ_{cr} is the stress in the compression flange caused by M_{cr} acting on the cracked composite section.

The calculation of the elastic critical moment, M_{cr} , may be based on the "continuous inverted U-frame" model. As shown in Figure 6-4, this model takes into account the lateral displacement of the bottom flange causing bending of the steel web, and the rotation of the top flange which is resisted by bending of the slab.

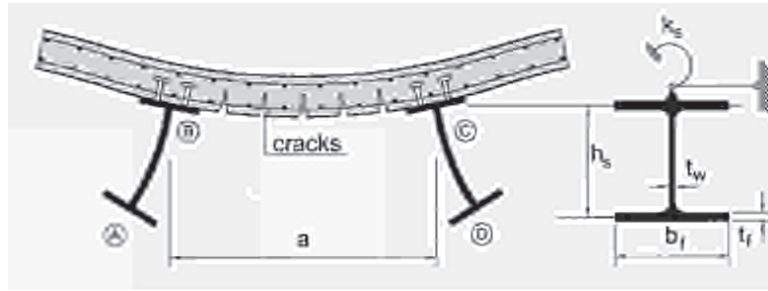


Figure 6-4: Inverted-U frame resisting to lateral-torsional buckling

At the top-steel flange level, a rotational stiffness, c_{ϑ} , per unit length of steel beam may be adopted to represent the effect of the U-frame:

$$c_{\vartheta} = \frac{k_1 k_2}{k_1 + k_2} \quad (6-5)$$

where:

k_1 is the flexural stiffness of the cracked concrete or composite slab in the direction transverse to the steel beam, which may be taken as:

$$k_1 = \alpha E_a I_2 / a \quad (6-6)$$

with $\alpha = 4$ for a slab continuous across the steel beam, and $\alpha = 2$ for a simply supported slab;

a is the spacing between the parallel beams;

$E_a I_2$ is the "cracked" flexural stiffness per unit width of the concrete or composite slab, as defined in 5.4.2.2 of Eurocode 4-1-1, where I_2 should be taken as the lower of the value at midspan, for sagging bending, and the value at the supporting steel member, for hogging bending;

k_2 is the flexural stiffness of the steel web, to be taken as:

$$k_2 = \frac{E_a t_w^3}{4(1 - \nu_a^2) h_s} \kappa_{hole} \quad (6-7)$$

$$\kappa_{hole} = 1 - \frac{2L_{hole}}{L} \text{ for a single opening according to Figure 6-5.}$$

$$\kappa_{hole} = 1 - \frac{3d}{4s} \text{ for multiple circular openings of diameter } d \text{ and spacing } s.$$

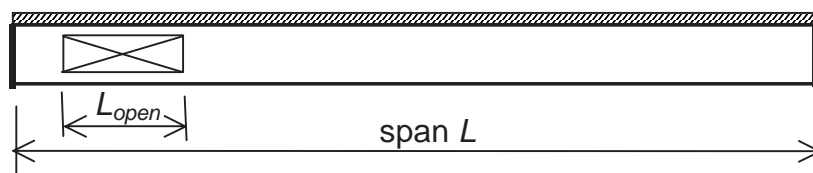


Figure 6-5: Continuous composite beam with opening in the web

The critical bending moment can be calculated from the following formula (6-8)

$$M_{cr} = \frac{1}{k_z} \left[\frac{\pi^2 E J_{\omega D}}{(\beta L)^2} + GJ_{T,eff} \right] \quad (6-8)$$

where:

$$(GJ_T)_{eff} = A (1,5 - 0,5\psi) GI_T$$

GI_T St Venant torsional rigidity of the steel section

A, ψ coefficients depending on the moment distribution, see Figure 6-7

$$EJ_{\omega D} = E(J_{\omega\omega} + z_D^2 J_{az})$$

$J_{\omega\omega}$ the warping section constant of the steel section

J_{az} the second moment of area of the steel section around the vertical axis

β is given in Figure 6-7 as function of η

$$\eta = \sqrt{\frac{c_\vartheta L^4}{EJ_{\omega D}}} \quad (6-9)$$

$$k_z = \left[\frac{(z_D + z_M)^2 + i_p^2}{z_e} + 2 z_D - r_{Mz} \right] \frac{J_{ay}}{J_{st,y}} \quad (6-10)$$

$$z_e = \frac{J_{ay}}{z_{st} A_a} \quad (6-11)$$

$$r_{Mz} = \left(\frac{1}{I_y} \int z (y^2 + z^2) dA \right) - 2 z_M \quad (6-12)$$

$$i_p^2 = (J_{ay} + J_{az}) / A_a$$

A_a is the area of steel section

J_{ay} is the second moment of area of the steel section around the horizontal axis

$J_{st,y}$ is the second moment of area of the composite section neglecting concrete around the horizontal axis.

Other notations are defined in Figure 6-6.

Figure 6-6: Notations for calculation of M_{cr} . S denotes the shear centre and M the centre of gravity of the steel section

A simplified rule is also given in Eurocode 4-1-1 stating that a check of LTB is not needed if certain conditions are satisfied. The rule has here been modified to account for openings in the web. The steel member should be an IPE section or a HE section or another hot-rolled or welded section of similar shape with $A_w / A_a \leq 0.45$, the same depth h , and satisfy the condition:

$$\left(\frac{h_s}{t_w} \right)^3 \frac{t_f}{b_f K_{hole}} \leq 10^4 \varepsilon^4 \quad (6-13)$$

where :

A_a is the area of the structural steel section;

A_w is the area of the web.

Additional notations are given in Figure 6-4.

Figure 6-7: Effective length factor β as function of restraint parameter η for various moment distributions

6.6 Semi-continuous joints

A semi rigid joint is characterized by its strength, stiffness and deformation capacity. A hole in the web close to the end of the beam may influence these characteristics, a fact that could be taken into account. However, this would be a quite elaborate task and the result would most likely be too complicated for practical use. Instead the aim was finding limitations for the placing of the hole such that the joint properties are not affected.

Computer simulations of a beam to column connection have been undertaken [10]. The simulations show no notable influence from the hole on the behaviour of the joint. This would imply that the hole may be placed as close as $0,75h_w$ from the end of the beam without influencing the joint or even closer if the hole is large. As the number of simulations is limited a safety margin is reasonable. The recommendation should therefore be that the edge of the hole should be not closer to the end than h_w .

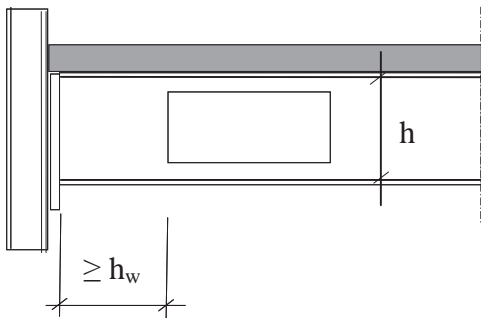


Figure 6-8: Limits with respect to joint for an unstiffened opening

If there is a need to place the hole closer to the end a vertical stiffener is suggested at the edge of the hole closest to the end. As an engineering judgement the stiffener should be taken as single sided with an area of $0,2A_w$ and the distance to the end should not be less than $0,5h_w$.

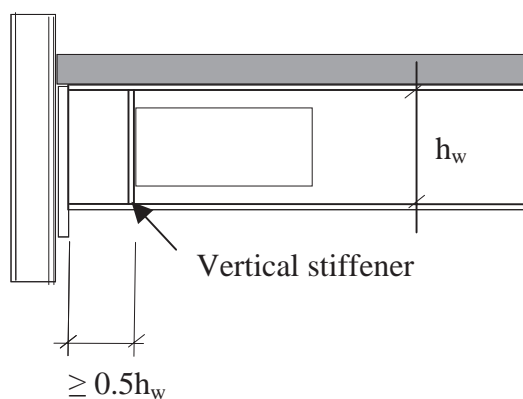


Figure 6-9: Limits with respect to joint for a stiffened opening

6.7 References

- [1] Eurocode 4-1-1 Design of composite steel concrete structures. Part 1-1: General rules and rules for buildings, EN 1994-1-1: 2004.
- [2] Hanswille, G., Lateral Torsional Buckling of Composite Beams. Comparison of more accurate methods with Eurocode 4, Proceedings of the Engineering Foundation Conference Composite Construction IV, Banff, 2002.
- [3] Höglund, T., Bärförmåga hos tunnväggig I-balk med cirkulärt eller rektangulärt hål i livet. Meddelande nr. 87, Institutionen för byggnadsstatik, KTH, Stockholm, 1970.
- [4] Eurocode 3-1-1 Design of steel structures. Part 1.1: General rules and rules for buildings, prEN 1993-1-1 : November 2003.
- [5] SCI, Design of composite beams with large openings for services. Document RT959, London, 2003.
- [6] Steifenlose Stahlskelettragwerke und dünnwandige Vollwandträger, Berechnung und Konstruktion, Europäische Konvention für Stahlbau (EKS), Verlag von Wilhelm Ernst & Sohn, Berlin 1977.
- [7] Eurocode 2-1-1 Design of concrete structures. Part 1: General rules and rules for buildings, prEN 1992-1-1: July 2002.
- [8] Eurocode 3-1-5, Design of steel structures. Part 1-5: Plated structural elements, prEN 1993-1-5: September 2003.
- [9] Eurocode 3-1-8, Design of steel structures. Part 1-8: Design of joints, prEN 1993-1-8: November 2003.
- [10] Part 2 of this final report.

European Commission

EUR 21345 — Steel products and applications for building, construction and industry
Large web openings for service integration in composite floors

*C. Müller, O. Hechler, A. Bureau, D. Bitar, D. Joyeux, L. G. Cajot, T. Demarco, R. M. Lawson,
S. Hicks, P. Devine, O. Lagerqvist, E. Hedman-Pétursson, E. Unosson, M. Feldmann*

Luxembourg: Office for Official Publications of the European Communities

2006 — 120 pp. — 21 × 29.7 cm

Technical steel research series

ISBN 92-79-01723-3

ISSN 1018-5593

Price (excluding VAT) in Luxembourg: EUR 35